Journal of Geoscience and Environment Protection, 2025, 13(10), 135-208
https://www.scirp.org/journal/gep
ISSN Online: 2327-4344
ISSN Print: 2327-4336

Paleoproterozoic Belt/Basins's Plutonic Masses and Country Rocks: Implications on Lithostructurale Architecture of Kedougou Kenieba Inlier (South-East Senegal and South-West Mali)

Mame Codou Ndiaye[1*], Mamadou Ndiaye[2], Papa Malick Ngom[2], Abdoulaye Landoure[3], Alain Nicaise Kouamelan[4], Andrea Moscariello[3], Antoine de Haller[3], Mababa Diagne[5], Rashid Ali Isdine Dao[6], Serigne Saliou Sylla[5], Matar Ndiaye[1]

[1]National Superior School of Mines and Geology, Cheikh Anta Diop University, Dakar, Senegal
[2]Geology Department, Faculty of Sciences and Technics, Cheikh Anta Diop University, Dakar, Senegal
[3]Department of Earth Sciences and Environment, University of Genova, Genova, Switzerland
[4]UFR of Earth Sciences and Mineral Resources, University of Felix Houphouet-Boigny, Abidjan, Ivory Coast
[5]Department of Earth Sciences and Environment, Amadou Makhtar Mbow University, Diamniadio, Senegal
[6]Department of Earth Sciences, Joseph Ki-Zerbo University of Ouagadougou, Ouagadougou, Burkina Faso
Email: *mamecodou1.ndiaye@ucad.edu.sn, lalinguere100@yahoo.fr

How to cite this paper: Ndiaye, M. C., Ndiaye, M., Ngom, P. M., Landoure, A., Kouamelan, A. N., Moscariello, A., de Haller, A., Diagne, M., Dao, R. A. I., Sylla, S. S., & Ndiaye, M. (2025). Paleoproterozoic Belt/Basins's Plutonic Masses and Country Rocks: Implications on Lithostructurale Architecture of Kedougou Kenieba Inlier (South-East Senegal and South-West Mali). *Journal of Geoscience and Environment Protection, 13,* 135-208.
https://doi.org/10.4236/gep.2025.1310010

Received: August 16, 2025
Accepted: October 27, 2025
Published: October 30, 2025

Abstract

This study focuses on Paleoproterozoic plutonic masses and their host rocks located within the Mako belt and associated basins. The objective is to identify their implications for the lithological and tectonic structure of the Kedougou-Kenieba Inlier through an approach integrating geological mapping, petrography, structural analysis, geochemistry, geophysics and geochronology. Indeed, the lithostructural and geochemical characterization of the plutonic masses shows that Dioudioukounkou is a peralkaline calc-alkaline granite from a volcanic arc located in an oceanic context of an active compressive margin. The post-orogenic granite of Dioudioukounkou is 385 ppm enriched in light rare earth elements. The metaluminous Koulountou pluton and the peraluminous Tiguida pluton represent island arc granites. Tiguida is syncollisional and associated with a low percentage of light rare earth elements with a LaN/SmN ratio below the detection limit and a $Na_2O + K_2O$ content of 6.89%, which is the highest alkaline content in Sesam. Koulountou is a post-collisional granite marked by an active compressive margin environment. It is enriched in light rare earth elements with a LaN/SmN ratio of 2.55. Tinkoto and Diabba are hosted in tholeiitic and calc-alkaline volcanics intersected by calc-alkaline plu-

tonites. Dioudioukounkou shows a concordant U-Pb age of zircon of 2156.1 Ma ± 5.6 Ma. This age appears to correspond to the phase of major magmatic activity associated with early Eburnean deformation D1 comparable to CiscoW. Tinkoto and Koulountou formed at 2109.3 Ma ± 6.0 Ma and 2106.7 Ma ± 8.1 Ma, respectively. Tinkoto is older and linked to the main CiscoM shear corresponding to D2. Koulountou is linked to the second order structures of CiscoM. The geophysical signatures of high to medium magnetic intensities highlight a succession of tectonovolcanic arcs: the arc in context of an oceanic volcanic arc associated with CiscoW, the arc in context of an island arc associated with CiscoM, the arc in context of a back-arc basin associated with CiscoE or D3, and the arc in context of an intracontinental volcanic arc associated with the CiscoF shear contact of Faleme or D4. The basins are defined in low to medium magnetic zones and correspond to the Diale back-arc basin and the Kofi intracontinental basin. These formations are intersected by the volcanic arc granite of Dioudioukounkou, the island arc granites of Koulountou and Tiguida, the back-arc basin granites of Tinkoto and Saraya, and finally the pluton of the intracontinental basin of Gamaye. The latest lithostructural architecture of the Kedougou-Kenieba inlier highlights the tectonomagmatic complexes of Maco, Sesam, Diabba and Kofi, which constitute the regional substrate enclosing these plutonites. The geodynamic evolution of these complexes is linked to a single magmatic event associated with tectonomagmatic episodes. Diabba, which represents the back-arc basin, shows an overturned funnel-shaped geosynclinal architecture, while the intracontinental Kofi basin reveals an hemigraben configuration opened at the end of late orogenic phase behind the intracontinental Faleme collision arc.

Keywords

Paleoproterozoic, Plutonic-Masses, Tectonomagmatic, Arcs, Basins, Belt

1. Introduction

Paleoproterozoic Inliers provide natural windows onto structures buried in the continental crust. They provide access to deep stratigraphic sequences, generally associated with highly complex structural and geodynamic processes. In ancient mountain ranges, they play a key role in reconstructing crustal architectures and geodynamic trajectories. The Kedougou Kenieba Inlier is located within a geologically complex area that has been heavily affected by tectonic events, notably the Eburnean orogeny approximately 2.2 to 2.0 Ga ago. It has been explored little, but it is of undeniable scientific and economic interest. The lithostructural interpretation of the Kedougou-Kenieba Inlier is often limited by the heterogeneity of the available data and difficulties of correlating local observations on a regional scale. Previous studies have mainly focused on field surveys or isolated or regionally segmented lithostratigraphic approaches, leaving uncertainties about the overall architecture of the Kedougou-Kenieba Inlier. Also, the structural configuration of Kedougou-Kenieba Inlier was initially based on four (4) deformation phases con-

ventionally designated D1, D2, D3, and D4. Even if this division establishes the major trends of Paleoproterozoic evolution, it lacked fine spatialization and coherent structural integration with shear corridors recognized within the field. To overcome these limitations, our work proposes an integrated approach combining, first, a detailed lithostructural, lithogeochemical, and geochronological analysis of the Mako-Diale transition zone, then extended to a correlation with regional geophysical and radiochronological results involving new data supplemented by conclusions from existing work within the entire Kedougou-Kenieba Inlier. The main objective of this study is to define the lithostructural architecture of Kedougou-Kenieba Inlier based on local results correlated with data from the segmented area of the entire inlier. This suggests establishing a petrographic, aeromagnetic, radiometric, geochemical, and geochronological characterization of the large plutonic masses within the tectonomagmatic complexes of Maco, Sesam, Diabba, extended to Saraya, Faleme, and Gamaye plutons and host formations. The geophysical and geochemical signatures of the large plutonic masses and their surrounding rock formations highlight implications of their geodynamic context in structuring the lithostructural architecture of Kedougou Kenieba Inlier and the genesis of associated orogenic deposits. This implies reconstructing the magmatic and tectonic history of the plutonic formations and their host-rocks standing as a regional substrate, identifying the relationships between magmatism, tectonics, and lithology, and finally proposing a geodynamic model for the Kedougou Kenieba Inlier. By proposing a coherent reconstruction of the architecture of Kedougou-Kenieba Inlier, this study contributes to the enrichment of regional knowledge and can serve as a reference for future work in similar contexts. The integrated approach we have adopted is part of a scientific approach aimed at reducing the uncertainties associated with geological extrapolations in complex areas. Not only does it provide a better understanding of tectono-stratigraphic and tectonomagmatic relationships, but it also opens up new perspectives for structural mapping, mineral exploration, and geodynamic modeling.

2. Geological Context

Paleoproterozoic formations of the West African craton are associated with several generations of intrusive formations. Their emplacement led to contact metamorphism of varying degrees in the surrounding rocks. Hirdes et al. (1992) made a general summary of the various studies carried out by different authors, enabling them to distinguish granitoids associated with Paleoproterozoic formations:

Granitoids of the Winneba type in Ghana which are the only ones to have arisen with any certainty from the remobilization of an Archean crust (Taylor et al., 1988). They outcrop in the sedimentary basin of the same name.

High-K or Bongo-type granitoids dated at 1968 Ga and, linked to Tarkwaïan intersected sediments. They outcrop in the Bole-Navrongo belt (Ghana).

Basin granitoids or Cape Coast granitoids or Baoule granitoids in Côte d'Ivoire. They are always associated with sedimentary basins and form large concordant syn-

or late-tectonic batholiths, surrounded by a thick halo of contact metamorphism. Their ages range from 2.15 to 2.05 Ga.

Belt-type granitoids or Dixcove-type granitoids in Ghana or Boudounkou-type granitoids in Senegal (Bassot, 1963; Bessoles, 1977). Their ages vary between 2.08 and 1.95 Ga. They are intrusives in Birimian volcanic belts and form small, often circular, late to post-tectonic massifs. They are often isotropic and therefore rarely structured or foliated, and are surrounded by an aureole of contact metamorphism, a few meters wide. Boudounkou-type granitoids are found in the Mako Supergroup.

Other classifications have been proposed by authors such as Roques (1948) in Dioh, Junner (1940), Bodin (1951), Bassot (1963), and Bessoles (1977).

Roques (1986) distinguished the following in AOF (Afrique Occidentale Française): concordant birimian batholiths, heterogeneous in nature, with clear schistosity and contact metamorphism; discordant batholiths, homogeneous in nature and with calc-alkaline affinity, characterized by an absence of schistosity and a weak halo of contact metamorphism; discordant batholiths with alkaline affinity.

Bassot (1966), Witschard (1965), Dia (1988), Dioh et al. (1990), Gueye (1995), Dia et al. (1997), and Gueye et al. (2008) have proposed different ages and emplacement contexts for the Kedougou Kenieba inlier. Granitoids intruding Mako volcanic belt are represented by biotite granodiorites and hornblende granodiorites, while those intruding the volcanosediments and sediments are made up of granodiorites as well as diorites and quartzite diorites.

Several authors have proposed a classification of the granitoids of Kedougou-Kenieba inlier in general and of the Mako Supergroup in particular. These include:

Hirdes et al. (1992) distinguished between biotite basin granites and amphibole belt granites.

Dioh et al. (2006) carried out a petrographic and geochemical study highlighting calc-alkaline granitoids evolving over time from sodic to potassic terms with: i) the layered plutonic complex outcropping to the North of the inlier, formed of sodic calc-alkaline granitoids showing similarities with adakites; ii) amphibole granitoids with TTG characteristics (Badon-Kakadian, Tinkoto, Mamakono, Soukouta massifs, etc.); iii) potassic granitoids with orthopyroxene and a high calc-alkaline content; iv) orthopyroxene-clinopyroxene potassic granitoids deposited preferentially in the Diale-Dalema series (Balamgouma and Boboti massifs); v) biotite granites deposited in the meta-sedimentary series (Kenieba, Saraya and Gamaye massifs).

Gueye et al. (2008) defined the following on the basis of geochronological and lithostructural studies: the Badon granites and tonalitic gneisses of Tinkoto (2200-2198 Ma) that recorded the early Eburnian phase; the layered plutonic complex and granites of Laminia Kaourou (2160-2130 Ma), relatively early to contemporaneous with the major Eburnian phase (D1); Diombalou and Bouroumbourou granites oriented parallel to the schistosity; and Mamakono, Tinkoto, and Saraya granites and garnet leucogranites (2100-2070 Ma).

Apart from the large plutonic granitoids, ultramafic facies associated with granitoid host-formations are recognized throughout West Africa Craton: in Ghana

(Loh & Hirdes, 1999; Attoh et al., 2006; Dampare et al., 2019), Côte d'Ivoire (Pouclet et al., 2006), Mali (Sangare, 2008), Burkina Faso (Ouedraogo, 1985; Beziat et al., 2000; Castaing et al., 2003) and Senegal (Bassot, 1966; Dia, 1988; Ngom, 1995; Ngom et al., 1998; Ngom et al., 2010; Cissokho, 2010; Dabo et al., 2017; Labou et al., 2019).

Ultramafic facies are widespread in the bimodal volcanic belts of the Bouroum Yalogo and Loraboue furrows in Burkina Faso (Zonou, 1987; Beziat et al., 2000), Kadiolo in Mali, Yaoure, Marabadiassa and Haute Comoe in Côte d'Ivoire (Fabre, 1987; Pouclet et al., 1996; Bundesanstalt für Geowissenschaften und Rohstoffe, Hannover, 1998; Pouclet et al., 2006) and Dixcove in Ghana (Attoh et al., 2006). Their lithological position and relationship to basalt flows are generally ambiguous. Some were emplaced before the D2 deformation phase, and others were after. In all cases, they are variously interpreted as the cumulative products of tholeiitic volcanism, or as the roots of oceanic crust, or as the early terms of granitoids (Cissokho, 2010).

In the Kadiolo volcanic belt (Mali), ultramafic-mafic rocks represented by dunites, wehrlites, lherzolites, gabbro-norites, norites, and diorites form discontinuous outcrops within the granitoids. The elongation of these basic ultrabasic rocks along NNE-SW to N-S faults could indicate their outcrop during relatively recent faults linked to Tertiary tectonic activity in the Taoudeni Basin (Femenias, oral com. in Sangare, 2008). They are interpreted as early accumulations of arc-type tholeiitic magmatism (IAT).

In the Ashanti belt (Ghana), the Akitekyi and Ahama ultrabasic complexes, differentiated into peridotites and pyroxenites, are associated with volcanic rocks (Loh & Hirdes, 1996).

In the southern part of the Ashanti belt, Dampare et al. (2019) identify two types of basalt above an ultramafic complex differentiated into dunites, harzburgites, pyroxenites, and gabbros. LREE-depleted Type I basalts display the geochemical signatures of back-arc basins. Type II basalts, enriched in LREE and LILE, show the geochemical characteristics of intra-oceanic island arcs.

In Ghana's Dixcove Belt (Attoh et al., 2006), the ultrabasic complex, differentiated into dunites, harzburgites, gabbros, and plagiogranites, contains rodingite.

In Senegal, Bassot (1963; 1966) showed that a tholeiitic suite of dispersed lenses of ultramafic rocks in tectonic contact with the mafic series can be found in the Mako village area within the MTZ zone of strong deformation (Ledru et al., 1989; 1991).

Ultramafic rocks appear in the form of polycrystalline massifs (lherzolite, harzburgite ± wehrlite) as at Lame, and bodies formed of a single rock type (wehrlite or lherzolite) as at Mako, Koulountou, and Sofia; UM rocks are affected by shear-contact with basalts, gabbros, and volcano-sedimentary rocks that encase them (Cissokho, 2010).

Several major phases of Eburnean deformation affecting the KKI during the Paleoproterozoic were recorded by Dabo & Aïfa (2010) and Ledru et al. (1991). The D1 phase, dated between 2.19 - 2.17 Ga, resulted in crustal thickening due to horizontal shortening transitioning from NE-SW to ENE-WSW (Diallo et al., 2020).

It is synchronous with the intrusion of large Tonalite-Trondhjemite-Granodiorite (TTG) batholiths within the Mako belt (Gueye et al., 2008). A large Nord-South strike-slip fault and shear zones characterized the D2 phase and mark a change in tectonic style from collisional to transcurrent deformation (Dabo & Aïfa, 2010). This tectonic phase, dated between 2140 Ma and 2100 Ma, is synchronous with the emplacement of several intrusions across the Proterozoic terranes of the West African Craton (Dabo & Aïfa, 2013; Dabo et al., 2018). Phase D3 is characterized by transcurrent or transtension tectonics and occurs between 2100 Ma and 2060 Ma (Dabo et al., 2018). Some authors have described the shear zone along the Faleme belt as the Senegalo-Malian Shear zone (SMS), formerly known as the Senegalo-Malian Accident. Other researchers have also questioned the existence of this structure and the qualifiers attributed to the signature, notably Allibone et al. (2020), even though the structure appears to control the useful substances in this zone with the arrangement of several deposits along this magnetic signature (Lawrence et al., 2013; Lambert-Smith, 2016). This structural configuration of Kedougou-Kenieba Inlier (KKI), within the West African craton, was initially based on a four (4) Phases deformation model conventionally designated D1, D2, D3, and D4. This division establishes major trends of Paleoproterozoic evolution.

Recently, Ndiaye et al. (2025) have established a new lithostructural model marked by the introduction of a new structural nomenclature (Shear-contact or Cisco) that assigns each phase a representative regional tectonic structure associated with a major lithological contact, making a clear contrast: CiscoW, CiscoM, CiscoE, and CiscoF. This 2D/3D model, formalized by Ndiaye et al. (2025), highlight relationships between lithologies, magmatism, deformation episodes affecting the different formations of Kedougou Kenieba Inlier and also the main shear zones describe as follow: The Western shear-contact (CiscoW) is a North-south to Northeast shear located between pillow lavas and andesitic to metavolcanic facies. The CiscoW forms the boundary between the Maco and Sesam domains. CiscoW corresponds to Sabodala Sinistral Mylonitic Shear Zone (SSZ). The Median shear-contact (CiscoM) set, as sinistral shear, is made up of two ranges of structures. A main branch that marks the lithostructural contact between Diabba and Sesam domains, followed by second-order structures. The main CiscoM is set with two branches: the northern branch, located to the north of the area of study, is oriented north-south. The main CiscoM southern branch is located to the south of the area of study and is oriented northeast. The Eastern shear-contact (CiscoE) is a NE-trending dextral strike-slip, mainly regional in extent. It forms the eastern boundary of the Diabba volcaniclastic formation. The CiscoE corresponds to the Main Transcurrent shear zone (MTZ). The main structure located at the level of the Faleme shear zone is recorded CiscoF.

The 2D/3D model of the Mako-Diale transition zone also highlights a litho-structural design showing three (3) domains (Maco, Sesam, Diabba evolving to three tectonomagmatic complexes: Maco oceanic crust, Sesam-arc, and Diale back-arc-ba-

sin (Diabba). Maco oceanic crust volcanism is unimodal (calc-alkaline) and associated with two tholeiitic series showing distinct magmatic sources in the context of a volcanic arc. The Sesam arc is marked by bimodal volcanism (tholeiitic and calc-alkaline), including Morbs tholeiites and also island arc tholeiites located at the edge of the continent. Diabba is marked by bimodal volcanism (tholeiitic and calc-alkaline), including continental MORBs tholeiites and MORBs or OIBs tholeiites. Plutonic masses within the Mako-Diale transition zone belong to three (3) different magmatic sources: Maco calc-alkaline diorite, Koulountou and Tinkoto granites, and tholeiitic diorite of Maco come from high-K mafic rocks, while Tiguida granite, Diabba granodiorite, and Maco tholeiitic gabbros belong to low-K mafic sources. The Dioudioukounkou granite is sourced from tonalite rocks.

The Kedougou-Kenieba inlier is intersected by several large plutonic masses: Badon-Kakadian Batholith, Dioumbalou, Bouroumbourou, Saraya, Tinkoto, Dioudioukounkou, Kouloutou, Tiguida, Soukouta, Gamaye granites... Different ages and emplacement contexts have been proposed by Bassot (1966), Dia (1988), Dioh et al. (1990), Gueye (1995), Dia et al. (1997), and Gueye et al. (2008). Radiochronological data from several large plutonic masses are defined by certain authors, in addition to other lithotectonic results from hosted formations. Existing radiochronological data are shown in **Table 1**.

Table 1. Summary of geochronological data of plutonic masses from the data of Kedougou-Kenieba Inlier.

Plutonics Formations	Ages (Ma)	Methods	Sources
Sandikounda Layered Plutonic Complex (SLPC)	2158 ± 8	Pb-Pb (zircon)	Dia et al. (1997)
Badon Granodiorite	2198 ± 2	Pb-Pb (zircon)	Gueye et al. (2007)
Laminia Pluton	2105 ± 8	Pb-Pb (zircon)	Dia et al. (1997)
Kaourou Pluton	2079 ± 6	Pb-Pb (zircon)	Dia et al. (1997)
Mamakono Granodiorite	2076 ± 3	U-Pb (zircon)	Hirdes and Davis (2002)
Tinkoto	2074 ± 5	Pb-Pb (zircon)	Gueye et al. (2007)
Saraya Batholith	2079 ± 2	U-Pb (monazite)	Hirdes and Davis (2002)
Boboti Pluton	2082.2 ± 0.9	U-Pb (zircon)	Hirdes and Davis (2002)
South Faleme Tonalite	2081.5 ± 1.1	U-Pb (zircon)	Hirdes and Davis (2002)
Gamaye Pluton	2045 ± 27	Rb-Sr (WR)	Bassot and Caen-Vachette (1984)

3. Materials and Methods

This study is based on an integrated approach combining field data, laboratory analyses, and regional geophysical processing, applied to a representative area

of the Kedougou-Kenieba Inlier. The petrographic study was carried out using thin sections and polished sections produced at the Felix Houphouët-Boigny University in Côte d'Ivoire. Geochemical analyses were carried out by X-ray fluorescence spectrometry, or XRF, at the University of Lausanne. The analyses of the samples provided geochemical data on the major plutonic masses and host formations in the study area. The limits of detection depend on the element concerned but are in the range 1 to 7 ppm for trace elements and 20 to 80 ppm for major elements.

The geochemical results were processed using the Geochemical Data toolkit. The QUEMSCAN analyses were carried out at the Department of Mineral Resources and Geofluids at the University of Geneva. Zircon U-Pb dating was carried out on three (3) magmatic rock samples: Ech.66, Ech.85, and Ech.98. The concordia ages were calculated using the program IsoplotR. All errors are reported at $_{1\sigma}$ (sigma).

In the lithostructural study, outcrops were identified, described, sampled, and represented on a detailed map. Geological mapping was used to produce interpreted lithological and structural maps. Field campaigns allowed direct observations of outcrops, description of lithological facies, and analysis of tectonic structures. The main criteria recorded include the nature and thickness of units, the geometry of folds, faults, and shear zones, and the relationships between magmatic intrusions and deformations.

Regarding geochemical study, representative samples were collected and analyzed in the laboratory using X-ray fluorescence and ICP-MS spectrometry to determine the elemental composition of the rocks, identify discriminating geochemical signatures (trace elements, rare earths), and reconstruct magmatic evolution and metallogenic processes.

Local lithostructural variations due to magnetism have been highlighted by aeromagnetic surveys measuring the Earth's magnetic field. These anomalies reflect geological structures in the Earth's crust, in particular the spatial geometry of rocks and the presence of lineaments interpreted as geological discontinuities (faults).

Minerals such as magnetite (Fe_3O_4), ilmenite, and pyrrhotite suggest the presence of endogenous rocks, mainly basic to ultrabasic. They are considered ferromagnetic and are responsible for the magnetic susceptibility of rocks, which can be studied on the ground or remotely using a magnetometer.

Spectral radiometry or gamma spectrometry is an airborne prospecting method that records the gamma radiation emanating from the first few centimeters of the ground. The radiometry was integrated and combined with fact-mapped data to mainly redefine geometric and geological characteristics of large plutonic masses by highlighting the ground levels of elements potassium (K), thorium (Th), and uranium (U). Each of these elements characterizes a specific type of facies; for example, potassium abundance indicates the presence of an acidic facies such as granite. In areas where outcrops and drilling data were insufficient

or non-existent, only radiometric and aeromagnetic considerations were taken into account.

For geochronological analyses, zircons from plutonic rocks were analyzed using mass spectrometry LA-ICP-MS to determine the ages of pre-, syn-, and post-tectonic plutonic masses (U-Pb). The geophysical analysis of airborne magnetic and radiometric data covering the entire inlier has been integrated to identify magnetic anomalies associated with deep structures, to map radiometric bodies (U, Th, K) likely corresponding to specific lithologies, and to correlate geophysical signatures with lithostructural observations. The correlation of local results to the regional scale was guided by objective criteria: the continuity of tectonic structures, consistency of geophysical anomalies, inter-site geochemical concordance, and compatibility with the Eburnean geodynamic framework.

The correlation is based on rigorously defined criteria: evaluation of existing results from different authors, continuity of observed tectonic structures, regional extension of lithostratigraphic units, homogeneity of geophysical anomalies (magnetic and radiometric), consistency of inter-site geochemical signatures, and compatibility of the interpretation with the regional geodynamic framework. These elements constitute methodological basis for our modeling.

4. Results

4.1. Petrographic and Mineralogical Characteristics of Maco, Sesam and Diabba Formations

4.1.1. Maco Formations

Maco lithologies (Dioudioukounkou hosting formations) are mainly represented by metabasalts, ultrabasic formations, and basic, intermediate, and acidic plutonites such as dunites, gabbros, diorites, granodiorites, and granites. Lithological contacts in this corridor are predominantly North-west trending. Foliation planes are oriented to the East-west and North-west. In places, North-South shears correspond to dolerite and gabbro dykes and sills.

1) Volcanic formations

The Maco metabasalts (**Figure 1**) have a microlitic texture and show massive or pillowed form.

Massive, dark-colored, weakly fractured metabasalts intersected by quartz veins are mainly located at the base of the Dioudioukounkou hill. Pillow basalts have a greenish color and are located in the northern part. Pillow lavas range in size from centimeters to decimeters. These rocks are affected by fractures, shears, and veins of folded and boudinated granodiorites.

Dacites are greyish-green effusive rocks rich in quartz and plagioclases. They are weakly porphyritic lavas with plagioclases phenocrysts and microphenocrysts. Calcite and quartz veinlets are noted.

2) Plutonic formations

Peridotites (Ech.86) are composed of serpentinite, olivine, tremolite, diopside, hedenbergite, and chlorite (**Figure 2**). The Diopside-hedenbergite is between the

olivine. Chromite, magnetite, pyrite, and hematite are accessory minerals.

The serpentinites (Figure 2) of Maco are sills that form chain-like hills in tectonic contact with major CiscoW shear-contact zones, sometimes offset by NW-SE faults. These ultramafic facies are affected by ductile deformation. They are holomelanocratic and mainly composed of serpentine (80.16%), Fe oxides (3.58%), olivine (1.97%), tremolite-actinolite (2.87%), chlorite (0.17%), Enstatite ferrosilite (1.91%), chromite (0.87%), diopside (0.19%), hedenbergite (0.63%), and horneblende (0.3%). The presence of Talc is notable as well as pervasive serpentine and serpentine veinlets.

Gabbros (Figure 3) in contact with ultrabasites are coarse to fine to medium grained rocks with a highly altered granular (igneous) texture (carbonated, epidotized, chloritized, leucoxenized) with late and early facies.

The diorites also show a gritty texture with well-individualized plagioclases and amphiboles.

Dolerites constitute the most recent formation. They spread out in several directions in the form of dykes, intersecting the other formations. Minerals include plagioclase, amphibole, and pyroxene relics. The dolerites contain mainly granodioritic, dioritic, basic to intermediate enclosures.

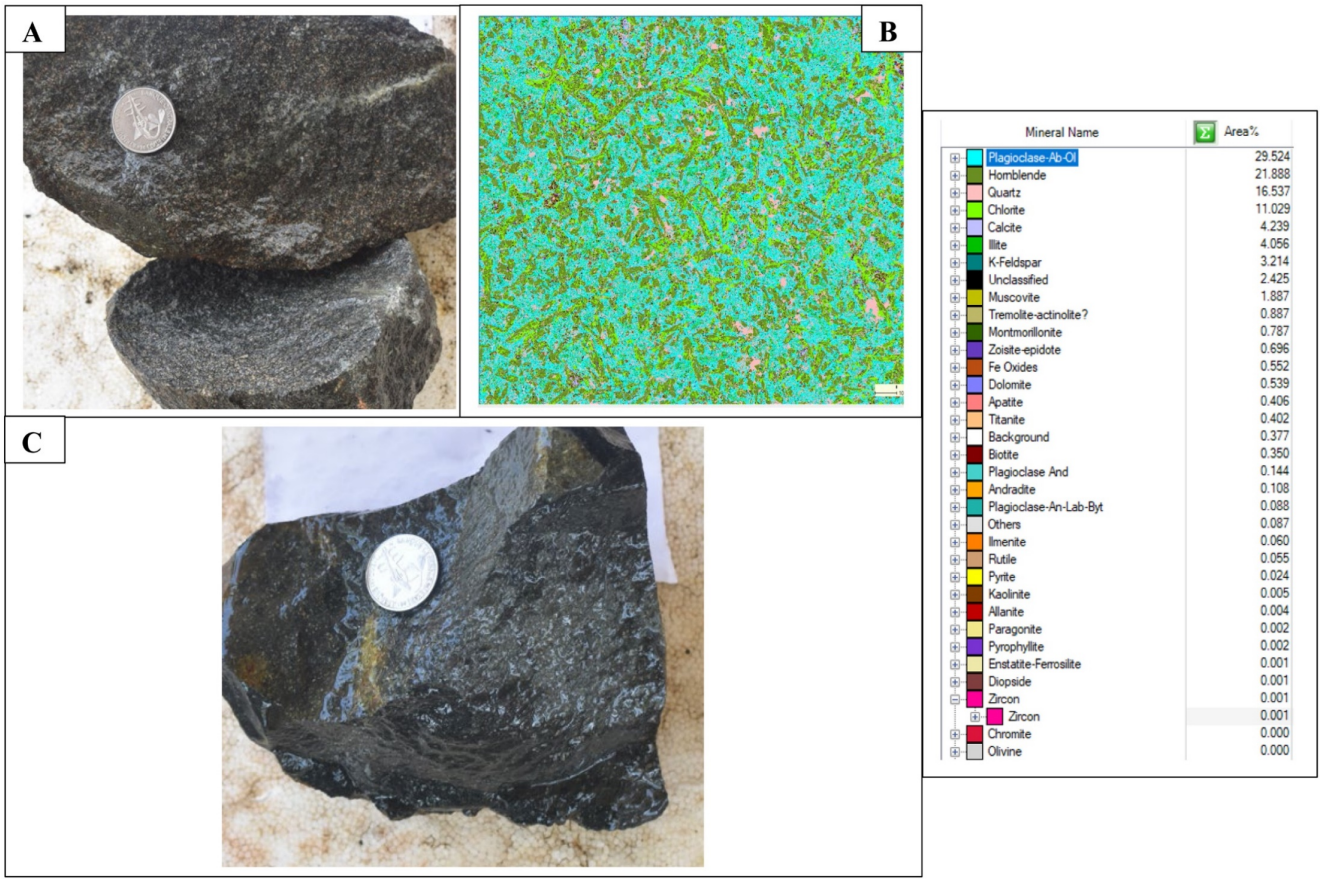

Figure 1. Mafic volcanic facies of Maco. A: Basalt (sample 70); B: QUEMSCAN analysis giving mineral composition sample 70; C: Basalts (sample 89).

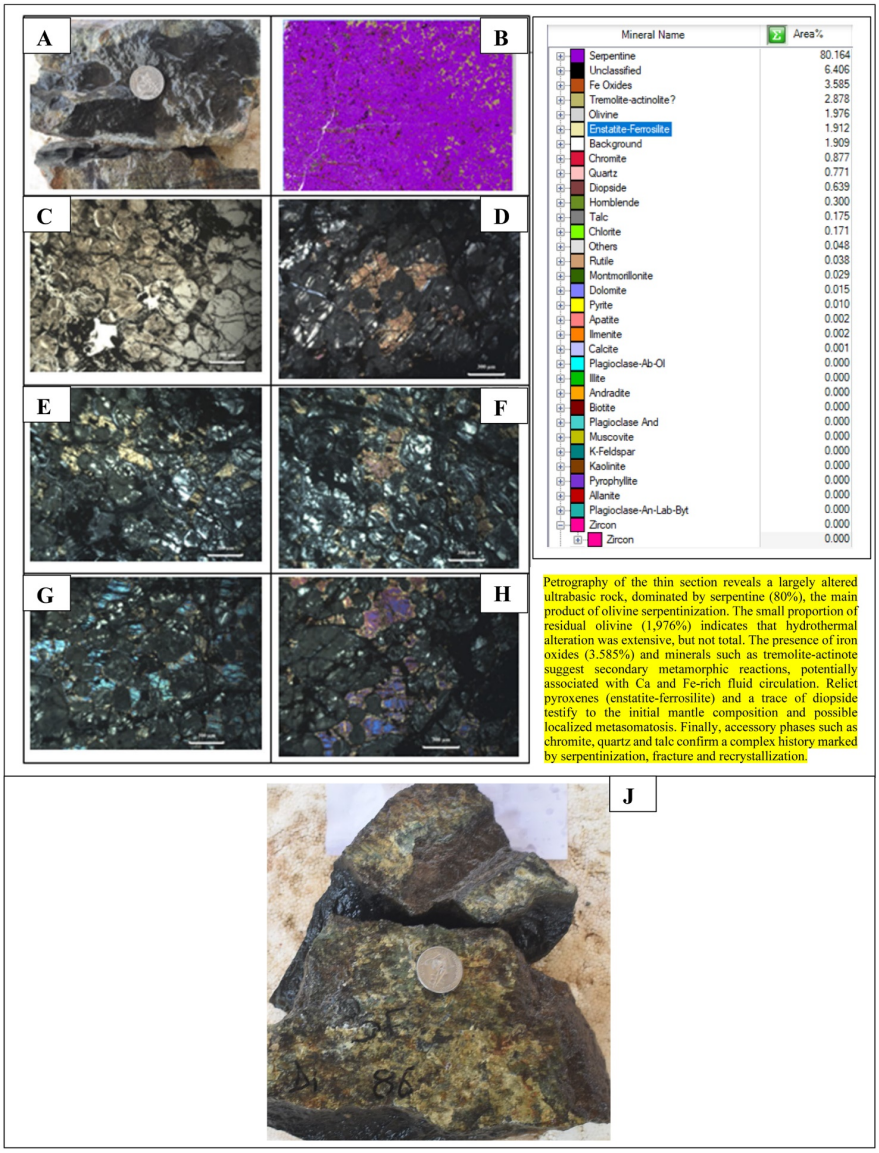

Figure 2. Microscopic details of Ultramafic facies from Maco. A: Sample 73 from outcrop rock; B: QUEMSCAN analysis giving mineral composition sample 73; C: Detail of micro-photo-graphs of serpentinized peridotite (sample 73) in polished section and natural light; I: QUEMSCAN analysis giving mineral composition (80%) serpentine; D, E, F, G, H: microphotographs of serpentinite (sample 73) in polished section and polarized light; J: Peridotite (sample 86).

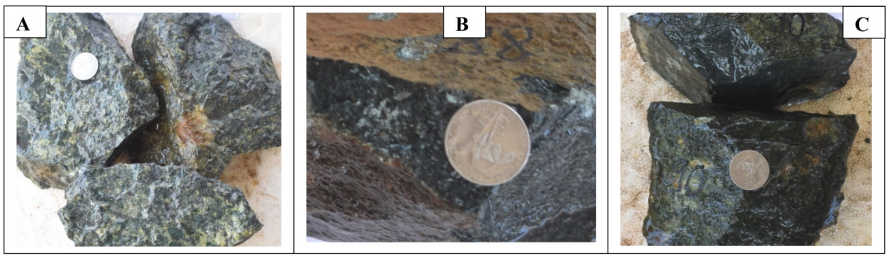

Figure 3. Mafic plutonic facies of Maco. A: Diorite, sample 63; B: Diorite, sample 88; C: Gabbro, sample 90.

The Dioudioukounkou massif is hosted by the Maco formation. Dioudioukounkou pluton (Figure 4) is a massive, circumscribed intrusive trending North-south, and seting in almost in oval shape, with irregular margins covering an area of around 60 km^2. The rock is composed of automorphous to subautomorphous plagioclases with a saussauritic core, ranging in composition from basic oligoclase in the center to acidic oligoclase at the periphery. Quartz is moderately abundant in small interstitial patches. Chlorobiotite and green hornblende are widespread. It is a homogeneous rock with two facies (Figures 4-6) containing basaltic and dacitic enclaves (Figure 7). Fine to medium-grained rock with a granular (igneous) texture.

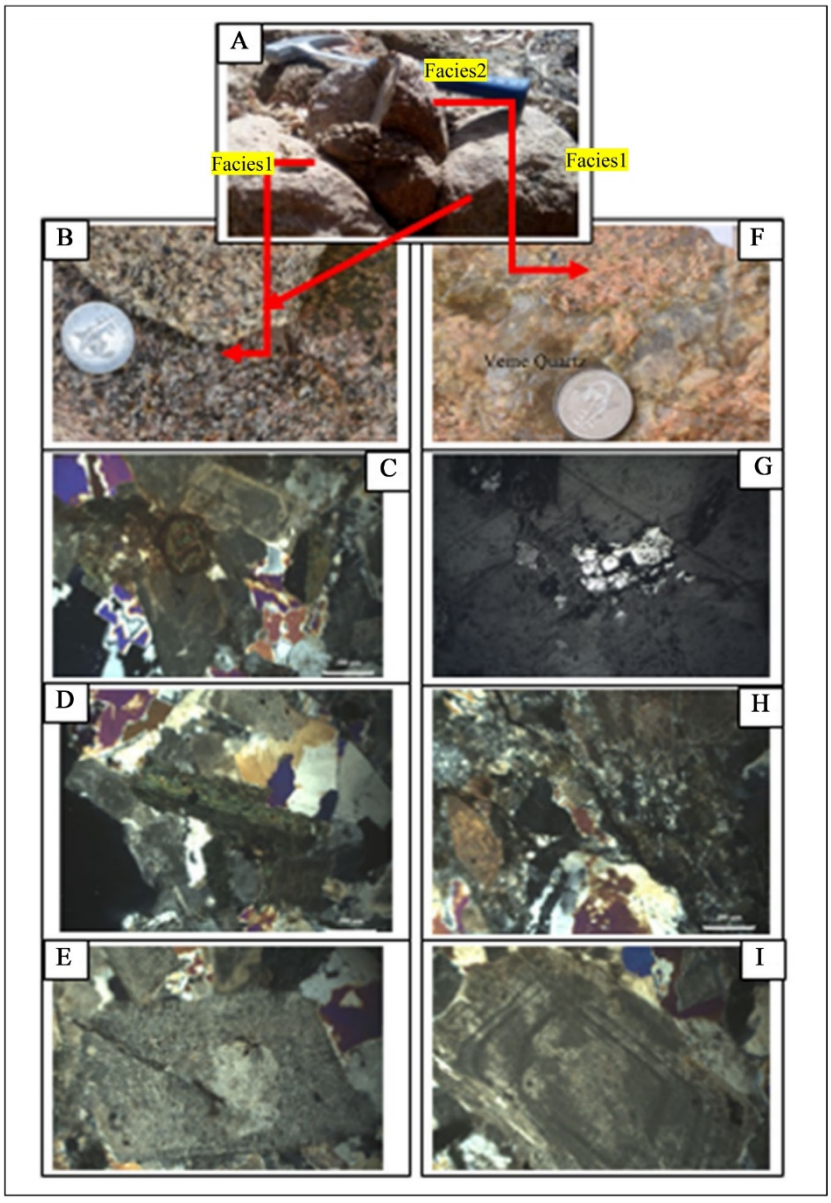

Figure 4. Facies of the Dioudioukounkou massif. A: Primary facies of the Dioudioukounkou massif, including a secondary facies in polished section along an oriented quartz vein; B, C, D, E: Microphotograph of the primary facies of Dioudioukounkou; F, G, H, I: Microphotograph of the secondary facies in polished section at Dioudioukounkou.

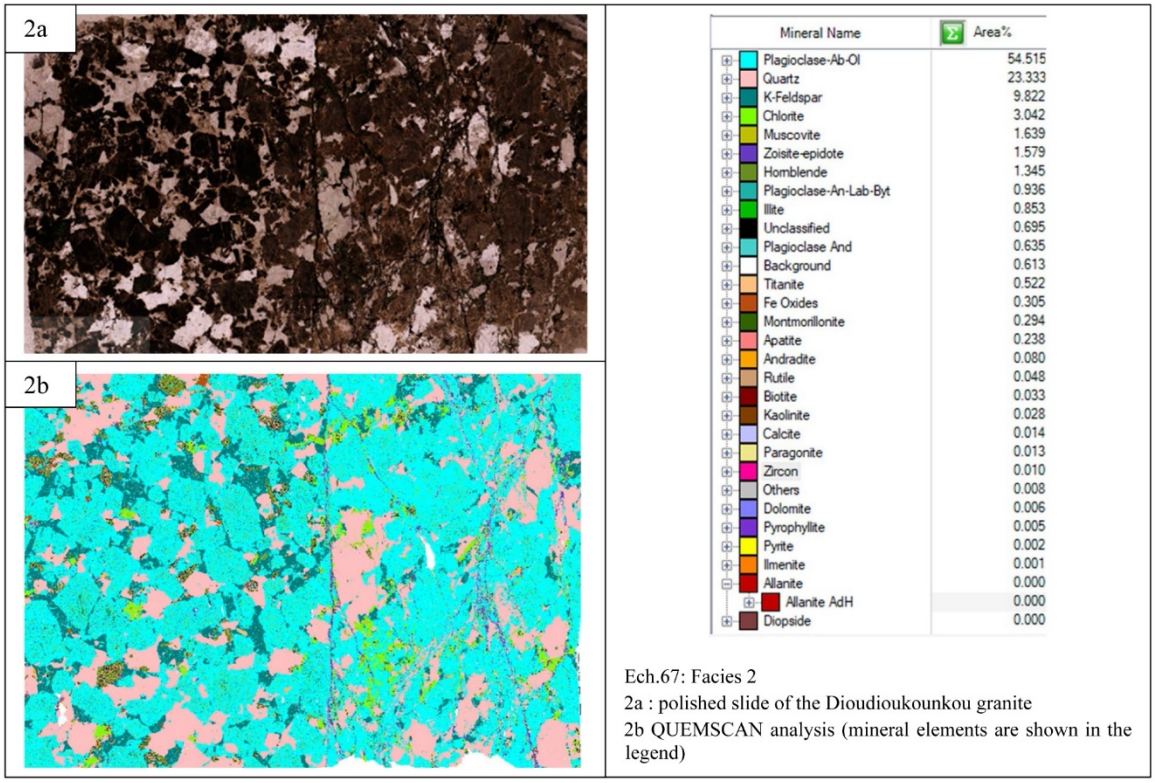

Ech.67: Facies 2
2a : polished slide of the Dioudioukounkou granite
2b QUEMSCAN analysis (mineral elements are shown in the legend)

Figure 5. Representative sample of Dioudioukounkou granite facies 2 (fine) enclaves in facies 2.

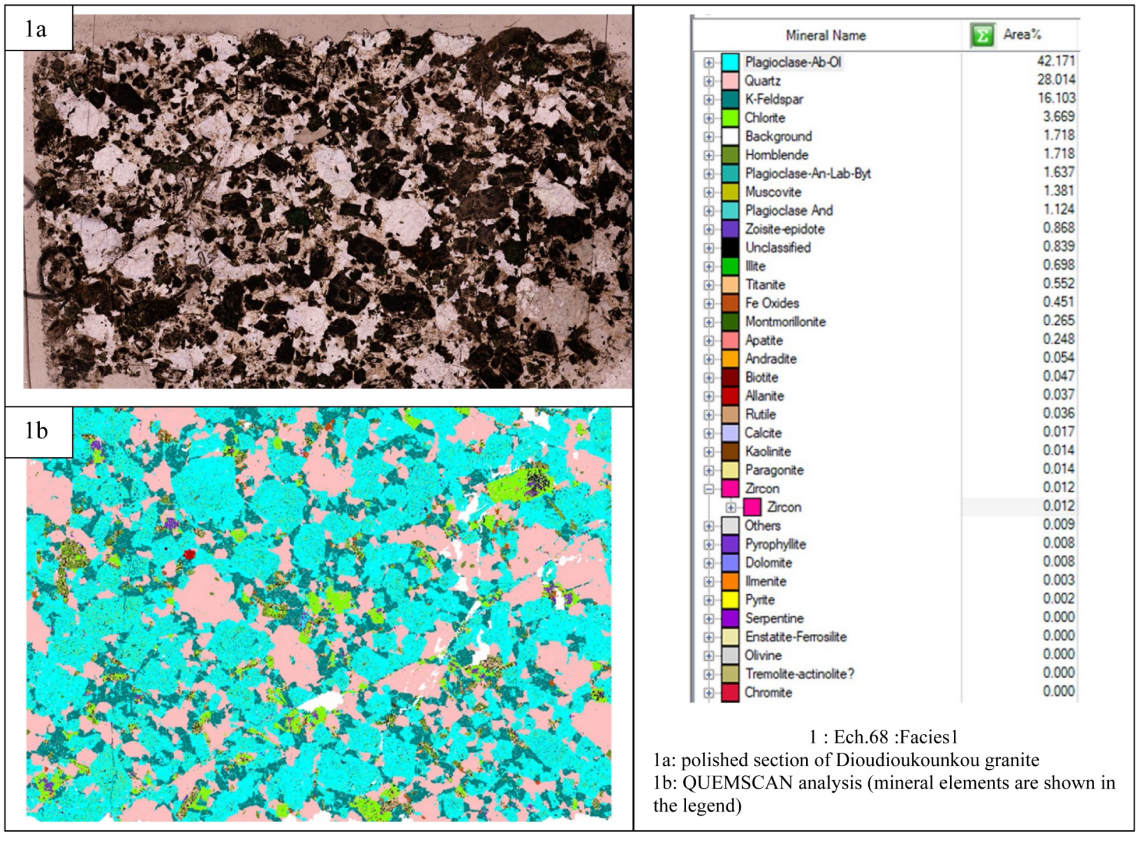

1 : Ech.68 :Facies1
1a: polished section of Dioudioukounkou granite
1b: QUEMSCAN analysis (mineral elements are shown in the legend)

Figure 6. Representative sample of Dioudioukounkou granite facies 1 (coarse).

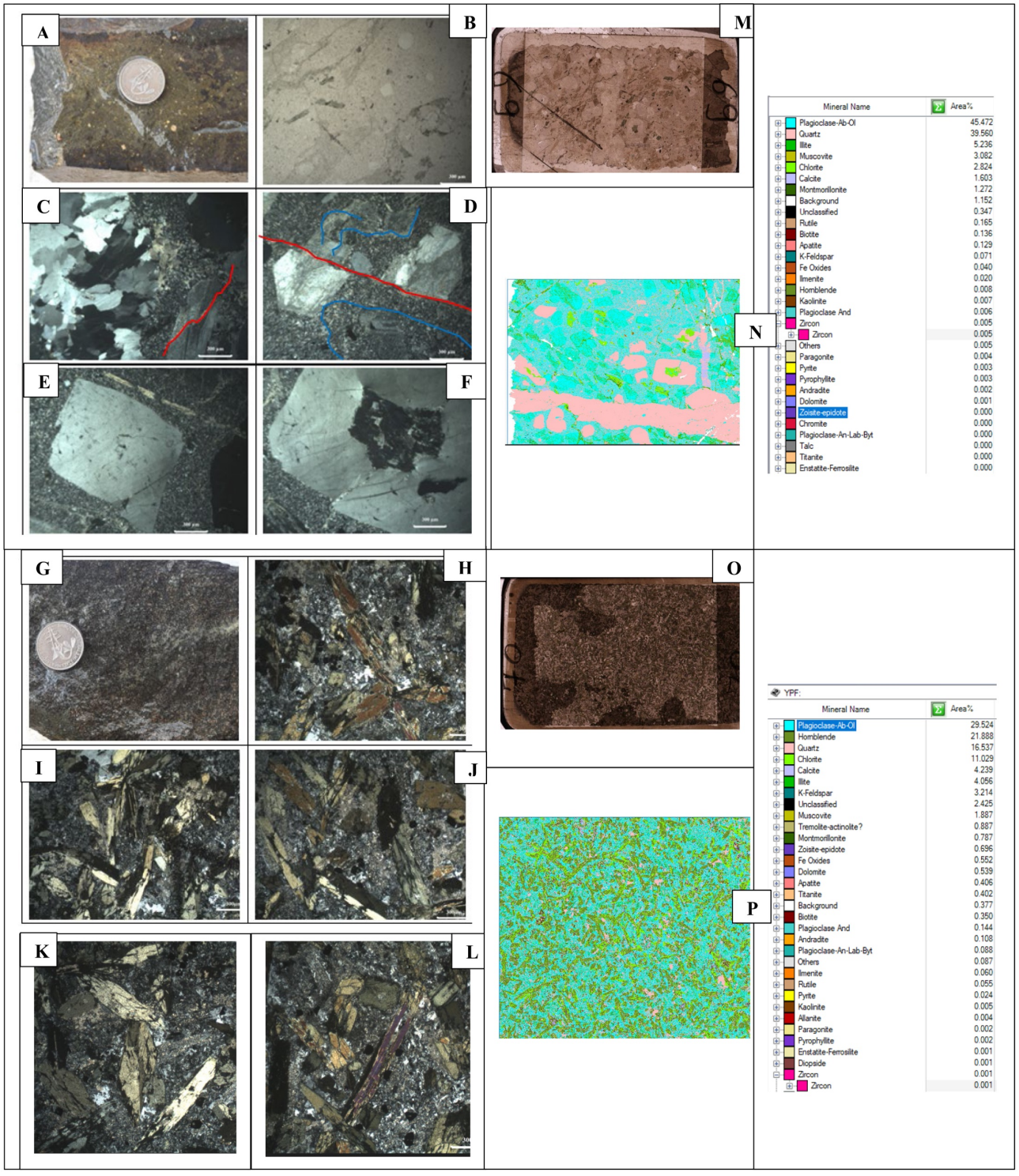

Figure 7. Facies of the Dioudioukounkou massif. A: Detail of microphotographs sample 69 of dacite enclave in thin section and polarized light; B, C, D, E, F, M: Microphotograph of dacite enclave showing proof of ductile and brittle deformation (micro folding and minerals cutted and displayed by faulting); G: detail of microphotographs of sample 70 of basaltic enclave in thin section and polarized light; H, I, J, K, L, O: Microphotography of basaltic enclave; N: QUEMSCAN analysis giving mineral composition of sample 69: Plagioclase-Ab-Ol (45.47%), Quartz (39.56%), Illite (5.23%), Muscovite (3.08%), Chlorite (2.82%), Calcite (1.62%), P: QUEMSCAN analysis giving mineral composition of sample 70: Plagioclase-Ab-Ol (29.52%), Horneblende (21.88%), Quartz (16.53%), Chlorite (11.02%), Calcite (4.23%), Illite (4.05%).

The facies has a strong, penetrating foliation linked to the preferential orientation of bands and irregular lenses of chlorite concentration and elongated fragments of the felsic component of the rock. The rock is composed of potassic feldspars (microcline), plagioclase, chlorite, sericite, and quartz, often in the form of aggregates. Chlorite has probably replaced ferromagnesian minerals, possibly including biotite. Occasional grains of dark grey-brown leucoxene are present, and a skeletal network of leucoxene is associated with chlorite. Clusters, disseminations, and silts of smaller leucoxene and rutile grains are also common. A carbonate mineral occurs sporadically in the matrix in the form of small aggregate bodies and chains. Inside these carbonate grains are pale pink in color and show well-developed fine lamellar twinning.

4.1.2. Sesam Formations

Koulountou and Tiguida are embedded in the Sesam formations. Lithologically, Sesam is characterized by the presence of andesitic volcanic formations (breccias, meta-andesite, metavolcanosediments, metatuffs) associated with andesitic volcanosediments. A complex of ultrabasic rocks, basic plutonic rocks, and mafic to felsic volcanics is associated with the Sesam formations (Figure 8).

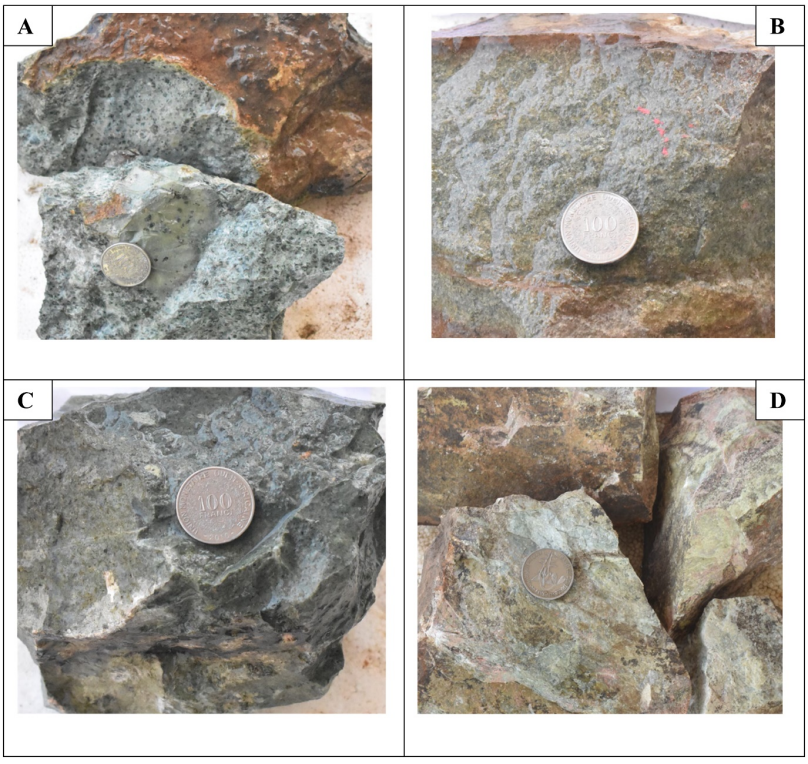

Figure 8. Sesam Facies. A: Andesitic basalt (sample 18); B: Andesite (sample 13); C: Andesite (sample 21); D: Koulountou Granodiorite (sample 92).

1) Volcanic formations

The breccias are associated with explosive andesitic volcanism. Andesitic flows alternate with agglomerates, tuffs, and abundant volcanic breccia. Agglomerates

contain polygenic and sub-angular lithic elements, sometimes stretched and oriented in a preferential direction, and are intermediate volcanic in nature, rarely dioritic. Volcanic breccias and agglomerates are associated with light-green tuffaceous material oriented N025 with a dip of 60˚ NW. The brecciated facies is deformed by schistosity marked by the stretching of millimetric to centimetric clasts arranged parallel to the direction of the tuffites.

Meta-andesites are greenish to greenish black in color and come in blocks of highly variable size. Meta-andesites are formed by accumulations of volcanic projections in fragments of varying sizes. They can be either massive or porphyritic.

Massive meta-andesites are a well-represented facies, composed mainly of amphiboles and plagioclases.

Metavolcanosedimentary rocks occur as lenses alternating with andesitic lavic facies, intersected by intrusive facies. The metavolcanosediments are made up of fine metatuffs. Petrographic study shows that andesitic tuffs are made up of terms of volcanodetritic or tectonic origin. These are essentially as composed as follows:

Metatuffs are facies corresponding to volcanic rocks that are sometimes highly silicified and chloritized. Lithic elements of volcanic origin are medium to fine in size and are joined by a greenish mesostasis. They can also be affected by brittle, ductile, and brittle-ductile deformations.

Andesitic metatuf is an epimetamorphic rock composed of mineral fragments with very fine, locally abundant recrystallized pelitic cement. Ferromagnesians are defertilized and sometimes replaced by opaque minerals. The rock is cut by veinlets filled with calcite, quartz, and chlorite associated with sparse opaque minerals. The marked schistosity is taken up locally by dextral shear channels (rich in chlorite and calcite).

Crystalline metatuffs are rocks composed of sub-angular mineral fragments and acid to intermediate rocks united by an abundant, finely recrystallized matrix. Mineral fragments are represented by abundant plagioclases showing well-preserved polysynthetic or double macles. Cement is scarce, recrystallized, and chloritized.

Dacites are amygdaloidal dacitic lavas with cavities filled with secondary quartz and other undifferentiated minerals. They feature calcite and quartz veinlets. Microscopic examination shows that the rock is a volcanic rock composed of plagioclase, quartz, and amphibole minerals. The rock is weakly porphyritic with plagioclase phenocrysts and microphenocrysts. The rock's texture is dominated by the appearance of uniformly distributed leucocratic bodies, composed mainly of quartz with albite, epidote, calcite, and chlorite. The main alterations identified are sericite, chlorite, epidote, and silica.

2) Plutonic formations

Ultramafic facies are represented by pyroxenites and amphibolites. Sesam pyroxenites are differentiated massifs enriched in pyroxenes at their summits, gradually giving way to pyroxenites consisting mainly of automorphous pyroxene crystals. White nodules of secondary calcite are exceptionally observed. They come into

contact with gabbros on certain ultramafic hills. The transition is gradual and marked by plagioclase enrichment. They are also intruded by meta-andesites and meta-basalts. These ultramafic formations are affected by ductile deformation corresponding to double folding. Amphibolites outcrop mainly north of Koulountou, at the contact between ultramafic and granodiorite. The minerals are essentially amphibole.

Gabbros show a segregation of light feldspars and dark minerals forming magmatic bedding. These feldspathic minerals can also form light-colored aggregates in mottled gabbros. They outcrop as kilometer high, massive, rarely fractured sills, generally oriented in the N040˚ birimian direction. Their texture is grainy, colored blackish-green or dark gray, more or less speckled with white. Micro-grained microgabbros are also present, especially in contact with andesites or rhyodacites.

Diorites have many similarities with gabbros, both in terms of composition and texture (equigranular, rarely porphyritic) and color (whitish due to plagioclases, sprinkled with black due to ferromagnesian minerals). With an often low extent, they outcrop to the West and always next to the gabbros and andesites. They could even constitute a transitional facies, which suggest a possible emposition by magmatic differentiation from the gabbros. Monzodiorites form a leucocratic rock with a grainy texture. They are very similar to granite, but with a high proportion of alkaline feldspars and plagioclases. They are found in the southwest of the grid, in the form of those that intersect the andesites and gabbros in a mean N040˚ direction, often reoriented under the influence of shear zones.

The Koulountou granite (**Figure 9**) is an elliptic-shaped massif that is thinned and stretched in its northern part in a NE direction. It takes the form of blocks that can be several meters in diameter. They consist mainly of plagioclase, amphibole, and quartz. They are strongly altered in carbonate-quartz, sericite, and pyrite. The main types of alteration are chlorite, sericite, carbonate, limonite, and leucoxene. The rocks are also crossed by aplites in places. Deformation is low and is made up of fractures. The walls of these fractures are lined with chlorite in places. Note that the late veins are more acidic, with a pinkish tinge tending towards a granitic composition. The minerals vary in size, becoming larger in the South toward the diorites. It is an equigranular rock (roughly equal amounts of potassic feldspar and protomylonitised plagioclase) with a medium-grained facies composed of plagioclase, quartz, amphibole, orthoclase, and biotite. They are millimeter to centimeter in size (up to one decimeter). These enclaves do not have a preferential orientation. Their generally rounded shape does not suggest syntectonic or synmagmatic deformation. The rock is affected by ductile deformation.

Tiguida massif (**Figure 10**) outcrops to the South of the Koulountou massif over several kilometers along strike N032 in an elliptical shape. It is a facies rich in potassic feldspar. It shows a large fracture network mainly oriented N050/80 with surface alteration revealing relics of acicular and coarse-grained quartz. Petrography reveals abundant and pervasive plagioclases. Quartz is moderately present in coarse grains

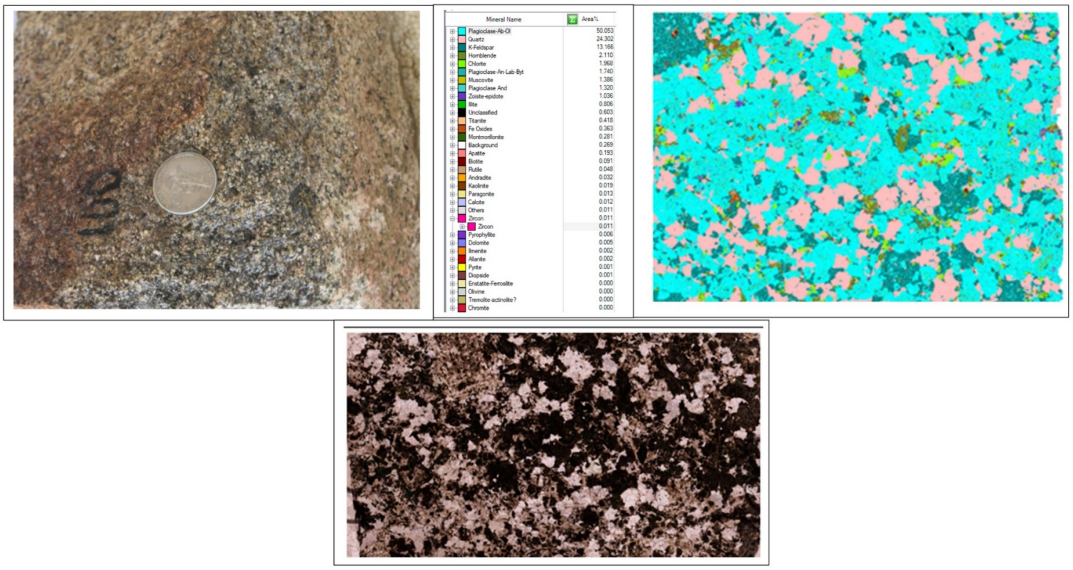

Figure 9. Facies of the Koulountou pluton. QUEMSCAN analysis giving mineral composition of sample 100: Plagioclases (50.05%), Quartz (24.30%), K feldspar (13.16%), Hornblende (2.11%), Chlorite (1.96%); F, G, H, I, J: Detailed microphotographs of microgranodiorite (sample 100); Pl: Plagioclase; Ort: Orthose; Hbl: Hornblende; Ilm: Ilmenite; Garnet (andradite); Opx: Orthopyroxen; Cpx: Clinopyroxen; Zr: Zircon; Qtz: Quartz; Bio: Biotite. Ferromagnesian minerals such as biotite and amphibole are visible in the altered parts. Koulountou contains enclaves that are essentially ultrabasic and basaltic. They are millimeter to centimeter in size (up to one decimeter). They are strongly altered in carbonate-quartz and pyrite.

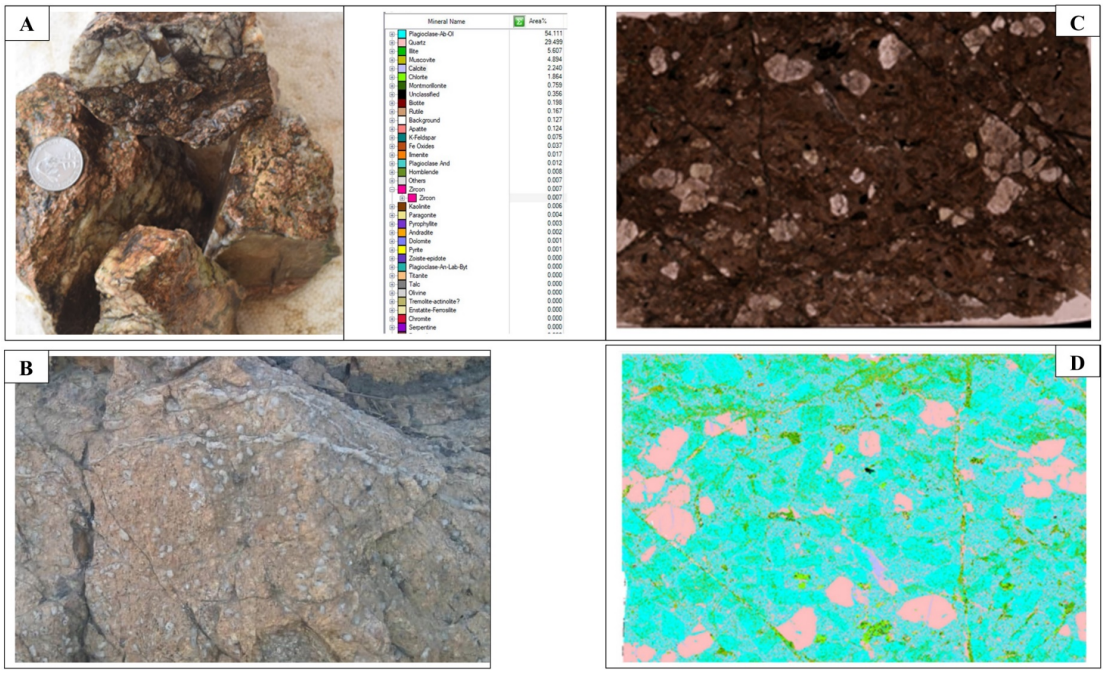

Figure 10. Facies of Tiguida pluton. A: sample 61 from outrop; B: Facies of the Tiguida granite showing abundant and accicular quartz grains, C: Detail of microphotographs of granite (sample 61) in polished section; D: QUEMSCAN analysis giving mineral composition of sample 61: Plagioclase-Ab-Ol (54.11%), Quartz (29.49%), Illite (5.60%), Muscovite (4.89%), Calcite (2.24%), Chlorite (1.86%); E, F, G, H: Details of microphotographs of fractures on granite (sample 62) in thin section and polarized light; Pl: Plagioclase; Garnet (andradite); Opx: Orthopyroxen; Cpx: Clinopyroxen; Qtz: Quartz; Bio: Biotite.

and veinlets. Muscovite is pasty and relatively abundant. Muscovite is pasty and rel-

atively abundant. are mainly composed of quartz (with local traces of calcite), albite, plagioclase, chlorite, and muscovite, and incidentally apatite, zircon, hematite, and magnetite with a granular texture. Both samples have a granular texture. Others, in addition to the granular texture, have quartz veins filled with muscovite, chlorite, and sericite.

4.1.3. Diabba Formations

Diabba formations are mainly composed of sedimentary facies (fine grained sediments, schists, quartz veins, cherts, metapelites, conglomerates, a large variety of grauwackes) associated with metabasalts, volcanoclastites, dacites, metarhyodacites (Figure 11, Figure 12).

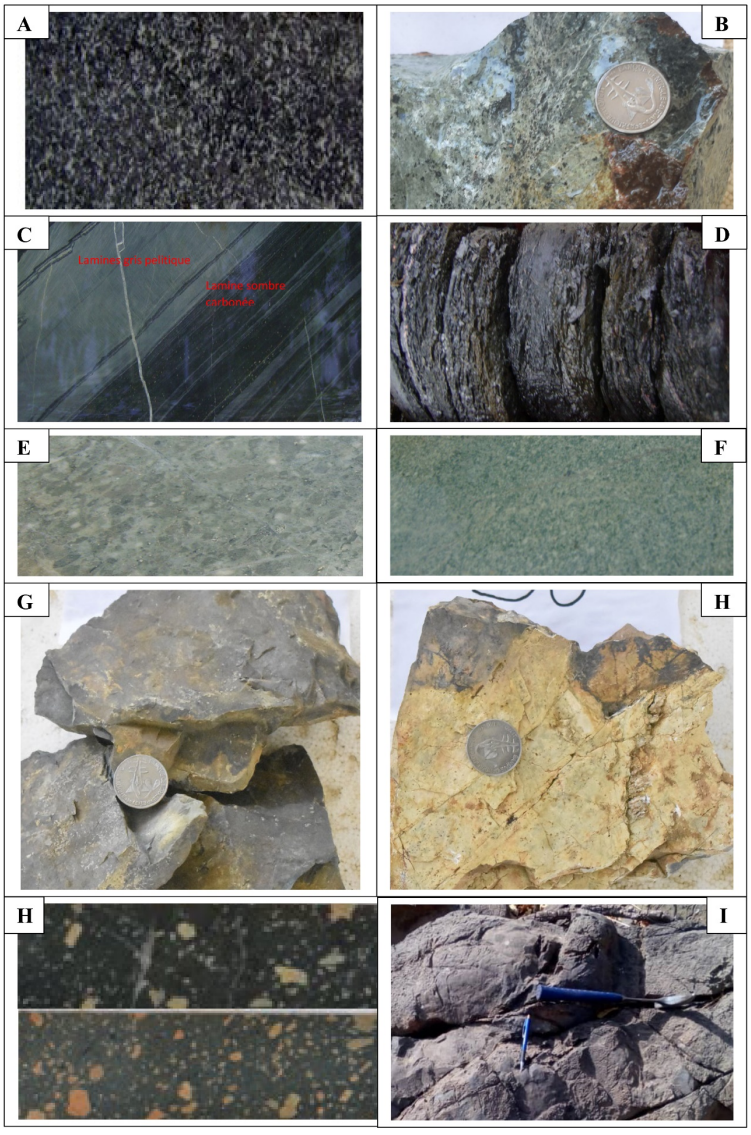

Figure 11. Diabba facies. A: Basalt (sample 375 from core samples); B: Andesitic basalt (sample 76); C: Graphitic pelite; D: Graphitic schist; E: Volcanic clastic with medium clasts; F: Volcanic facies with fine clasts; G: Fine sediment (sample 30); H: Chert (sample 38); I: Porphyritic facies of andesite with zoned plagioclases. I: Massive andesitic facies.

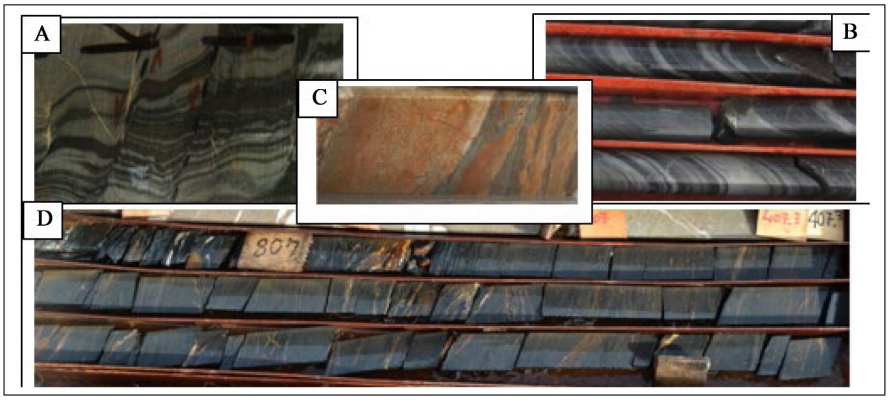

Figure 12. Stratification pattern. A: Stratification offset by a reverse fault system; B: Oblique stratification; C: Stratification offset by a load pattern; D: Perpendicular stratification.

1) Volcanic rocks

The metabasalts of Diabba volcanoclastic formations have a microlitic texture. Some facies may contain spinifex-textured plagioclases. Crystals are feathery and arborescent. The scarce mesostasis is partially devitrified. The massive basalts are melanocratic, poorly fractured, and cut by quartz veins. Microscopic study shows that these basalts from Diabba volcanoclastic formations are flows marked by skeletal needles of secondary actinote grouped in sheaves with no particular orientation. The actinote, which comes from the ouralitization of ancient pyroxenes, is chloritized and sometimes fibrous.

Metaandesites form elongated NE to NS bands. They are composed of plagioclases and ferromagnesian minerals in a sparse, recrystallized mesostasis. Massive metaandesites come in two varieties: a pale greenish variety with a microlithic texture, and a greenish-black variety comparable to andesitic basalts. Porphyritic andesites are more common in the eastern part.

Metarhyodacites outcrop as veins or sills in the northwestern part of Diabba. Petrography shows an aphyric texture of metarhyodacites. Quartz in small crystals, sometimes corroded by mesostasis, is automorphic, grouped in polycrystalline clusters, and sometimes associated with alkali feldspars. Alkali feldspars, which are totally altered, have their cross-sections studded with sericite flakes that obliterate their characteristic macles. Veins are abundant in the rock. In these veins, opaque minerals occupy the intercrystalline spaces or fill the intra-mineral microfractures or form fine streaks in the middle of the veins. Dacites are found along the CiscoE contact shear zone. These facies are marked by SiO_2 contents ranging from 59.32% to 60.50%.

Volcanoclastites are composed of polygenic felsic and mafic clasts of varying sizes in a rare matrix. The dominant clasts are mauve or green in color. Depending on the granulometry of the clasts, we can distinguish:

Clast or lapilli tuff facies are made up of large, sub-angular to stretched polygenic clasts several tens of millimeters in size, with a rare, ashy cement. They are rich in rock fragments and quartz grains. These facies are often associated with

highly sheared to brecciated graphitic contacts. These formations are also affected by intense silicification.

Facies with sub-rounded to sub-stretched clasts, up to 64 millimeters in size, of varied nature are probably andesitic, with a predominance of mauve or green clasts. Cement is tuffaceous, sparsely distributed, and of the same nature as the dominant clasts.

Facies with two millimeters sized clasts stretched in a preferential direction with a rare matrix. In highly deformed zones, the rock is close to metalutites, crystal metatuffs, or volcanodetritic meta-arenolutites.

Microscopic study shows that volcanoclastic facies correspond to a set formed by:

Volcanoclastic metalitharenites are composed of volcanic lithoclasts, hornblende, plagioclase clasts, and quartz united by a rare, finely recrystallized matrix (almost contiguous grains).

Volcanoclastic quartzofeldspathic meta-arenites with polygenic lithoclasts correspond to rocks formed of lithoclasts, plagioclases, and quartz united by an intensely calcitized quartzofeldspathic cement. The abundance of microlitic porphyritic andesitic lithoclasts may justify the name.

Rarely clast-bearing feldspathic volcaniclastic meta-arenites constitute a locally microlithic rock composed of mineral fragments and rocks in a relatively abundant, recrystallized cement. Lithoclasts are rare and very small, and the rock is highly deformed with competent brecciated beds. Schistosity is marked, and the rock is intensely invaded by fluid circulation.

Volcaniclastic meta-lutites are composed of ferromagnesians, quartz, and plagioclases bound together by abundant cement.

Volcanoclastic ash is a glassy matrix with no visible clasts. Cinerites show a strong network of alterations and quartz veins.

2) Sedimentary facies

Sedimentary facies are mainly metapelites or argillites (sometimes found in enclaves within intrusive facies), schists, quartz veins, and quartzites/cherts.

Quartzites are generally microcrystalline, consisting mainly of centrally located quartz with a NE-SW band. They often outcrop as massive blocks reworked by shearing, intense fracturing or foliation, or by andesitic volcanic events.

Quartz veins outcrop mainly in the western part of the Tinkoto pluton, cutting andesites, gabbros, and tuffs along strike N060˚ to N080˚, dipping steeply (70˚ to 90˚) to the northwest. They can extend for kilometers and are between 5 and 15 meters thick.

They are made up of bands of milky-white, sometimes dark-bluish, quartz veins, boudinated but rarely ferruginous. At the outcrop, bipyramidal quartz crystals have formed perpendicular to the general N060˚ to N080˚ elongation.

In the eastern part, quartz veins are present at various scales and affect all lithological units. They are generally oriented North-east to the North and North-south to the South. They can form decimetric to metric furrows.

Argillites or meta-argillites are marked by a more or less subvertical bedding associated with schistosity. The beds differ in color and competence. They are locally metamorphosed and apparently baked in the vicinity of plutonites.

The conglomerates are practically composed of epiclasts of sedimentary nature with sparse cement of fine pelitic nature. The facies is discontinuous, and the elements are polygenic in blunt to subrounded form, indicating transport between their source and depositional environment.

Coarse-grained to very coarse-grained grauwackes contain relatively coarse clasts in a sparse to abundant matrix. Apart from grain size, these facies can have all the characteristics of fine and medium-grained greywacke. This facies is dominant in the northern part of the prospect and is often interspersed with levels that are sometimes very graphitic and highly deformed, forming the wall of mineralization.

A much coarser grauwacke or conglomerate facies is often intersected in the drill holes. The facies is discontinuous with a conglomeratic appearance.

Medium-grained grauwackes show well individualized grains or small grays in a mostly chloritized and sericitized matrix, and the rock is generally traversed by a system of quartz, carbonate, or hematite veins and veinlets.

Graphitic metapelites are characterized by an alternating bedding of coarser clear beds and fine graphitic beds. Sericite levels and quartz and carbonate veins are associated with this N020-trending bedding with a dip of 70˚ to 85˚, which can be taken up by shearing.

Graphitic schists: when graphitic facies are sheared and affected by intense deformation, they are very schistose and strongly graphitized; they thus become graphitic schists and the shear zone. They may constitute a small edge passage or form a large package. Graphitic schists are more common in fine-grained volcanosediments. They may be intersected at the contact between volcaniclasts and intrusives.

Stratification can be observed on the drilled cores, particularly in the carbonate shales, which show alternating clear pelitic beds and graphitic sequences. These facies show stratification parallel, secant, or perpendicular to the core axis. The stratification may be offset by load figures or faults.

3) Plutonic formations

Serpentinites (**Figure 13**) are holomelanocratic rocks showing serpentine (52.7%), Fe oxides, olivine, tremolite-actinolite, chlorite, Enstatite-ferrosilite, chromite, diopside, hedenbergite, andradite, hornblende, and olivine. They outcrop mainly in the western and eastern parts of Diabba and appear as altered mounds often oriented N030 to N040 or embedded in gabbroic formations. These formations have undergone deserpentinization compared with the Maco serpentinites.

Gabbros (**Figure 14**) have a grainy texture and are composed of porphyritic pyroxenes. On contact with the andesites, they change to microgabbros, which have a micro-grained texture. Pyroxenes transformed into secondary amphiboles

are surrounded by a crown of chlorite, epidote, and pyrite. Two types of gabbro have been intersected along the corridor:

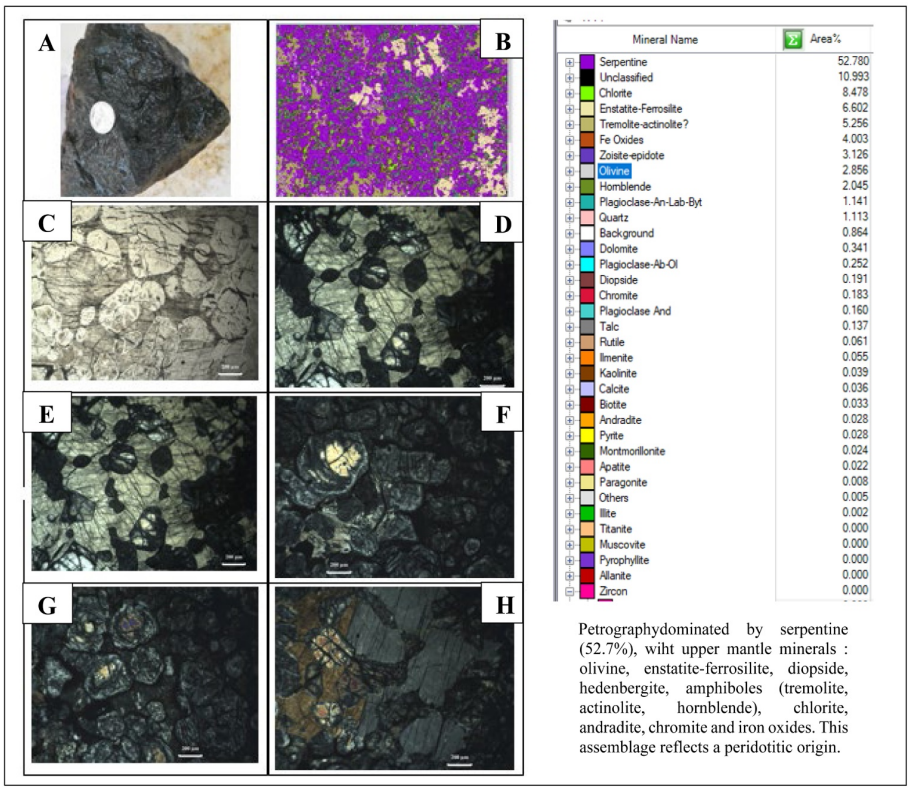

Figure 13. Serpentinites of Diabba. A: sample 47 from outcropping rock; B: QUEMSCAN analysis giving the mineral composition of sample 47; C: Detail of microphotographs of serpentinite (sample 47) in polished section and under natural light; I: QUEMSCAN analysis giving the mineral composition (52%) of serpentinite; D, E, F, G, H: microphotographs of serpentinite (sample 47) polished section and under polarized light..

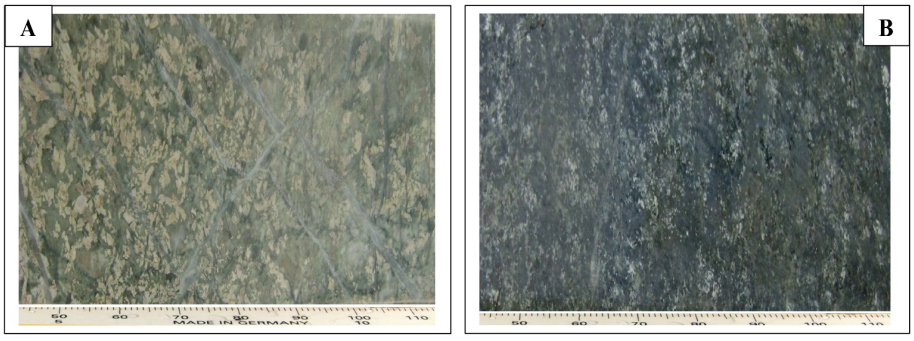

Figure 14. Gabbro facies of Diabba. A: Early altered gabbro with leucoxene; B: Strongly chloritized late gabbro.

A *late gabbro* with frank brecciated contacts is the least mineralized. It is massive with well-individualized plagioclases, some of which are very fine. It may also show strong chlorite alteration.

An *early gabbro* that intruded the volcanosedimentary sequence following the

major NE tectonic structure. This gabbro predates mineralization and is characterized by intense ductile and brittle deformation, pervasive silica, sericite, and sometimes carbonate alteration, mainly at its edges. Where the gabbro is altered and deformed, sometimes associated with hematite and leucoxenes, it hosts strong gold mineralization, whereas within the facies, the gabbro is massive, strongly altered in chlorite.

Diorites have a grainy texture marked by an assemblage of ferromagnesians, plagioclase crystals, biotite, and green hornblende. Microscopic examination confirms the presence of biotite with an automorphic rectangular cross-section, highly altered amphiboles, and destabilized plagioclases. Plagioclases are fine-grained and usually sericitized, with well-marked schist planes. They can also be medium-sized, stretched to sub-rounded, with the occasional presence of chlorite. The main alterations are sericite, calcite, epidote, and chlorite. The rock is locally schistose in the direction of the veins. Opaque minerals are locally massive or disseminated in the gangue.

Microgranodiorites are essentially composed of plagioclase, biotite, and quartz with a micrograined texture. The matrix is quartzofeldspathic and strewn with fine sericite flakes. The feldspars are completely altered, and only well-preserved quartz remains. Opaque minerals are abundant, sometimes in clusters.

Micromonzonites are composed of plagioclase, ferromagnesian minerals, and orthoclase in a quartz-feldspar microcrystalline matrix. The texture is microgritty porphyritic, and opaque minerals are fine and arranged in the cleavage planes, where they are abundant and disseminated.

Tinkoto massif (**Figure 15**) is a rounded to locally sub-rounded massif. This facies is in the form of metric-sized balls. It is found in river beds, valleys, and within the laterite armour. The texture is mostly grainy with a light whitish pink colour reflecting an uneven distribution of phenocrysts of alkali feldspars and quartz, plagioclases, and biotite flakes. In the south-western part, at the contact with the volcanic-sedimentary host rock, it changes to a porphyritic facies with large automorphic plagioclase crystals in a quartzofeldspathic matrix. This is an unconformable granite. Outcrops occur in the form of scattered blocks rarely exceeding ten meters in diameter. Irregular assemblages of dark micaceous minerals form Schlierens that stand out against the leucocratic background of the rock. Melanocratic enclaves can be recorded.

4.2. Geochemical Signature of Maco, Sesam, and Diabba Formations

4.2.1. Geochemical Signature of Maco Formations

This classification of volcanic rocks is based on the contents of major elements. However, given the high degree of alteration of facies, the classification and nomenclature of volcanic rocks are based on Jensen's (1976) FeT + TI-Al-Mg ternary diagram applied to volcanic rocks. The Jensen (1976) diagram applied to volcanic rocks shows that samples 89 and 70 are calc-alkaline basalts. sample 89 is massive and associated with the Maco domain. Sample 70 is a basalt enclave within Diou-

dioukounkou granite, thus belonging to Maco.

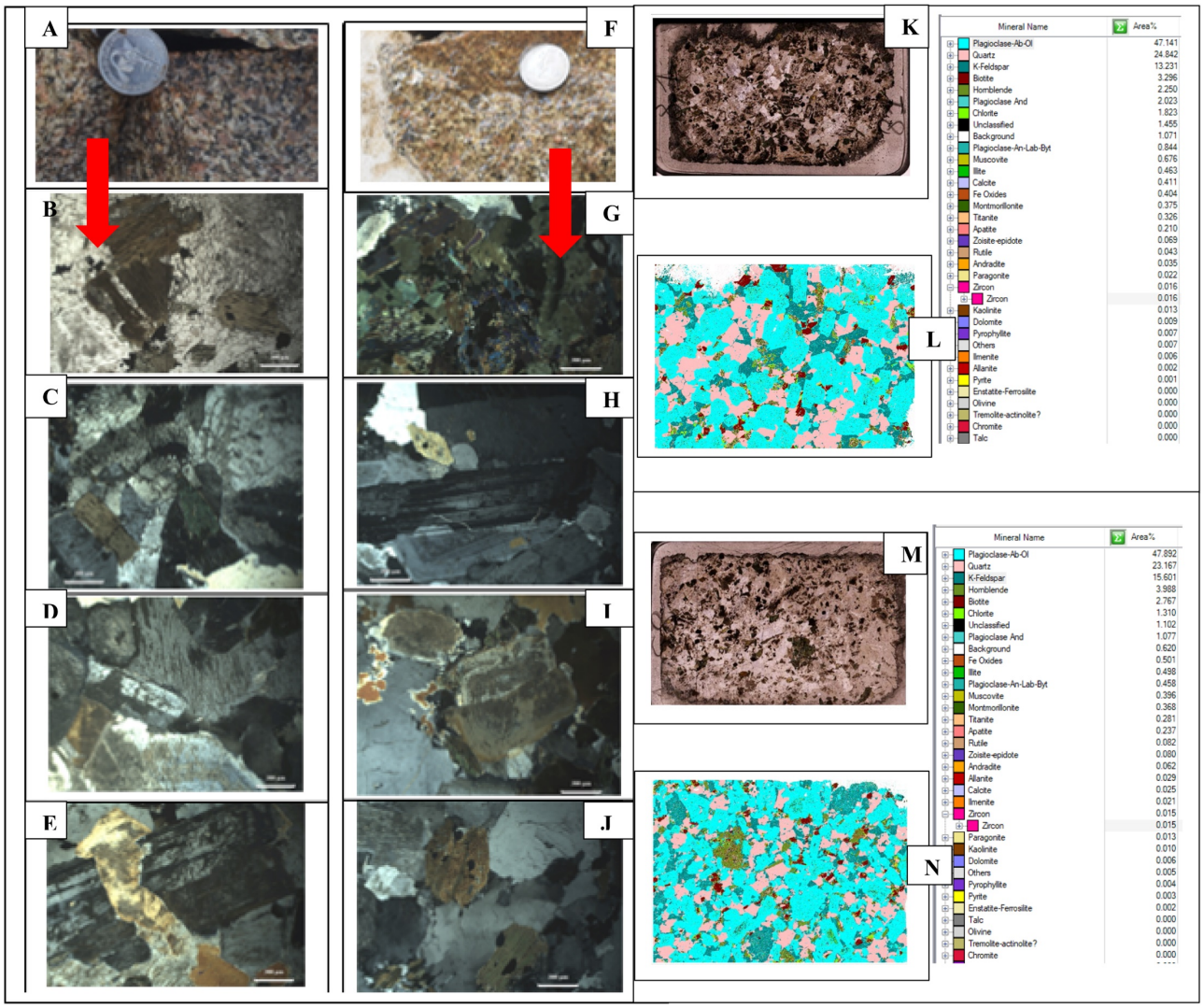

Figure 15. Facies of the Tinkoto pluton. A: Rock sample 81; B, C, D, E: detail of microphotographs of granite (sample 81) in polished section (K); F: Rock sample 85; G, H, I, J, L: QUEMSCAN analysis giving mineral composition of sample 81: Plagioclase-Ab-Ol (47.14%), Quartz (24.84%), Illite (0.46%), Muscovite (0.67%), Biotite (3.25%), Hornblende (2.24%); G, H, I, J: Details of microphotographs of on granite (sample 85) in thin section and polarized light (M); N: QUEMSCAN analysis giving mineral composition of sample 85: Plagioclase-Ab-Ol (47.89%), Quartz (23.16%), Illite (0.49%), Muscovite (0.39%), Biotite (2.66%), Hornblende (3.98%).

The classification of plutonics is based on the evolution of major elements through the diagram of Cox et al. (1979). Plotting the major elements on the TAS diagram (Cox et al., 1979) shows that Maco's plutonic formations are mainly composed of sub-alkaline to tholeiitic rocks, mainly basic to intermediate: gabbros (Ech.90) and diorites (Ech.63 and 88). The Cabanis and Lecolle (1989) diagram shows that calc-alkaline basalts (Ech.70, Ech.89) and tholeiitic diorites (Ech.88) lie within boundaries of compressive orogenic plates (island arc, active margin). Tholeiitic gabbros (Ech.90) and calc-alkaline diorites (Ech.63) fall within late-orogenic to post-orogenic intraplate domains (compressive to distensive).

1) Volcanic rocks

Calc-alkaline basalts

Maco's calc-alkaline basalts have SiO_2 contents ranging from 56.96 to 57.07% and alkalinity ($Na_2O + K_2O$) from 5.17 to 5.54%. These basalts are moderately magnesian, with MgO contents ranging from 4.77 to 6.40%. They are more ferriferous, with Fe_2O_3 contents ranging from 8.24 to 8.73% and Al_2O_3 from 14.25 to 16.14%. The basalts represented by samples 89 and 70 show cobalt contents of between 26.5 and 38 ppm, nickel 96.1 to 102.4 ppm, vanadium 174.1 to 195.1 ppm, and chromium 197.9 to 271.4 ppm. Zirconium contents range from 90.3 to 123.9 ppm, while radioactive element contents are: Th 2.3 to 6.6 ppm and U 1.9 to 4.5 ppm. The profile of calc-alkaline basalts is marked by enrichment in LILE (Cs, Rb, and Ba). There is also a depletion in HFSE (Nb, Ce, P, and Ti). Rare earth contents (∑REE) in Maco basalts range from 50.8 - 81.9 ppm. Rare-earth elements spectra normalized to the primitive mantle according to Sun and McDonough (1995) are relatively moderately steep with low to moderate fractionation rates, showing a LaN/YbN ratio of 1.59 for sample 89 and below the detection limit for sample 70. Enrichment in light rare earths elements is noted with a LaN/SmN ratio equal to 2.79 for sample 70. The basalts are enriched in LREE (16 to 50 times the primitive mantle). Maco calc-alkaline basalts are also marked by heavy rare earth element depletion, with the ratio (DyN/YbN) below the detection limit. Apart from Ytterbium, there are no heavy rare earth elements and no Europium anomalies (Eu/Eu*).

2) Plutonic rocks

a) Tholeiitic gabbros

Gabbros are represented by sample 90. Silica content is 52.06%. Alkali content ($Na_2O + K_2O$) is 3.47%. The gabbro's Al_2O_3 content is 16.46%. The Fe_2O_3 content is 10.85%. MgO content is 5.48%. Tholeiitic gabbros represented by sample 90 show cobalt contents of 45.7 ppm, nickel 147.9 ppm, vanadium 183.7 ppm, and chromium 72 ppm. Zirconium contents range from 165.9 ppm, while radioactive elements are: Th 3.1 ppm and U 2.2 ppm. The spectrum of tholeiitic gabbros is marked by enrichment in "LILE = large ion lithophile element" (Rb, Ba) and moderate depletion in HFSE "high field strength element" (K, P, and Ti). The rare-earth elements content (∑REE) of tholeiitic gabbros is equal to 64.6 ppm. The rare-earth spectrum, by Sun and McDonough (1995), normalized to the primitive mantle is moderately sloped with a LaN/YbN ratio equal to 2.02. The spectrum is softly enriched in light rare earth elements, with a LaN/SmN ratio equal to 1.17. The formations are enriched 14 times the primitive mantle. These spectra show positive U anomaly and negative K and P anomalies. No heavy rare earth elements are observed, and no Europium anomalies (Eu/Eu* and DyN/YbN below detection limit).

b) Tholeiitic diorites

They are represented by sample 88 from Maco. Silica content is 56.11%. Alkali content ($Na_2O + K_2O$) is 2.85% and Al_2O_3 content is 12.21% (88). Fe_2O_3 content is 10.36% (88); MgO is 6.32%. Tholeiitic diorites represented by sample 88 show

cobalt contents of 50.2 ppm, nickel 338.1 ppm, vanadium 137.6 ppm, and chromium 553.7 ppm. Zirconium content is 84.1 ppm, while radioactive elements are: Th 1.6 ppm and U below the detection limit. The spectrum of tholeiitic diorites is marked by an enrichment in LILE = "large ion lithophile element" (Cs, Rb, Ba) and a moderate depletion in HFSE "high field strength element" (Nb, P, and Ti). The rare earth content (∑REE) of the diorites is 37 ppm. Rare earth spectra show a LaN/YbN ratio below the detection limit. The spectrum shows low rare-earth enrichment with a LaN/SmN ratio below the detection limit. The formations are enriched 16 times the primitive mantle. These spectra show positive Nd, Th, and K anomalies and negative Nb and P anomalies. No heavy rare earths elements are observed, and no Eu anomalies (Eu/Eu* and DyN/YbN below detection limits).

c) Calc-alkaline diorites

Calc-alkaline diorites 58.99% represented by the sample 63 are 58, 99% silica content and 3.45% alkali content (Na2O + K2O). Al2O3 content is 14.31% and 7.65% Fe_2O_3. MgO content is 10.91%. Calc-alkaline diorites represented by sample 63 show cobalt contents of 30.3 ppm, nickel 90.9 ppm, vanadium 113.7 ppm, and chromium 133.3 ppm. Zirconium contents range from 138.9 ppm, while radioactive elements are: Th 2.6 ppm and U 1.1 ppm. Calc-alkaline diorites are marked by an enrichment in LILE = "large ion lithophile element" (Cs, Rb, Ba) and a moder-ate depletion in HFSE "high field strength element" (Nb, K, P, and Ti). Rare earth content (∑REE) of the diorites is 38.8 ppm. Rare earth spectrum shows a LaN/YbN ratio below the detection limit. The spectrum shows enrichment in light rare earth elements with a LaN/SmN ratio equal to 1.74. The formations are enriched 14 times more than the primitive mantle. The spectrum also shows positive anomalies in Th, K, Pb, and Zr. It also shows negative anomalies in Nb, Ce, P, and Ti. No heavy rare earths elements (DyN/YbN below detection limits) and Eu anomalies observed (Eu/Eu* below detection limits).

d) Peraluminous granite of Dioudioukounkou

The SiO_2 content is 73.28%, while the alkali content ($Na_2O + K_2O$) is 6.82%. This granite shows cobalt (5 ppm), nickel (8 ppm), vanadium (20 ppm), and chromium (83 ppm) contents. Zirconium content is 170 ppm. Radioactive elements are low: Th (10 ppm) and U (3 ppm). The Dioudioukounkou granite (Ech.66), compared with the multi-element diagram of Sun and McDonough (1989), shows a spectrum marked by enrichment in LILE = "large ion lithophile element" (Cs, Rb, with a negative anomaly in Ba) and depletion in HFSE "high field strength element" (Nb, Ce, P, and Ti). A negative zirconium anomaly is notable. Rare earth content (∑REE) is 286.1 ppm. Rare-earth spectra normalized according to Sun and McDonough (1995) have a relatively medium to high slope. These rocks show low fractionation rates with LaN/YbN ratios of 17.45 and light rare earth enrichment with a LaNSmN ratio equal to 4.61. The Dioudioukounkou formations are 103 times enriched in primitive mantle. Dioudioukounkou granite is enriched in Ytterbium 8 times the primitive mantle. No heavy rare earths or Europium anomalies are observed.

4.2.2. Geochemical Signatures of Sesam Formations

1) Volcanic rocks

This classification of volcanic rocks is based on the content of major elements. The diagram of Le Bas et al. (1986) was used to classify the different formations in the Mako-Diale transition zone. Volcanic facies of Sesam are essentially formed by andesitic basalts and andesites.

a) Tholeiitic andesitic basalts

It is represented by sample 18 with an SiO_2 content of 55.93% and alkalinity ($Na_2O + K_2O$) of 3.19%. The andesitic basalt from the Sesam has an MgO content of 8.78%, a Fe_2O_3 content of 9.12% and an Al_2O_3 content of 12.44%. Andesitic basalts are represented by sample 18. The multi-element diagram by Sun and McDonough (1989) shows a spectrum marked by enrichment in LILE = "large ion lithophile element" (Rb, Ba) and depletion in HFSE "high field strength element" (Th, Nb, Ce, P). Positive anomalies in U, K, and Zr are also notable. Rare earth content (∑REE) is 23.2 ppm. Rare-earth spectra normalized according to Sun and McDonough (1995) have a relatively medium slope. These rocks show low fractionation rates with a LaN/YbN ratio below the detection limit. Rare earth enrichment is also low, with the LaN/SmN ratio below the detection limit. The formations are enriched 12 times more than the primitive mantle. Apart from Ytterbium, there are no heavy rare earths, and no Europium anomalies (Eu/Eu* below the detection limit).

b) Tholeiitic andesites

They are represented by sample 13 with fine lithic elements. Sesam andesites have SiO_2 contents of 54.89%, alkalinity ($Na_2O + K_2O$) of 4.41%. The MgO content is 2.07%, while the Fe_2O_3 content is 9.69%. The Al_2O_3 content is high at 13.37%. The tholeiitic andesites of Sesam, represented by sample 13, show cobalt contents of 23.5 ppm, nickel 5.5 ppm, vanadium 162.5 ppm, and chromium 21 ppm. Zirconium121, 6 ppm. Radioactive elements are low: Th 3.6 ppm and U 1.9 ppm. The multi-element diagram by Sun and McDonough (1989) shows a spectrum marked by enrichment in LILE = "large ion lithophile element" (Cs, Rb, Ba) and moderate depletion in HFSE "high field strength element" (Nb, Th, Ce). Positive Uranium and K anomalies are notable. The rare earth content (∑REE) of tholeiitic andesites is 46.3 ppm. Rare-earth spectra normalized according to Sun and McDonough (1995) are low slope with a LaN/YbN ratio of 1.44. A slight enrichment in light rare earths elements is noticeable, with a LaN/SmN ratio of 1.16. The formations are 260 times richer than the primitive mantle. Apart from ytterbium, there are no heavy rare earths or Eu anomalies (Eu/Eu* below detection limit).

c) Calc-alkaline andesites

They are represented by sample 21. Calc-alkaline andesites with fine lithic elements have a SiO_2 content of 59.44%. The alkali content ($Na_2O + K_2O$) is 4.58%. MgO content is 5.7%, Fe_2O_3 content is 6.32% and Al_2O_3 content is high (13.67%). Sesam andesites represented by sample 21 show cobalt contents of 29.1 ppm, nickel 153.5 ppm, vanadium 94.7 ppm, and chromium 359.8 ppm. Zirconium contents range from 102.7 ppm, while radioactive elements are low: Th 4.8 ppm and U 3.2

ppm. The multi-element diagram by Sun and McDonough (1989) shows a spectrum marked by enrichment in LILE = "large ion lithophile element" (Rb, Ba) and moderate depletion in HFSE "high field strength element" (Nb, Ce, P). Positive anomalies in Uranium, K, and Pb are notable. The rare earth content (∑REE) of calc-alkaline andesites is 32.3 ppm. Rare-earth spectra normalized to Sun and McDonough (1995) have a faintly visible slope. The LaN/YbN ratio of these rocks is below the detection limit. There is a slight enrichment in light rare earth elements, with the LaN/SmN ratio below the detection limit. There are no heavy rare earth elements and no Eu anomalies (Eu/Eu* below detection limit).

2) Plutonic formations

The classification of plutonic rocks is based on the evolution of major elements. It is carried out with the help of the diagram by Cox et al. (1979). Plotting the major elements on the TAS diagram (Cox et al., 1979) shows that the plutonic rocks of Sesam are mainly represented by quartz diorites or granodiorites (Ech.92) in addition to Koulountou and Tiguida granites.

A) Metaluminous granodiorites

The calc-alkaline granodiorites of the Sesam are metaluminous and represented by sample 92 from the southern part of the Koulountou massif. Analysis of the Cox et al. (1979) diagram shows that these Koulountou granodiorites are in the subalkaline to tholeiitic rock range. The calc-alkaline granodiorites of Sesam have an SiO_2 content of 64.46%. Alkali content ($Na_2O + K_2O$) is 4.24%. Their MgO content is very low (1.47%), and Al_2O_3 is 12.29%. Sesam granodiorites (Ech.92) show cobalt contents of 8.3 ppm, nickel 14.7 ppm, vanadium 31.4 ppm, and chromium 113.2 ppm. Zirconium levels are 226 ppm, while radioactive elements are low: Th 5.2 ppm and U 1.7 ppm. The multi-element diagram by Sun and McDonough (1989) shows a spectrum marked by enrichment in LILE = "large ion lithophile element" (Cs, Rb, Ba) and moderate depletion in HFSE "high field strength element" (Nb, Ce, P, Ti). Positive anomalies in U, K, Pb, and Zr, Nd, and Sm are notable. Rare earth element contents (∑REE) of granodiorites range from 111.3 ppm. Rare-earth spectra normalized to Sun and McDonough (1995) are low slope. These rocks show average fractionation rates with LaN/YbN ratios of 3.54. There is a slight enrichment in light rare earth elements, with a LaN/SmN ratio of 1.94. The formations are 35 times enriched in the primitive mantle.

b) Koulountou metaluminous granite

The Koulountou granite is represented by sample 97. Its SiO_2 content is 67.75%. Alkali content ($Na_2O + K_2O$) is 7.47%. Koulountou granites from Sesam (sample 97) show cobalt contents of 12.3 ppm, nickel 51.4 ppm, vanadium 46.6 ppm, chromium 106.6 ppm, zirconium 130.5 ppm, and low levels of radioactive elements: Th 10.3 ppm and U 6.3 ppm. The multi-element diagram by Sun and McDonough (1989) shows a spectrum marked by enrichment in LILE = "large ion lithophile element" (Rb, Ba) and moderate depletion in HFSE "high field strength element" (Nb, Ce, P, Ti). Positive anomalies in U, K, Pb, and Zr, Nd, and Sm are notable. The rare-earth content (∑REE) of the granites is 176.6 ppm. The rare earth ele-

ments spectrum normalized to Sun and McDonough (1995) has a shallow slope. These rocks show low fractionation rates with LaN/YbN ratios below the detection limit. There is an enrichment in light rare earth elements, with the LaN/SmN ratio equal to 2.55. The formations are enriched 90 times the primitive mantle. Apart from ytterbium, there are no heavy rare earth elements, and no Europium anomalies (Eu/Eu* below the detection limit).

c) Tiguida peraluminous granite

They are represented by sample 59, which belongs to the Sesam domain. It outcrops to the south of the Koulountou massif over several kilometers along strike N032 in an elliptic form. It is a facies rich in potassic feldspar. Tiguida rock is composed of plagioclase, amphibole, quartz, and potassic feldspar. It has a large fracture network, mainly oriented N050/80, with surface alteration revealing relics of coarse quartz grains. Tiguida contains 72.48% SiO_2, 6.89% alkali ($Na_2O + K_2O$), 15.59% Al_2O_3 and 1.87% Fe_2O_3. The Tiguida calc-alkaline granite (Ech.59) shows cobalt levels below the detection limit, nickel 9.4 ppm), vanadium (38.4 ppm), and chromium (81.9 ppm). Zirconium levels (80.8 ppm). Radioactive elements are low: Th (2.6 ppm) and U (1.9 ppm). The multi-element diagram by Sun and McDonough (1989) shows a spectrum marked by enrichment in LILE = "large ion lithophile element" (Cs, Rb, Ba) and moderate depletion in HFSE "high field strength element" (Th, Nb, Ce, P, Ti). Positive anomalies in U, K, and Pb are notable. The rare earth content (∑REE) of the Tiguida granite is 28.7 ppm. Rare-earth spectra normalized to Sun and McDonough (1995) are low slope. These rocks show low fractionation rates with LaN/YbN ratios below the detection limit. There is low enrichment in light rare earth elements, with LaN/SmN ratios below the detection limit. The formations are enriched 12 times the primitive mantle. There are no heavy rare earths, and no Europium anomalies (Eu/Eu=below detection limit).

3) Volcanosediments

Volcanosedimentary facies of the Sesam show tholeiitic variety (Ech.3) with an alkaline content ($Na_2O + K_2O$) of 1.05% and a calc-alkaline variety with an alkaline content of 4.84%. Volcanosedimentary rocks from Sesam (Ech.3 and 15) contain cobalt (74.9 - 35.3 ppm), nickel (77.9 - 189.2 ppm), vanadium (157.3 - 216.9 ppm), and chromium (331.4 - 300.4 ppm). Zirconium levels (56.6-118.7 ppm) and radioactive elements are: Th (2.4 - 5.1 ppm) and U (2 - 2.5 ppm). The multi-element diagram by Sun and McDonough (1989) shows a spectrum marked by enrichment in LILE = "large ion lithophile element" (Cs, Rb, Ba) and depletion in HFSE "high field strength element" (Th, Nb, Ce, P). Positive anomalies in U, K, Pb, and Nd are notable. Rare earth contents (∑REE) in volcanosediment range from 34.4 - 66.3 ppm. Rare-earth spectra normalized to Sun and McDonough (1995) are low slope. The tholeiitic variety shows very low levels of light rare earth elements (LaN/SmN below the detection limit). The calc-alkaline variety, on the other hand, is moderately enriched in light rare earths elements (LaN/SmN ratio 2.22). The formations are enriched 14 to 22 times more than the primitive mantle.

There are no heavy rare earth elements and no Europium anomalies (Eu/Eu* below the detection limit).

4.2.3. Geochemical Signature of Diabba Formations

1) Volcanic formations

This classification of volcanics is based on the major element content of the formations in the Diabba area. The nomenclature of the various formations is based on Le Bas et al. (1986). Volcanic facies of Diabba are essentially formed by basalts, andesitic basalts, andesites, and dacites.

a) Tholeiitic basalts

They are represented by sample 375, with its spinifex structure. These basalts contain 47.63% SiO_2 and 4.31% alkali ($Na_2O + K_2O$). These basalts are moderately magnesian with MgO contents of 5.92% and more ferriferous with Fe_2O_3 contents of 13.96%. Their Al_2O_3 content is 15.49%. The Diabba basalts (Ech.375) show cobalt contents of 48.8 ppm, nickel 44.7 ppm, vanadium 152.7 ppm, and chromium 110.2 ppm. Zirconium levels are 127.5 ppm, while radioactive elements are: Th 3.2 ppm and U 2.4 ppm. The multi-element diagram by Sun and McDonough (1989) shows a spectrum marked by enrichment in LILE = "large ion lithophile element" (Cs, Rb, Ba) and depletion in HFSE "high field strength element" (Th, Nb, Zr). Positive anomalies in U, La, and P are notable. The rare-earth elements content (∑REE) of Diabba spinifex basalts (Ech.375) is 122.4 ppm. Rare earth elements spectra normalized according to Sun and McDonough (1995) have a relatively medium slope. These rocks show high fractionation rates, with a LaN/YbN ratio of 11.9. They are enriched in light rare earth elements, with a LaN/SmN ratio of 3. The formations are enriched 50 times more than the primitive mantle. Apart from Ytterbium, there are no heavy rare earth elements and no Europium anomalies (Eu/Eu* below the detection limit).

b) Tholeiitic andesites basalts

They are represented by sample 76 with an SiO_2 content of 53.06% and an alkali content ($Na_2O + K_2O$) of 2.59%. It has MgO and Fe_2O_3 contents of 7.28% and 9.9% respectively. Their Al_2O_3 content is high at 10.70%. Andesitic basalts from Diabba (Ech.76) show cobalt (44.3 ppm), nickel (254.7 ppm), vanadium (152.7 ppm), and chromium (489 ppm). Zirconium levels are 63.9 ppm, while radioactive elements are: Th 2.1 ppm and U 1.4 ppm. The multi-element diagram by Sun and McDonough (1989) shows a spectrum marked by enrichment in LILE = "large ion lithophile element" (Cs, Rb, Ba) and depletion in HFSE "high field strength element" (Nb, Ce, P). Positive anomalies in U, K, Sr, and Nd are also notable. The rare earth elements content (∑REE) of andesitic basalts is 34.2 ppm. Rare earth elements spectra normalized according to Sun and McDonough (1995) have a relatively medium slope. These rocks show low fractionation rates with a LaN/YbN ratio below the detection limit. Rare earth elements enrichment is low, with the LaN/SmN ratio below the detection limit. The formations are enriched 16 times the primitive mantle. Apart from Ytterbium, there are no heavy rare earths and no Europium

anomalies (Eu/Eu* below the detection limit).

c) Calc-alkaline andesites

They are mainly represented by samples 219 and 52. Diabba's calc-alkaline andesites are porphyritic or have coarse-grained lithic elements. Alkaline proportions ($Na_2O + K_2O$) range from 5.39% to 6.18%. MgO content ranges from 3.01% to 5.13%. Their Fe_2O_3 content ranges from 6.77% to 7.66%. Their high Al_2O_3 content ranges from 14.29% to 16.49%. Diabba andesites (Ech.219, Ech.52) show cobalt contents of 20.7 - 22.9 ppm, nickel 52.1 - 52.7 ppm, vanadium 128.7 - 132.9 ppm, and chromium 110.1 - 189.9 ppm. Zirconium levels are 129.8 - 132.3 ppm, and radioactive elements are Th (4 - 4.3) ppm and U (2.5 - 3.9) ppm. The multi-element diagram by Sun and McDonough (1989) shows a spectrum marked by enrichment in LILE = "large ion lithophile element" (Cs, Rb, Ba) and depletion in HFSE = "high field strength element" (Th, Nb, Ce, P, Ti). Positive anomalies in U, K, Pb, and Nd are notable. Rare earth elements contents (∑REE) in Diabba andesites range from 60.9 - 62.2 ppm. Rare-earth spectra normalized to Sun and McDonough (1995) are very shallow-sloped. These rocks show high fractionation rates with a LaN/YbN ratio below the detection limit. There is low enrichment in light rare earth elements, with the LaN/SmN ratio below the detection limit. The formations are enriched 21 to 28 times the primitive mantle. There are no heavy rare earth elements, and no Eu anomalies (Eu/Eu* below the detection limit).

d) Calc-alkaline dacites

They are mainly represented by samples 341 and 230 from Diabba. Sample 230 is located on the CiscoE shear-contact zone. The dacites correspond to the fine to coarse-grained volcaniclastic facies within the Diabba domain. These facies are marked by SiO_2 contents ranging from 59.32% to 60.50%. Sample 341 has a slightly higher alkaline content ($Na_2O + K_2O$) (4.38%) than sample 230 (3.97%). The MgO content of Diabba dacites varies between 1.94% and 2.13%, while Fe_2O_3 content ranges from 4.90% to 5.37%. Their Al_2O_3 content varies between 12.92 and 17.03%. The Diabba dacites (341, Ech.230) contain cobalt (10.8 - 32.5 ppm), nickel (25.4 - 72 ppm), vanadium (63.9 - 132.9 ppm), and chromium (69.7 - 189.9 ppm). Zirconium levels (108 - 141.4 ppm) and radioactive elements are: Th (3 - 5.4 ppm) and U (1.5 - 1.8 ppm). The multi-element diagram by Sun and McDonough (1989) shows a spectrum marked by enrichment in LILE = "large ion lithophile element" (Cs, Rb, Ba) and depletion in HFSE "high field strength element" (Nb, Ce, P, Ti). Positive anomalies in U, K, Pb, and Nd are also notable. Rare earth elements contents (∑REE) of Diabba dacites range from 39.9 - 108.9 ppm. Rare-earth spectra normalized according to Sun and McDonough (1995) are gently sloping. These rocks show a LaN/YbN ratio below the detection limit. Light rare earth elements are enriched with a LaN/SmN ratio of 5.3. The formations are enriched 19 times more than the primitive mantle. There are no heavy rare earth elements, and no Eu anomalies (Eu/Eu* below the detection limit).

2) Plutonic formations

Due to the wide variety of intrusive formations, signature studies are only avail-

able for the Diabba granodiorite near Massawa along the MTZ and the Tinkoto granite (Figure 15).

a) Peraluminous granodiorites

The calc-alkaline granodiorites of the Diabba domain are peraluminous. They are represented by sample 317 taken from the CiscoE shear-contact zone, with a SiO_2 content of 67.93%. The alkaline content is 6.14% and the CaO content is 2.83%. The Diabba granodiorites (Ech.317) show cobalt (7.5 ppm), nickel (20.7 ppm), vanadium (55.8 ppm), and chromium (95.9 ppm) content. Zirconium content is 91.7 ppm. Radioactive elements are: Th (2.2 ppm) and U (1.8 ppm). These granodiorites are plotted on the multi-element diagram of Sun and McDonough (1989) in Figure 16. The analysis shows a spectrum marked by enrichment in LILE = "large ion lithophile element" (Cs, Rb, Ba) and moderate depletion in HFSE "high field strength element" (Nb, Ce, P, Ti). Positive anomalies in U, K, Pb, and Zr are notable.

b) Metaluminous granite of Tinkoto

The Tinkoto granite in the Diabba area (Ech.81) has cobalt (10 ppm), nickel (17.9 ppm), vanadium (62.1 ppm), and chromium (109.8 ppm). Zirconium content is (96.2 ppm), and radioactive elements are: Th (7.2 ppm) and U (4.5 ppm). The multi-element diagram by Sun and McDonough (1989) shows a spectrum marked by enrichment in LILE = "large ion lithophile element" (Cs, Rb, Ba) and depletion in HFSE = "high field strength element" (Th, Nb, Ce, P, Ti). Positive anomalies in U, K, Pb, and Nd are notable. Rare earth elements contents (∑REE) in the Tinkoto granite range from 75.6 ppm. Rare earth elements spectra normalized to Sun and McDonough (1995) are low slope (Figure 17). These rocks show low fractionation rates with LaN/YbN ratios below detection limits. They are enriched in light rare earths with a LaN/SmN ratio equal to 3.75. The formations are enriched 40 times the primitive mantle. There are no heavy rare earth elements, and no Eu anomalies (Eu/Eu* below detection limits).

3) Metasedimentary facies

They are represented by samples 30 (fine sediment) and 38 (Chert). Their SiO_2 contents are 50.87 (Ech.30) and 76.40% (Ech.38). The Fe_2O_3 content is high (15.20%) for sample 30, compared with 1.68% for sample 38. Similarly, CaO content is high (5.26%) for sample 30 versus 0.55% for sample 38. Sedimentary facies are represented by samples 30 (fine sediment) and 38 (Chert). Petrography shows that Ech.30 is composed of albite, quartz, plagioclase, and K-feldspar. This sedimentary formation bears pyrite, chalcopyrite, and quartz-carbonate veins, and there is a presence of martitization (transformation of magnetite to hematite). Diabba metasediments (Ech.30, Ech.38) show high levels of cobalt (47.9 ppm), nickel (3.8 - 81.9 ppm), vanadium (314.2 ppm), and chromium (106.2 - 172.5 ppm). Alkali contents ($Na_2O + K_2O$) are 3.39 (Ech.30) and 6.98 (Ech.38). Zirconium contents range from 34.6 to 76 ppm. Radioactive elements recorded correspond to: Th (2.6 - 2.7 ppm) and U (2.1 - 2.5 ppm). The multi-element diagram by Sun and McDonough (1989) shows a spectrum marked by

enrichment in LILE = "large ion lithophile element" (Cs, Rb, Ba) and depletion in HFSE "high field strength element" (Th, Nb, Ce, P, Ti). Positive anomalies in U, K, and Pb are notable (**Figure 17**). Rare earth elements contents (∑REE) of the metasediments range from 17.2 to 40.9 ppm. Rare earth elements spectra normalized to Sun and McDonough (1995) are low slope. These rocks show low fractionation rates, with a LaN/YbN ratio of 0.87. There is a slight enrichment in light rare earth elements, with a LaN/SmN ratio of 0.88. Apart from ytterbium, there are no heavy rare earth elements, and no Eu anomalies (Eu/Eu* below the detection limit). The multi-element diagram by Sun and McDonough (1989) shows a spectrum marked by enrichment in LILE = "large ion lithophile element" (Cs, Rb, Ba) and depletion in HFSE "high field strength element" (Th, Nb, Ce, P, Ti). Positive U, K, and Pb anomalies are notable. Rare earth elements contents (∑REE) of metasediments range from 17.2 to 40.9 ppm. Rare-earth spectra normalized to Sun and McDonough (1995) are low slope. These rocks show low fractionation rates, with a LaN/YbN ratio of 0.87. There is a slight enrichment in light rare earth elements, with a LaN/SmN ratio of 0.88. Apart from ytterbium, there are no heavy rare earth elements and Eu anomalies (Eu/Eu* below detection limit).

5. Comparative Study of Geochemical Signatures of Maco, Sesam, and Diabba

Comparative geochemical studies of the large plutonic masses of Maco, Sesam, and Diabba and their country rocks reveal calc-alkaline volcanism, calc-alkaline plutonism, tholeiitic volcanism, and tholeiitic plutonism.

5.1. Calc-Alkaline Volcanism

Calc-alkaline volcanism of the Mako-Diale Transition Zone occurs at Maco, Sesam, and Diabba. **Maco calc-alkaline** volcanism (**Figure 16**) is unimodal. It is represented by basalts (Ech.89, Ech.70) sitting on a compressive active margin geodynamic environment associated with a volcanic arc. **Sesam calc-alkaline volcanism** shows calc-alkaline andesites (Ech.21) and calc-alkaline volcanosediments in an island arc environment. **Diabba calc-alkaline volcanism** is marked by calc-alkaline andesites (Ech.52; Ech.218) and calc-alkaline dacites (Ech.341; Ech.230). This volcanism sits on a compressive active margin geodynamic environment associated with an island arc. Trace element compositions are also plotted on the multi-element diagrams of Sun and McDonough (1989; 1995). The evolution of the trace element contents (**Figure 16**) of the samples in the Sun and McDonough (1995) multi-element spectrum shows that formations of the Mako-Diale transition zone are enriched in LILE = large ion lithophile element and HFSE = high field strength element. Spectral analysis also shows a series of positive anomalies in U, K, Pb, Nd, and a series of negative anomalies in Nb, Ce, P, and Ti. All calc-alkaline volcanics show a positive U anomaly and negative Nb anomaly.

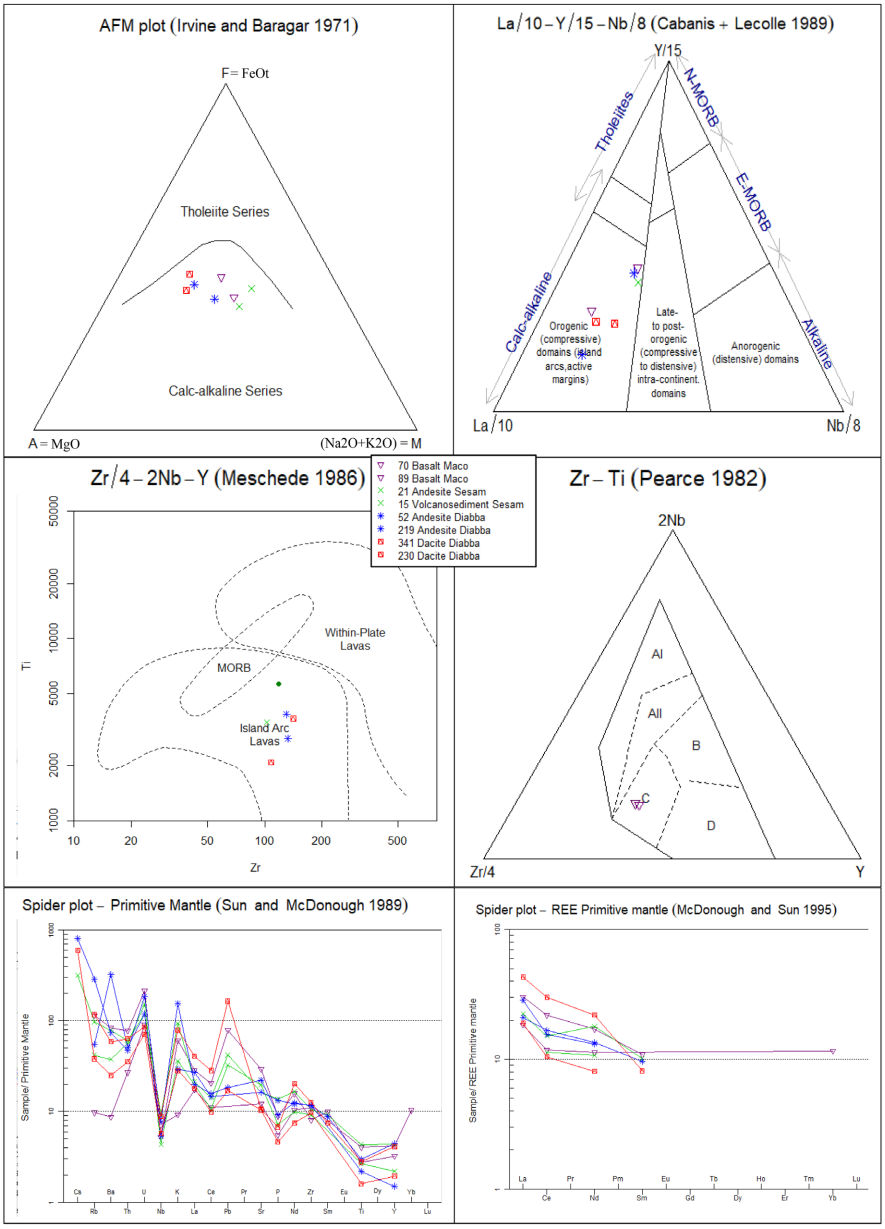

Figure 16. Geochemical signature of calc-alkaline volcanics. AFM diagram of Irvine and Baragar (1971) showing the volcanic affinity of the rocks of the Mako-Diale transition zone (ZTMD); La/10-Y/15-Nb/8 ternary diagram of Cabanis and Lecolle (1989) applied to the volcanic rocks of the ZTMD; Th/Yb-Ta/Yb diagram of Pearce (1982) applied to the intermeiary and acid calc-alkaline volcanic rocks of the ZTMD; Meschede (1986) applied to Maco basalts; AI-AII = Within-Plate Alkaline Basalts, AII-C = Within-Plate Tholeiites, B = P-type Mid-Ocean Ridge Basalts, D = N-type Mid-Ocean Ridge Basalts and C-D = Volcanic Arc Basalts; ZTMD = transition zone of Mako-Diale, diagram by Pearce and Gale (1977) and Th/Yb-Ta/Yb diagram by Pearce (1982) applied to basic and intermediate rock. The combined diagrams show that Maco's calc-alkaline volcanism is based on a compressive active margin associated with a volcanic arc. It is characterized by the presence of volcanic arc basalts (Ech.89, Ech.70). The calc-alkaline volcanism of Sesam is set as volcanics belonging to an island arc environment associated with: calc-alkaline volcanosediments with an affinity for island arc lavas (Ech.15); and calc-alkaline andesites with affinity for island arc lavas (Ech.21). The calc-alkaline volcanism of Diabba sets in a compressive active margin. It is associated with an island arc represented by island arc lavas (Ech.52; Ech.218); and island arc lavas (Ech341; Ech.230); Multi-element spectra normalized to the primitive mantle applied to calc-alkaline volcanics; Multi-element spectra of Sun and McDonough (1989) and multi-element spectrum of the evolution of trace element contents of Sun and McDonough (1995) showing a series of positive anomalies in U, K, Pb, Nd, and a series of negative anomalies in Nb, Ce, P, Ti. All the calc-alkaline volcanics show a positive anomaly in U and a negative one in Nb.

5.2. Calc-Alkaline Plutonism

The calc-alkaline plutonism of the Mako-Diale Transition Zone is notable in the Maco, Sesam, and Diabba domains. **Maco calc-alkaline plutonism** is represented by calc-alkaline diorites (**Figure 17**) associated with a geodynamic environment of volcanic arc granitoids (VAG).

Sesam calc-alkaline plutonism is associated with volcanic arc granitoids and intraplate granitoids; the volcanic arc granitoids, "VAG" are calc-alkaline and correspond to Koulountou granodiorites (Ech.92) and Tiguida granite (Ech.59). They are marked by an orogenic (compressive) active margin environment; the "WPG" intraplate granitoids are calc-alkaline and represented by the calc-alkaline Koulountou granite (Ech.97) sitting on an orogenic (compressive) active margin environment. **Diabba calc-alkaline plutonism** is represented by the Tinkoto granite (Ech.81) and the Diabba granodiorite (Ech.317). It is based on a geodynamic compressive active margin environment associated with arc granitoids.

Multi-element spectra of Sun and McDonough (1989) and the multi-element spectrum of the evolution of trace element contents of Sun and McDonough (1995) show a series of positive U, K, Pb, Nd anomalies and a series of negative Nb, Ce, P, Ti anomalies. All calc-alkaline plutonic facies of the Mako-Diale transition zone show a positive U anomaly and a negative Nb anomaly (**Figure 17**).

5.3. Tholeiitic Volcanism

Tholeiitic volcanism of the Mako-Diale Transition Zone (ZTMD) has not been intersected at Maco (**Figure 18**). It is represented in the Sesam and Diabba domains. It occurs in the form of tectonovolcanic episodes belonging to distinct geodynamic environments: intraplate basalts (intraplate lavas) with MORBs affinity (Ech.375 = Diabba basalt); active margin (compressive) andesitic basalts with MORBs affinity (Ech.76 = Diabba andesitic basalt); andesites (Ech.13 = Sesam andesite) with intraplate lavas affinity; active margin andesitic basalts (Ech.18 = Sesam andesitic basalt) with island arc lavas affinity; active margin tholeiitic volcanosediments (compressive) with island arc lavas affinity.

The trace element compositions of all samples from the Sesam domain are plotted on the multi-element diagrams of Sun and McDonough (1989). The evolution of the trace element contents of the samples in the multi-element spectrum of Sun and McDonough (1995) shows (**Figure 18**) that the formations of the Sesam domain are enriched in LILE = large ion lithophile element and HFSE = high field strength element. Spectral analysis also shows a series of positive U, K, Sr, Pb, Nd, and Sm anomalies, and a series of negative Nb, Ce, P, and Ti anomalies. All Sesam lithologies show positive U and Ta anomalies and a negative Nb anomaly.

5.4. Tholeiitic Plutonism

Tholeiitic plutonism is found exclusively in Maco (**Figure 19**). It is marked by the presence of tholeiitic gabbros from intra-continental sources (pre-plate collision zone) and tholeiitic diorites from mantle sources (fractionate mantle zone).

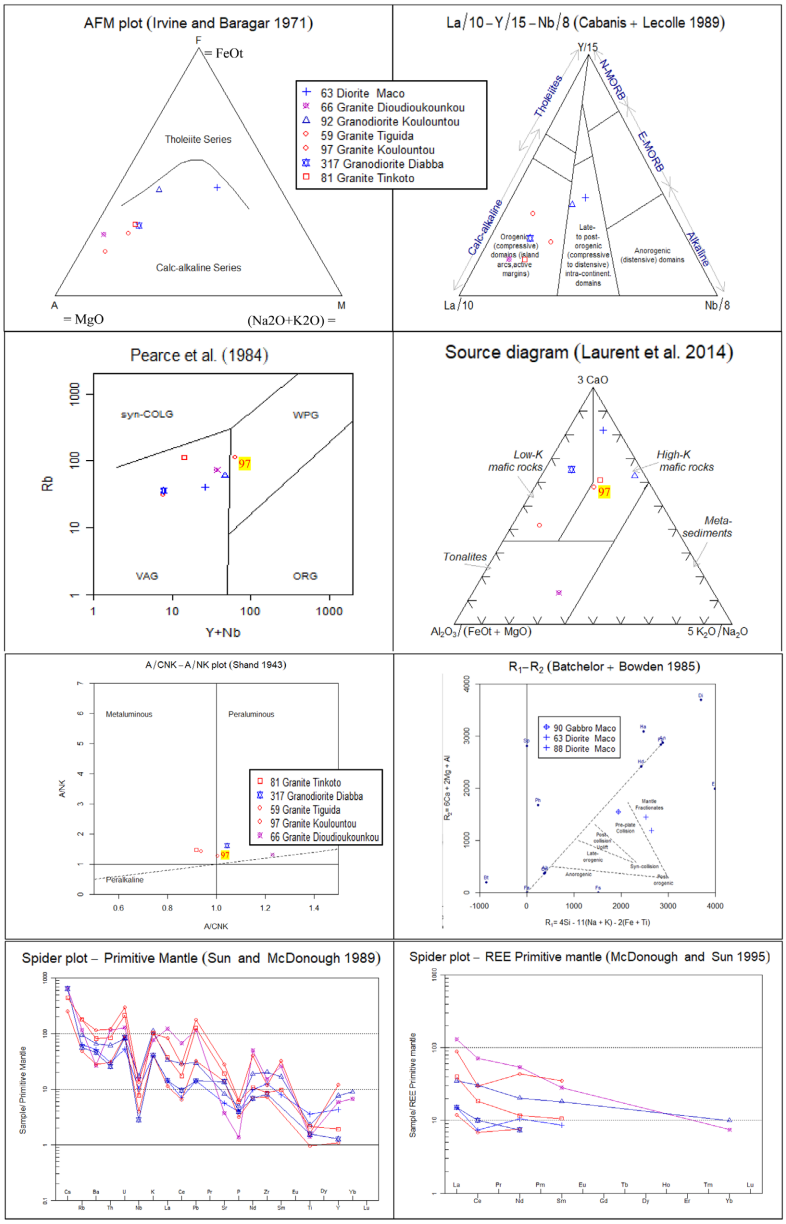

Figure 17. Geochemical signature of calc-alkaline large plutonic masses. The AFM diagram of Irvine and Baragar (1971) distinguishes a single magmatic series for large plutonic masses: the calc-alkaline series represented by Koulountou granite (Ech.97), Tiguida granite (Ech.59), Tinkoto granite (Ech.81), Dioudioukounkou granite (Ech.66), Diabba granodiorite (Ech.317), Maco diorite (Ech.63) and Diabba granodiorite (317); Shand's diagram (Shand, 1943) applied to large plutonic masses of Mako-Diale transition zone shows that three (3) facies are peraluminous and correspond to the following samples: sample 66 from the Maco domain, sample 59 from the Sesam domain and sample 317 from Diabba domain. The other two (2) facies are metaluminous. They correspond to Tinkoto (sample 81) and Koulountou (sample 97) granites belonging respectively to Diabba and Sesam domains. The Batchelor and Bowden (1985) diagram applied to granitoids shows that tholeiitic gabbros are in the 'pre-plate collision' zone. On the other hand, the tholeiitic diorites (Ech.88) and calc-alkaline diorites (Ech.63) of Maco are in the 'fractionate mantle' field. The diagram of Laurent et al. (2014) shows that large plutonic masses belong to three (3) different sources. Koulountou (Ech.97) and Tinkoto granites are sourced from high-K mafic rocks, while Tiguida granite and Diabba granodiorite belong to low-K mafic rocks. The Dioudioukounkou granite is sourced from tonalite rocks. Multi-element spectra normalized to the primitive mantle applied to calc-alkaline plutonite rocks; Multi-element spectra of Sun and McDonough (1989) and multi-element spectrum of the evolution of trace element contents of Sun and McDonough (1995) showing a series of positive anomalies in U, K, Pb, Nd, and a series of negative anomalies in Nb, Ce, P, Ti. All the calc-alkaline plutonic facies in the Mako-Diale transition zone show a positive U anomaly and a negative Nb anomaly.

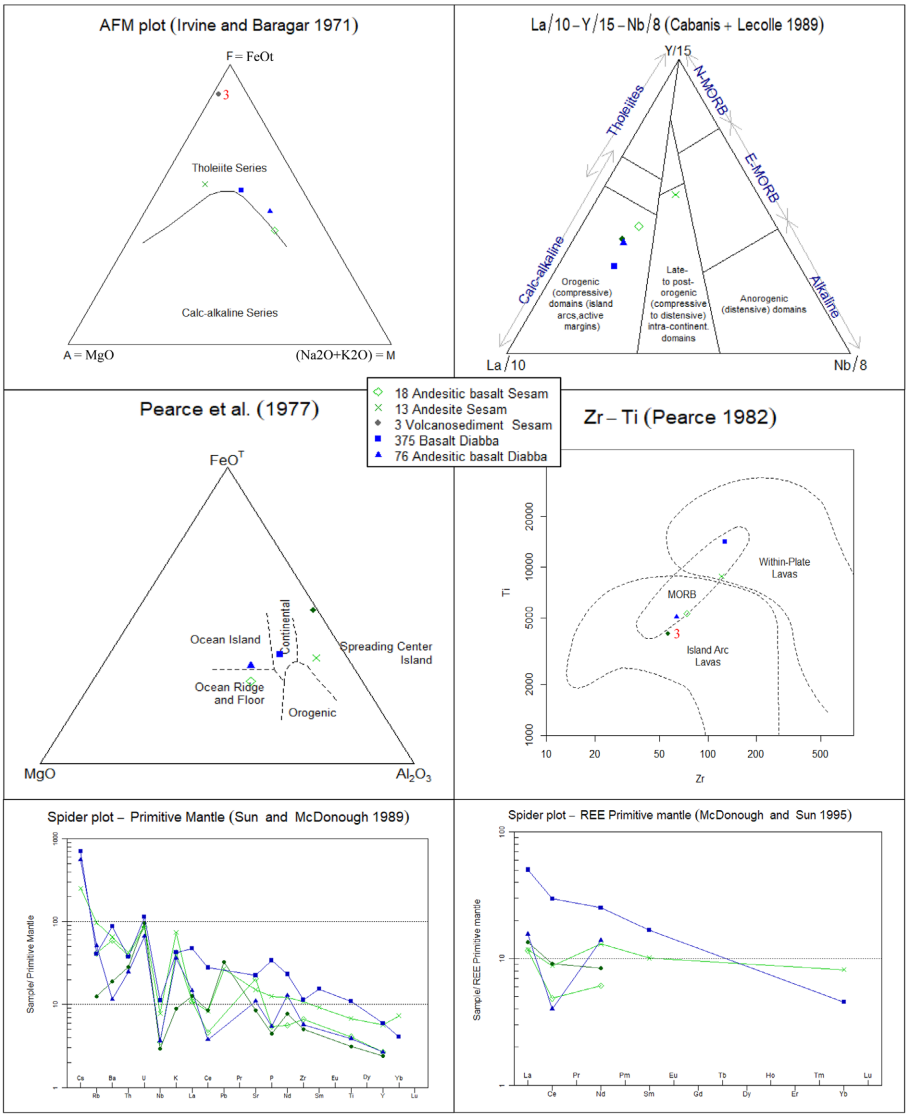

Figure 18. Geochemical signature of tholeiitic volcanics. AFM diagram of Irvine and Baragar (1971) showing the volcanic affinity of the rocks of the ZTMD; La/10-Y/15-Nb/8 ternary diagram of Cabanis and Lecolle (1989) applied to the volcanic rocks of the ZTMD; Th/Yb-Ta/Yb diagram of Pearce (1982) applied to the intermediate and acid calc-alkaline volcanic rocks of the ZTMD; Meschede (1986) applied to Maco basalts; AI-AII = Within-Plate Alkaline Basalts, AII-C = Within-Plate Tholeiites, B = P-type Mid-Ocean Ridge Basalts, D = N-type Mid-Ocean Ridge Basalts and C-D = Volcanic Arc Basalts. AFM diagram by Irvine and Baragar (1971) showing the magmatic affinity of rocks; La/10-Y/15-Nb/8 ternary diagram by Cabanis and Lecolle (1989); diagram by Pearce and Gale (1977), and Th/Yb-Ta/Yb diagram by Pearce (1982) applied to basic and intermediate rock. The diagram by Pearce and Gale (1977) shows that the tholeiitic andesitic basalts of Sesam (Ech.18) are in the 'Ocean ridge and floor' field. The tholeiitic andesites (Ech.13) of Sesam have MORB affinity in the context of the Spreading Center of the Island. The Diabba tholeiitic andesitic basalts are found in the Ocean island field, while the Diabba tholeiitic basalts (Ech.375) are found in the continental domain. The volcanosediments (Ech.3) of Sesam are in the "Spreading Center of Island" field and are tholeiites. Pearce's diagram (Pearce, 1982) shows that the tholeiitic basalts (Ech.375) are Mid-oceanic ridge basalt MORBs with an affinity for within-plate lavas. The andesitic basalts of Sesam (Ech.18) are Mid-oceanic ridge basalt (MORBs) with an affinity for island arc. The andesitic basalts of Diabba (Ech.76) are Mid-oceanic ridge basalt (MORBs) or Ocean Island basalt (OIBs) with island arc. The Sesam volcanosediments (Ech.13) are arc tholeiites showing an affinity with island arc lavas. Sesam volcanosediments represent andesitic (explosive volcanic) deposited material with facies ranging from coarse to fine (ash) lithic elements.; Multi-element spectra of Sun and McDonough (1989) and multi-element spectra of the evolution of trace element contents of Sun and McDonough (1995) showing a series of positive anomalies in U, K, and a series of negative anomalies in Nb, Ce. All lithologies show a positive U anomaly and a negative Nb anomaly.

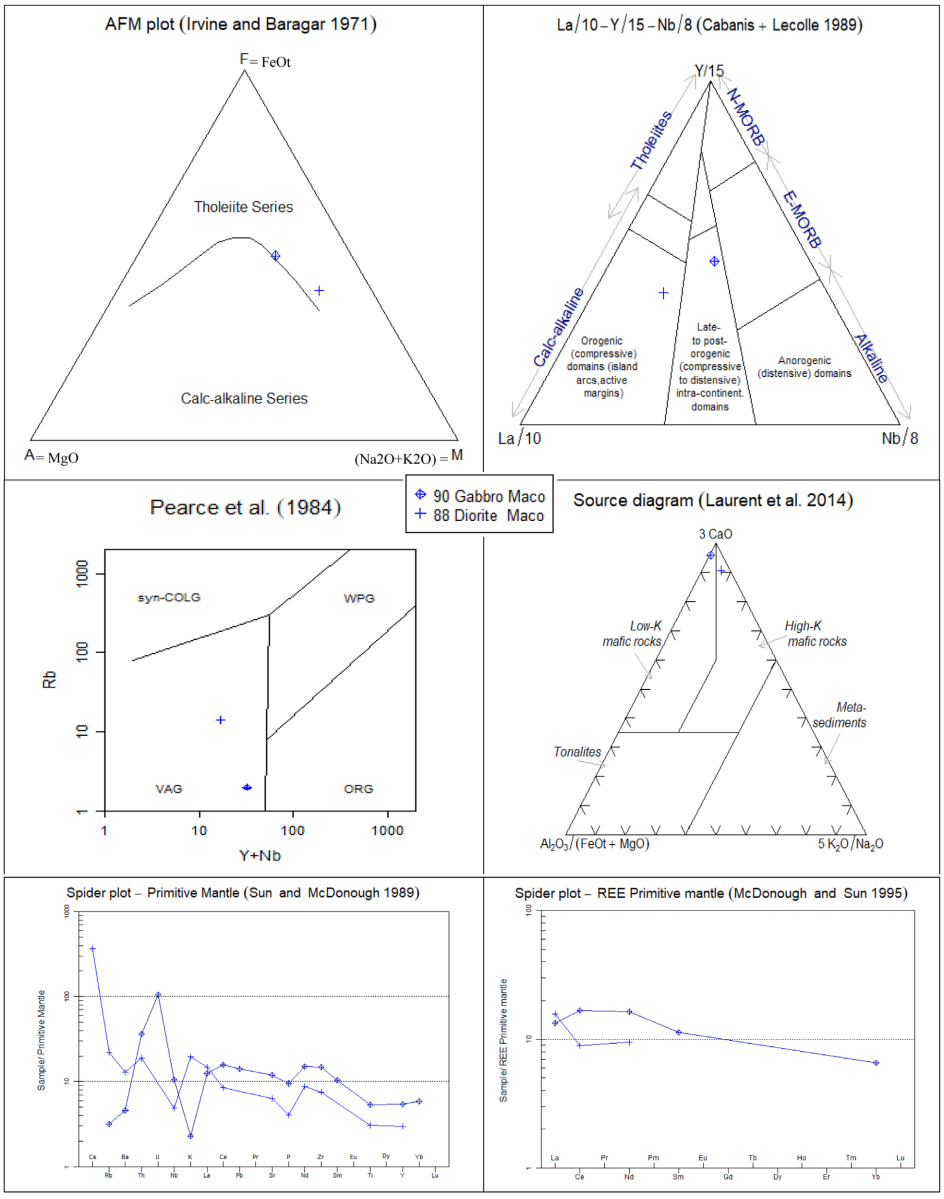

Figure 19. Geochemical signature of tholeiitic plutonism of Maco. The AFM diagram of Irvine and Baragar (1971) shows that tholeiitic plutonism is represented by the gabbros (Ech.90) and diorites (Ech.88). The diagram by Laurent et al. (2014) shows that tholeiitic plutonism of Maco domain is marked by the presence of tholeiitic gabbros from an intra-continental source (pre-plateau collision zone) and tholeiitic diorites from a mantle source (fractionate mantle zone). Maco's tholeiitic gabbros come from a mafic magmatic source with a low potassium content (Low K mafic rock). The tholeiitic diorites of Maco are derived from a mafic magmatic source with a high potassium content (High K mafic rock). In short, Maco's tholeiitic plutonism highlights two tholeiitic series from different sources. The diagram of Pearce et al. (1984) applied to the basic to intermediate plutonic formations of Maco shows that the tholeiitic gabbros, tholeiitic diorites, and calc-alkaline diorites are in the volcanic arc granitoids (VAG) zone. The Batchelor and Bowden (1985) diagram applied to granitoids shows that tholeiitic gabbros are in the "pre-plate collision" zone. The tholeiitic diorites (Ech.88) and calc-alkaline diorites (Ech.63) of Maco are in the "fractionate mantle" field.; Multi-element spectra normalized to the primitive mantle applied to the tholeiitic plutonic rocks of the Mako-Diale transition zone. Multi-element spectra from Sun and McDonough (1989) and the multi-element spectrum of trace element content evolution from Sun and McDonough (1995) show a series of positive anomalies in U (Gabbro) and K (Diorite) and a series of negative anomalies in Nb (Gabbro) and P (Gabbro, Diorite). For large samples, as in **Figure 19**, statistical tests such as the T-test and Karl Pearson's correlation will not be significant when considering two variables. However, even though they are two samples, we are not thinking in statistical terms here; the idea is to show the behavior of volcanic tholeiites in relation to plutonic tholeiites, which technically cannot be placed in the same multi-elements diagram with volcanic tholeiites.

Maco's tholeiitic gabbros are derived from a mafic magmatic source with low potassium content (Low K mafic rock). Maco's tholeiitic diorites, on the other hand, derive from a mafic magmatic source with a high potassium content (High K mafic rock). In short, Maco's tholeiitic plutonism reveals two plutonic tholeiitic series from different sources. The trace element compositions of the samples are plotted on the multi-element diagrams of Sun and McDonough (1989). The evolution of the trace element contents of the samples in the multi-element spectrum of Sun and McDonough (1995) shows (**Figure 19**) that the rocks of the Sesam domain are enriched in LILE = large ion lithophile element and HFSE = high field strength element. Spectral analysis also shows a series of positive U, K anomalies and a series of negative Nb, Ce anomalies. All lithologies show a positive U anomaly and a negative Nb anomaly.

5.5. Evidence of Magmatic and Tectonic Sources and Metallogenic Implications

The magmatic sources of the Paleoproterozoic crustal growth in the Kedougou-Kenieba Inlier and the WAC have been previously constrained by isotopic studies (Abouchami et al., 1990; Ngom et al., 2010). The Paleoproterozoic rocks of the Mako Volcanic Belt display positive $\varepsilon_{Nd(t)}$ values ranging from 2.2 to 4.3, with low initial Sr isotopic compositions (0.700 to 0.704) in **Figure 20**. The low initial Sr isotopic composition rules out a pre-existing continental crust as a possible source. The isotopic results indicate that the Kedougou-Kenieba Inlier is derived from homogeneous, juvenile mantle-derived material (Pawlig et al., 2006). The composition is isotopically close to that of the depleted mantle of DePaolo (1981) (Pawlig et al., 2006; Ngom et al., 2010).

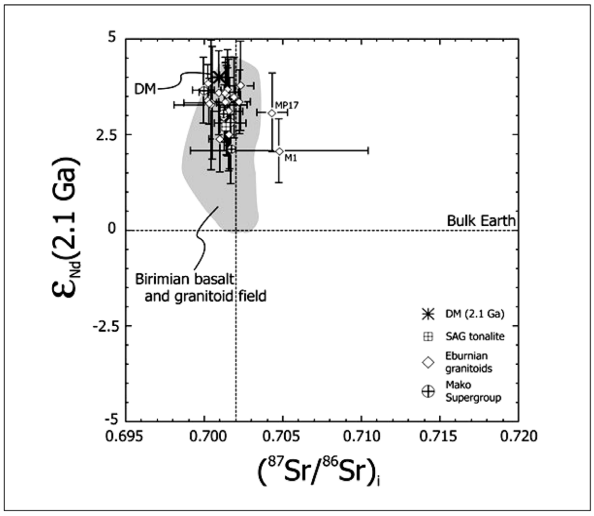

Figure 20. Plot of $\varepsilon_{Nd(t)}$ versus initial $^{87}Sr/^{86}Sr$ ratios for SAG tonalite, the Mako Volcanic Belt, and the Eburnian granitoids of the KKI recalculated to the Eburnian orogeny at 2.1 Ga. DM denotes the contemporaneous depleted mantle composition from DePaolo (1981). Grey field labeled "Birimian basalt and granitoid field" represents compositions of Birimian basaltic and felsic lithologies from the WAC taken from Abouchami et al. (1990), Boher et al. (1992), Taylor et al. (1992), Gasquet et al. (2003), and Pawlig et al. (2006).

Magmatism expressed through Maco, Sesam, Diabba, and Kofi and their country rocks is reflected in calc-alkaline volcanism, calc-alkaline plutonism, tholeiitic volcanism, and tholeiitic plutonism. Calc-alkaline volcanism of the Mako-Diale Transition Zone occurs at Maco, Sesam, and Diabba. The calc-alkaline plutonism of the Mako-Diale Transition Zone is notable in Maco, Sesam, and Diabba. The tholeiitic volcanism of the Mako-Diale Transition Zone (ZTMD) has not been intersected at Maco. It is represented in the Sesam and Diabba domains. It occurs in the form of tectonovolcanic episodes belonging to distinct geodynamic environments: intraplate basalts (intraplate lavas) with a volcanic arc. Tholeiitic plutonism is found exclusively in Maco. Calc-alkaline volcanism of the Mako-Diale Transition Zone occurs at Maco, Sesam, and Diabba. The tholeiitic plutonism of Maco is marked by the presence of tholeiitic gabbros from an intra-continental source (pre-plate collision zone) and tholeiitic diorites from a mantle source (fractionate mantle zone). Maco's tholeiitic gabbros come from a mafic magmatic source with a low potassium content (Low K mafic rock). In contrast, the tholeiitic diorites of Maco are derived from a "High K mafic rock" mafic magmatic source with a high potassium content. In summary, the Maco tholeiitic plutonism highlights two tholeiitic series from different sources. The magmatism of the Sesam arc is marked by MORBs tholeiites associated with arc tholeiites and calc-alkaline series: tholeiites 3 of Sesam (Ech.18: andesitic basalt) with MORBs affinity from active margin (Ocean Ridge and floor), tholeiites4 of Sesam (Ech.13: andesite) with intracontinental MORBs affinity (Spreading center of island) and tholeiites with insulair arc lavas affinity (Ech.3: volcanosediments) and calc-alkaline 2 series of Sesam with insular arc affinity fed by two sources with distinct geotectonic contexts (Ech.21: andesite in orogenic context and Ech.15: volcanosediment with insular arc affinity in Ocean Ridge and floor context). The Diabba is marked by tholeiitic volcanisms and calc-alkaline volcanisms: Diabba tholeiites 5 (basalt) with affinity for intraplate lavas (continental zone); Diabba tholeiites 6 (andesitic basalt) with MORBs or OIBs affinity (oceanic islands zone), and Diabba calc-alkaline series 3 (andesites) with island arc affinity (orogenic). Large plutonic masses from Maco Sesam and Diabba belong to three (3) different magmatic sources: Koulountou (Ech.97) and Tinkoto granites and Koulountou granodiorite come from high-K mafic sources, while Tiguida granite and Diabba granodiorite are derived from low K mafic rocks. Dioudioukounkou granite belongs to tonalite source (Ndiaye et al., 2025). In the same spirit, composite intrusions from Dalema-Faleme Series shows for three different sources: the low K samples intrusions are mostly devoid of any Eu anomaly and have a slight enrichment of the MREEs compared to the HREEs with the (Dy/Yb)N ratios varying between 1.0 and 1.5; the medium to high K intrusions, including granodiorite and monzogranite, respectively, from Boboti and Nafadji plutons, originated from a more evolved lower crustal source with a lower εNd (+2.67 and + 2.97) and the high K leucogranite samples stand out with a strong negative Eu anomaly, a greater ratio of (Dy/Yb) N, which varies between 2.04 and 2.37 (Faye et al., 2023).

Petrographic and tectonic studies show that Maco formation hosting Dioudioukounkou granite, is represented by volcanics (metabasalts) and ultrabasic, basic, intermediate, and acidic plutonic formations represented by gabbros, diorites, granodiorites, granites, and also serpentinites in tectonic contact with the western shear contact CiscoW.

Koulountou and Tiguida granites are hosted by the Sesam formation, mainly represented by andesitic volcanics (breccias, meta-andesite, metavolcanosediments, metatuffs) associated with andesitic volcanosediment (andesitic explosive volcanics deposited with facies ranging from coarse to fine-ash-lithic elements) and other plutonic formations such ultrabasites. The petrographic and contextual studies highlight that Diabba's main lithologies are composed of sedimentary facies (fine-grained sediments, schists, quartz veins, cherts, metapelites, conglomerates, grauwackes) associated with volcanoclastic rocks and plutonic formations composed of granites, granodiorites, and serpentinites in tectonic contact with the shear zone, CiscoE.

A study of the trace element compositions of calc-alkaline magmatism samples shows that positive neodymium (Nd) anomalies in calc-alkaline volcanics and plutonites indicate contributions from mantle sources. Positive neodymium (Nd) anomalies also indicate magmatic differentiation processes where magma has evolved incorporating Nd-rich mantle materials. Positive uranium (U) anomalies in calc-alkaline volcanics and plutonites suggest hydrothermal processes (positive uranium anomaly may indicate that rocks have been affected by hydrothermal fluids, which can transport and concentrate Uranium) and magmatic enrichment (it may also suggest that rocks have undergone specific magmatic processes that have led to uranium enrichment). Negative niobium (Nb) anomalies in calc-alkaline volcanics and plutonites suggest a crustal source (negative niobium anomaly may indicate that the rocks originate from a crustal source, as niobium is often depleted in crustal materials compared to mantle materials). They may also testify to magmatic fractionation processes (this can also be the result of magmatic fractionation processes, where niobium is removed from liquid phase and incorporated into resistant minerals).

Overall, anomalies observed may suggest that calc-alkaline volcanics and plutonics formed in a tectonic context where Western shear-contact (CiscoW), which constitutes the D1 phase of deformation associated with crustal growth, CiscoM corresponding to the D2 phase associated with the opening of the Diabba back-arc basin, and CiscoE representing the phase called MTZ, argue in favor of subduction.

Also, the presence of serpentinized peridotites (serpentinites), andradite (a type of garnet that often forms in high-pressure, low-temperature environments) within large plutonic masses (Dioudioukounkou, Koulountou, Tiguida, Tinkoto) and the positive U anomaly testify to hydrothermal processes typical of subduction zones. The study of tholeiitic magmatism shows that the positive U anomaly in volcanic and plutonic tholeiites suggests that the formations have been affected by hydro-

thermal fluids, which can transport and concentrate uranium. It may also suggest that the formations have undergone specific magmatic processes leading to uranium enrichment. A positive tantalum (Ta) anomaly in volcanic tholeiites suggests a mantle contribution, as tantalum is often enriched in material originating from the earth's mantle. A positive Ta anomaly may indicate a significant mantle contribution. It may also testify to magmatic processes (differentiation) where tantalum is concentrated in certain mineral phases. The negative niobium (Nb) anomaly in volcanic and plutonic tholeiites indicates that the rocks originate from a crustal source, as niobium is often depleted in crustal materials compared to mantle materials. It also bears witness to magmatic fractionation, where niobium is removed from the liquid phase and incorporated into resistant minerals. The anomalies observed may suggest that volcanic and plutonic tholeiites are formed in a tectonic context where hydrothermal and magmatic processes played an important role. This may include subduction environments or crust-mantle interactions. Examination of the tectonic context, marked by the CiscoM shear-contact corresponding to the D2 phase associated with the opening of Diabba and the CiscoE corresponding to D3, argues in favour of subduction. Also, the presence of serpentinized peridotites (serpentinites along the CiscoM and CiscoE), andradite (a type of garnet that often forms in high-pressure, low-temperature environments) in the large plutonic masses (Koulountou, Tiguida, and Tinkoto) and the positive U anomaly testify to hydrothermal processes typical of subduction zones.

The Maco peridotite is associated with a mylonitic shear zone, marking an interface of deep ductile deformation in the mantle lithosphere. The deformation favored the circulation of hydrothermal fluids, inducing extensive serpentinization (serpentine >80%) and crystallization of secondary metasomatic phases such as tremolite and diopside. This mineralogical assemblage is typical of active subduction related tectonic settings. The presence of calcic pyroxenes and relics of olivine indicates a complex transformation, with possible local recrystallization or deserpentinization in response to a re-increase of metamorphic conditions.

The extensive serpentinization of peridotites within the Maco oceanic formation hosting Dioudioukounkou garnet granite is a marker of regional metamorphism, probably linked to a subduction context leading to the hydration of peridotite lenses in tectonic contact with the western shear contact CiscoW equal to the Sabodala shear (SSZ) and their transformation into serpentinites. This serpentinization may have played a key role in the development of Sofia and Sabodala non-refractory deposits.

Indeed, geochemical studies by Ngom et al. (2008) on the green rocks of the Mako supergroup confirm a bimodal volcanic heterogeneity, with tholeiitic and calc-alkaline episodes, favorable to the development of complex metallogenic systems. The ultramafic rocks of the Mako supergroup, notably peridotites and pillow basalts (Ngom et al., 2008; Gueye et al., 2008), display characteristics favorable to serpentinization, a hydration process of ferromagnesian minerals. This phenomenon is evidenced by the presence of minerals such as chlorite, epidote, calcite

and actinote in green schist-type metamorphic zones (Bassot, 1987; Dioh, 1986).

Furthermore, Sofia Escario Perez's (Escario Perez, 2018) experimental work on hydrothermal flows in the lithospheric mantle demonstrates that serpentinization of peridotites leads to carbonation and oxidation reactions, generating fluids rich in H_2 and CO_2, capable of transporting and concentrating metals such as Ni, Co, Cr, and sometimes gold.

Furthermore, Dessimoulie (2019), in her thesis on the geochemistry of serpentinization, points out that this process modifies the chemical composition of peridotites and enriches rocks in trace elements and metals, reinforcing the idea that serpentinization can play a key role in the formation of economically exploitable deposits.

The deserpentinization, induced by thermal gradients linked to plutonic intrusions (e.g., Badon Kakadian batholith, Tinkoto and Mamakono massifs), releases fluids rich in H_2, CO_2, and metals (Gueye et al., 2008; Pawlig et al., 2006). These fluids interact with the surrounding rocks, promoting the mobilization and concentration of metals such as Ni, Cr, Co, and potentially gold.

The work done by Guillou, Ndiaye, and Samama (2009) has highlighted the existence of pseudomorphic siliceous vein paleosurfaces in the Saraya region, testifying to ancient hydrothermal systems linked to deep fluid circulations. These structures are interpreted as evidence of crustal-scale fluid-rock interactions, similar to those observed in the Massawa and Sofia deposits.

Diabba serpentinite has a matrix dominated by serpentine (52.7%), accompanied by minerals typical of the upper mantle: olivine, enstatite-ferrosilite, diopside, hedenbergite, amphiboles (tremolite, actinolite, hornblende), chlorite, andradite, chromite, and iron oxides. This assemblage reflects a peridotitic origin, probably linked to an oceanic lithosphere that underwent an intense serpentinization process through the penetration of cold fluids along abyssal fractures. The partial de-serpentinization observed is evidence of progressive burial in a subducted context. This process induces the dehydration of serpentinized phases and the release of fluids enriched in volatile and lithophilic elements (H_2O, CO_2, Ba, Pb, Sr, LREE). These fluids participate in the melting of supra-subducted mantle and the genesis of hydrated arc magmas, characterized by strong oxidation and geochemical anomalies (negative Nb-Ta, LREE enrichment).

These studies are converging towards an integrated understanding of the role of serpentinization/deserpentinization in metallogeny of ancient terrains.

The deserpentinization of the Diabba peridotite lenses (52% serpentine compared to Maco 82% serpentine) in tectonic contact with the shear zone is CiscoE, which in turn would have favoured the dehydration of the peridotites and the transformation of serpentine into olivine. This process, combined with the release of metal-rich hydrothermal fluids (and carbon in this sedimentary back-arc context), channeled along the CiscoE. This deserpentinization would have played an important role in the development of the Massawa refractory deposit associated with graphite. Conversely, serpentinization of the peridotites would have favored

reconcentration of metal-rich fluids (in the context of an oceanic volcanic arc) along the western shear-contact zone CiscoW.

The study of peridotite lenses in tectonic contact with the median shear contact (CiscoM) in the context of the formation of the island arc hosting Koulountou and Tiguida garnet granites and the study of peridotite lenses in tectonic contact with the Faleme shear contact (CiscoF) in the context of intracontinental arc was not carried out in this study, but the setting of the CiscoM and CiscoF is a major advantage for the possibility of reconcentration of mineralizing hydrothermal fluids through serpentinization or deserpentinization of peridotites. In the context of this island arc and intracontinental arc for future searches of potential deposits of useful substances such as gold and related metals, serpentinized peridotites are proposed as rock tracers, and olivine and serpentine as mineral tracers.

Geochemical signature of High K leucogranite from Dalema-Faleme suggests an evolved and a reduced chemical composition of the high-K leucogranite melts derived from a crustal source, while low K intrusions suggest a formation from an oxidized magma and a control of hornblende during magmatic petrogenesis (Faye et al., 2023). A potential Ionized Oxidation-style gold and copper mineralization is possible due to the presumed presence of a rigid lithospheric crustal margin, represented by the Faleme Belt, delineated to the East by the CiscoF and to the West by Eastern Diale-Dalema Sedimentary rocks. The Western edge of this rigid crustal block is marked by the intrusion of the Saraya Batholith, which separates the now highly deformed Diale-Dalema Sediment. The prominent presence of skarn mineralization in the Faleme zone is consistent with the entry of oxidizing fluids during magmatism. Magnetite skarn mineralization can be directly mapped with magnetic data and is characterized by strong remanent magnetizations. A potential for possible kimberlite/lamporite veins has been recognized by a number of distinct strongly magnetic anomalous responses, in magnetically weak sediments and granite in the southeast and in the inferred crustal margin (Fugro Airborne Surveys Interpretation Team, 2000).

6. Geophysical Characterization of Kedougou Kenieba Inlier Formations

To define the various lithostructural units and their implications on the structuring of Kedougou Kenieba Inlier, the lithostructural characterization of Maco, Sesam, and Diabba, a detailed geophysical study was carried out at the scale of the entire Kedougou Kenieba Inlier.

Geophysical data (aeromagnetic and radiometric) used in this study are those acquired by FUGRO on behalf of the Direction of Geology and Mines (DMG) of Senegal and those from Barrick Gold. The lithostructural study consists of characterizing the different lithological and structural facies in the area using geophysical and cartographic methods. The lithostructural characterization in this subchapter mainly concerns the major structures, the large lithostructural units they delimit, and certain large plutonic masses such as, Kakadian, Soukouta, Dioudioukounkou, Koulountou, Tiguida, Tinkoto, Falombo, Bouroumbourou, Saraya, Ga-

maye, and other Faleme massifs... The data collected enable the highlighting of lithostructural contrasts and the redefining of an interpreted lithostructural architecture of Kedougou-Kenieba Inlier.

Aeromagnetic and Radiometric Data

The aeromagnetic, and cartographic results compiled over the entire Kedougou Inlier highlight four zones **(Figures 21(A)-(F))** with distinct magnetic signatures**:** a zone of high magnetic intensity to the West with a fluid texture, an intermediate zone of medium to high magnetic intensity with an anastomosing deformed semi-linear texture, a zone of low to medium intensity marked by a linear texture and a zone (the easternmost) with dual magnetic response: Eastern part has a patchy, semiglobular texture while the western part is homogeneous. These zones are delimited by four major shear-contact: Western shear-contact CiscoW (SSZ = D1), Eastern shear-contact CiscoE (MTZ = D3), Median shear-contact CiscoM (D2) located between CiscoW and CiscoE, and the Faleme structure, which we refer to here as Faleme shear-contact CiscoF (D4). The Faleme Volcanic Zone is quite distinct and is defined by a region of high magnetic intensity. It is bounded to the East by the North-South sinistral shear-contact of the Faleme (CiscoF). Its Eastern margin is bounded by a North-South shear. The CiscoW, CiscoM, CiscoE, and CiscoF delineate four (4) major lithostructural domains (Maco, Sesam, Diabba, and Koffi). These domains are intersected by formations showing strong to weak aeromagnetic expression, clearly demonstrating distinct units or concentric/curvilinear profiles representative of granitoids.

Radiometric anomalies are aligned with the CiscoW, CiscoM, CiscoE, and CiscoF shear zones, indicating active geological structures where radiometric elements have been mobilized by recent fluids or tectonic processes. Significant correlations between radiometric anomalies and deformation zones have been noted, demonstrating that the distribution of U, Th, and P indicates active tectonics and deep subsurface dynamics.

Radiometric and aeromagnetic data covering the entire Kedougou Kenieba Inlier were used to define the granitoid contours of the area. Compilation of radiometric data (Uranium, Thorium, and Potassium distribution maps) with field mapping enabled us to delineate the granitoid contours of the study area. Kakadian, Soukouta, Dioudioukounkou, Tinkoto, Falombo, Saraya, Bouroumbourou, Koulountou, Tiguida, Faleme plutons, and Gamaye were clearly identified by their radioelement concentrations, highlighted by the specification of their respective colors on the various maps.

The Kakandian Batholith forms several granitic to granodioritic plutons, approximately 5 to 30 km in diameter. The literature reports the presence of specific plutons, precisely named and considered independent from the main body, which is the Kakadian Batholith. These plutons include the Sandikounda plutonic complex, the Laminia Kaourou plutonic complex, and the amphibole gneiss complex (Dia et al., 1997). However, geophysical studies do not confirm this segmentation because

the magnetic and radiometric characteristics are too similar to distinguish them from one another. Therefore, in the context of this study, these bodies are considered as a single entity. Figure 22 shows a pluton of the Kakadian Batholith. There are four subdivisions within this granite (grd 5, grd 10, grd 12, and grd 13). The magnetic characteristics are typical, with high intensities and a spotted to sub-linear texture and are identical to those observed throughout the batholith. The latter also shows a strong signature specific to potassium (appearing in red in the ternary radiometric image), making it easy to identify. The locally concentric orientation lines deviate around the intrusion bodies. The composite intrusion suite that includes the Kakadian Batholith is represented by a large high-intensity domain with a corresponding high pseudo-gravity value. High-frequency anomalies and concentric orientation lines correlate with late to post-tectonic granitic bodies. The East-west-oriented zone of high magnetic intensity intersecting the figure is interpreted as a late mafic dyke on the right (Fugro Airborne Surveys Interpretation Team, 2000).

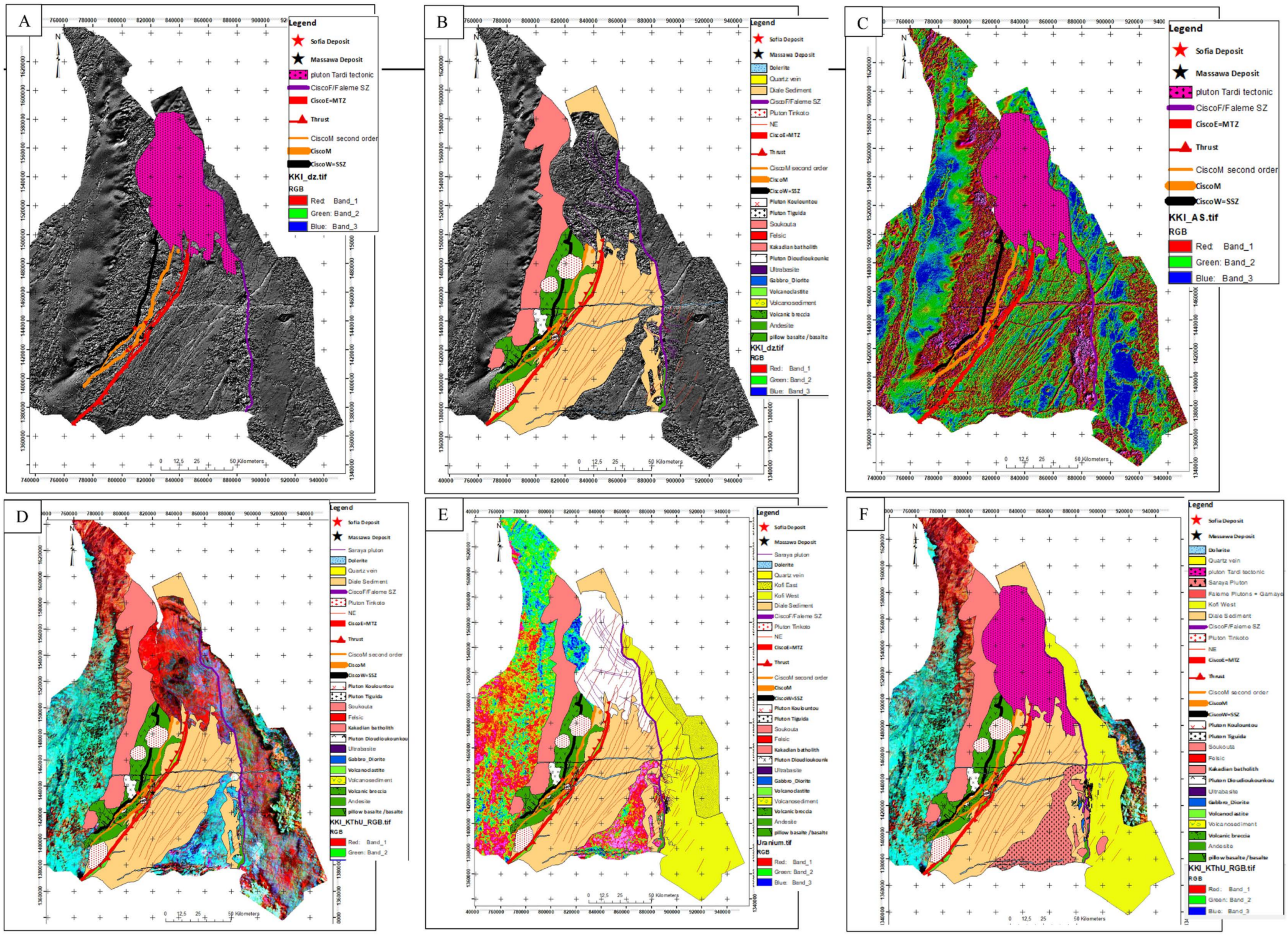

Figure 21. Electromagnetic and radiometric data covering the entire Kedougou Kenieba Inlier; A, B: Magnetic intensity map (grey-scale 1DV) showing the major structures of the Kedougou Kenieba Inlier (1DV = First vertical derivative of total magnetic intensity—IMT—of low latitude reduced to the pole (BLRAP) in grey scale) and analytical magnetic signal showing the structures and lithological limits. D, F: Radiometric maps of variations in the spatial distribution of the gradient of triptic concentrations of uranium, thorium, and potassium, where red, blue, and green represent high, moderate, and low values, respectively; E: Radiometric map of variations in the spatial distribution of the uranium concentration gradient.

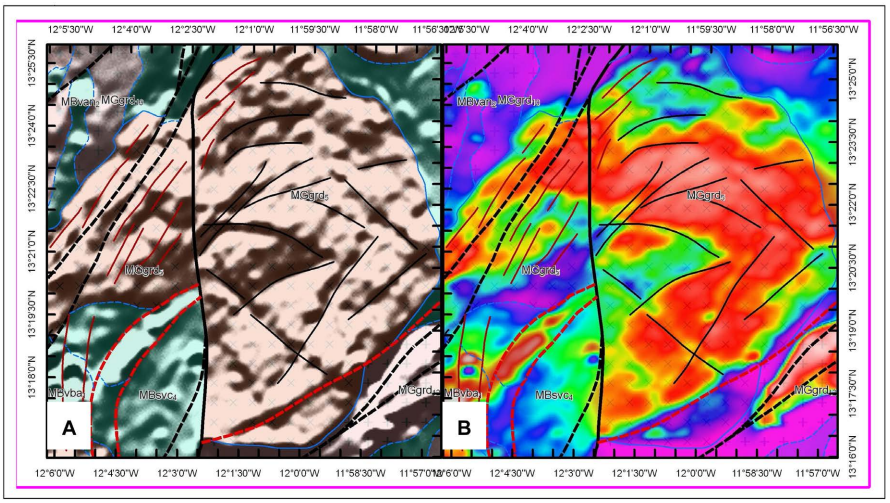

Figure 22. Example of a granitic pluton in the Kakadian Batholith; four subdivisions have been de-fined in the granite (grd 5, grd 10, grd 12, and grd 13) in the Fugro Airborne Surveys Interpretation Team Technical Report Airborne Geophysical Project 9ACP/SE/009. A) Image from the 1DV BLRAP. B) Image from the BLRAP IMT; particularly high magnetic intensity compared to the surrounding volcanic rocks (svc4 vba1).

The Uranium distribution map shows the well-defined contours of the plutonic masses in the study area. Uranium concentration in the Dioudioukounkou pluton is highly heterogeneous, reflecting the diversity of facies within the Dioudioukounkou pluton. Uranium levels are highest in the southeastern and northwestern parts of the pluton, while the rest of the district has low to medium concentrations. Tinkoto massif also has high Uranium concentrations evenly distributed over the pluton, with the exception of the South-western part, where concentrations are medium to poorly distributed. Koulountou shows moderately high uranium levels throughout the massif, with the exception of the Northern and South-eastern parts. The Tiguida massif has low uranium concentrations. The Saraya batholith is characterized by high to medium Uranium grades, with low to medium grades in the northern and southern parts. The lowest contents are found in the North-eastern part. The distribution of Thorium concentration of Dioudioukounkou massif shows that the highest pourcentages are concentrated in the North-western part and moderately in the South-eastern part. In contrast, the Tinkoto massif shows average to low Thorium concentrations. Thorium contents are low in the Koulountou and Tiguida massifs. Thorium grades in the Saraya granite are high in the South-western part and low in the North-eastern part. For the Potassium concentrations distribution (**Figure 23**), the highest grades are found in the southern part of the Koulountou massif, in the northeastern part of the Tiguida massif, in the southeastern part of the Tinkoto pluton, and in the central western part of Dioudioukounkou. The radioelement distribution map shows that the Tiguida massif contains higher concentrations of Potassium than Uranium and Thorium. The batholith shows very low magnetic intensity, with a flat texture that is difficult to distinguish. However, the radiometric image clearly highlights

the Saraya batholith, which is distinguished by its high potassium content.

Saraya Batholith shows a weak magnetic response, making the geometric boundaries ambiguous, which has been clarified using radiometric data. Saraya has high potassium content in the northeast and relatively low levels in the rest of the masif. The meta-sediments to the East of the Saraya Batholith appear less penetrative and host a number of elongated granitic plutons associated with the Saraya Batholith Complex. North-northeast and Northeast-trending shear zones are notable in this part. The meta-sediments located at the West of the Saraya Batholith are highly deformed. The Gamaye massif shows low potassium content. Faloumbo and Bouroumbourou plutons show curviligne magnetic response entirely within Maco for Falombo, showing a homogeneous potassic, pink leucogranite at the west of Sabodala deposit, and between Maco and Sesam for Bouroumbourou, showing an older phase comprising a group of biotite granite suites at the North-east of the deposit (Figure 23).

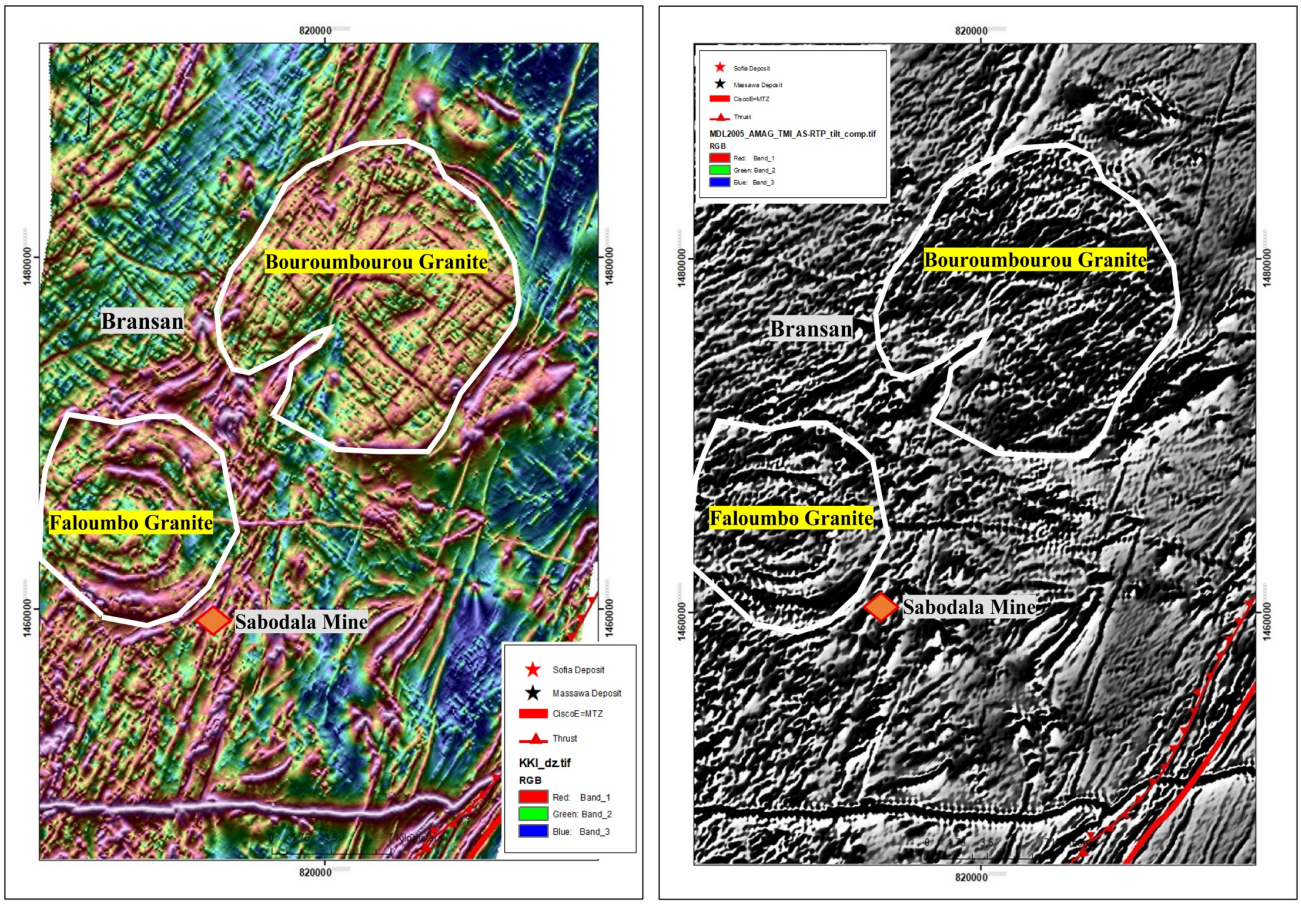

Figure 23. Total magnetic intensity map showing geometric contours of Faloumbo and Bouroumbourou plutons onto aeromagnetic images of Sabodala and Bransa zones.

These intrusive plutons are associated with mafic and felsic sills and dykes.

Aeromagnetic, radiometric, cartographic, geochemical, geochronological, and petrographic studies show that the Kedougou Kenieba Inlier is marked by

the presence of four (4) regional structures: the Western shear-contact (CiscoW = SSZ = D1), the Eastern shear-contact (CiscoE = MTZ = D3), the median shear-contact (CiscoM = D2) located between CiscoW and CiscoE, and the Faleme shear-contact (CiscoF = D4). These structures delimit four major lithostructural domains evolving into tectonomagmatic complexes: Maco oceanic crust, Sesam arc, Diale back arc basin, and Koffi, intersected by facies grouping small massifs and large plutonic masses. Small massifs are made up of gabbros, diorites, and acid intrusives. They are distributed along three directions, NE and NNE to NS. The large plutonic masses are mainly represented by Kakadian, Soukouta, Bouroumbourou, Dioudioukounkou, Koulountou, Tinkoto, Tiguida, Saraya, Boboti, Gamaye massifs...and the tardi tectonic granite on top of Kedougou Kenieba inlier.

7. LA-ICP-MS Zircon Geochronology

Zircon U-Pb dating was carried out on three (3) magmatic rock samples (Ech.): Ech.66, Ech.85, and Ech98. When observed under cathodoluminescence, most of the zircons showed oscillatory and sector zoning typical of igneous origins. The zircons are euhedral to subhedral and colorless. Representative SEM-CL images of each rock are presented in Figure 24. The Concordia ages were calculated using the program IsoplotR. All errors are reported at $_{1\sigma}$ (sigma).

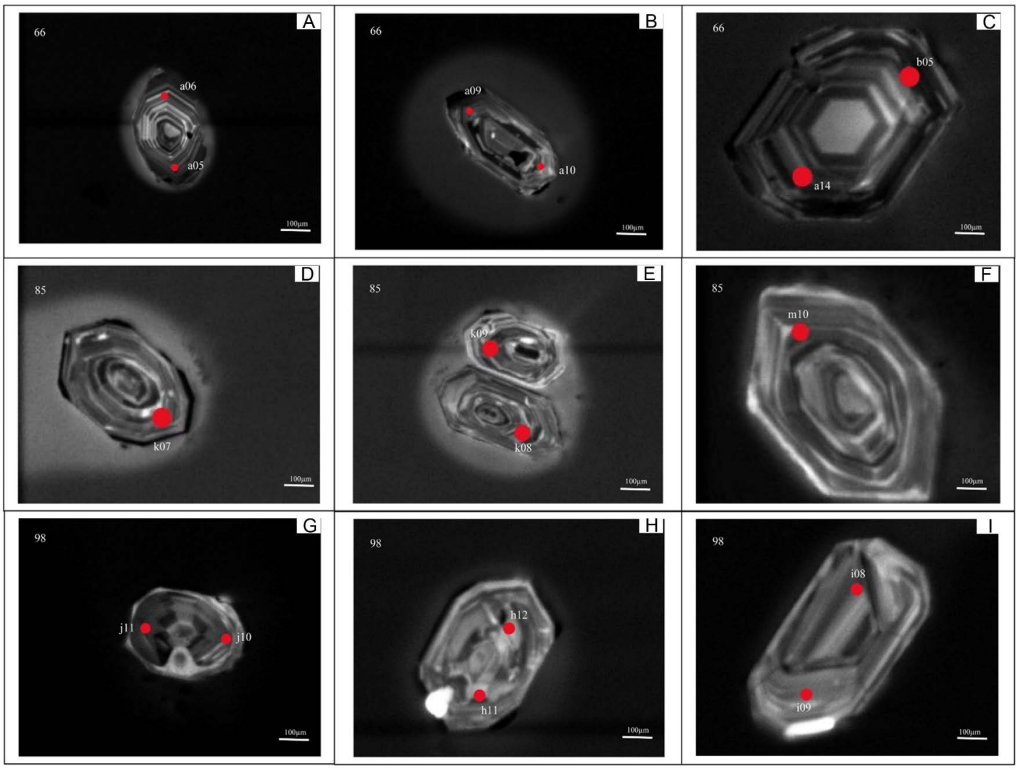

Figure 24. Representative cathodoluminescence images with analytical points in red circle. A, B, C: Sample 66 (ech.66) from Dioudioukounkou granite; D, E, F: Sample 85 (ech.85) from Tinkoto pluton; G, H, I: Sample 98 (ech.98) from Koulountou pluton.

7.1. Dioudiounkounkou Pluton

Zircons from the Dioudioukounkou (Ech.66.) granite (Figure 24) are mainly subhedral and vary in size (<150 µm). Magmatic growth zoning is well developed in most of the grains. A total of 33 zircon grains were analyzed, resulting in a total of 44 spots. Thirty-three analyses were plotted on a concordia diagram. Most of the data are discordant, with just a few on the concordance line. The discordant data are interpreted to be caused by recent Pb-loss. A regression line fitted to the concordant and discordant spots intersects the isochron at 2156.1 Ma ± 5.6 Ma (MSWD = 1.3), with a lower intercept around the origin (Figure 25(A)). This corresponds well with a weighted mean 207Pb/206Pb of 31 most concordant points of 2154.6 Ma ± 7.6 Ma (MSWD = 0.67) (Figure 25(B)). The upper discordia intercept of 2156.1 Ma ± 5.4 Ma is interpreted to represent the age of magmatic emplacement.

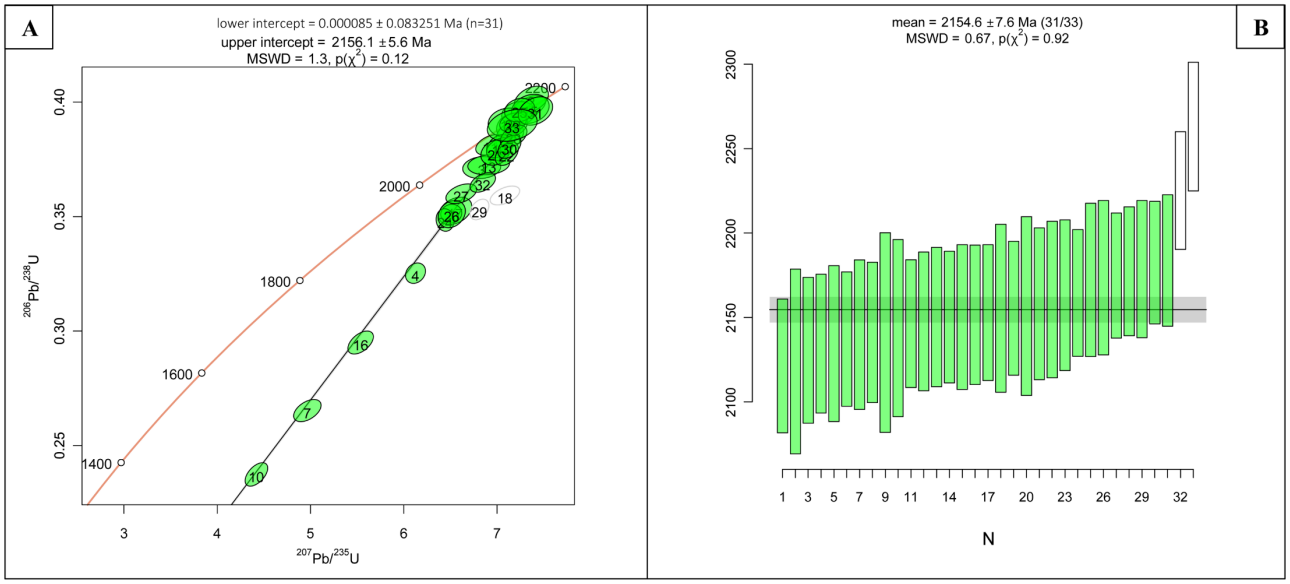

Figure 25. Geochronological diagrams of Dioudioukounkou granite (Ech.66). A: Concordia diagram showing discordia; B: The weighted mean $^{207}Pb/^{206}Pb$ age.

7.2. Tinkoto Pluton

Forty-two (42) spot analyses were made on thirty-eight (38) prismatic zircon grains of Tinkoto granite (Ech.85). SEM-CL imaging shows zonation in all zircon grains. Forty (40) analyses were plotted on a concordia diagram. A significant number of analyzed spots are discordant. This is interpreted to be caused by recent Pb-loss. A discordia line was fitted to a subset of 36 spots with an upper intercept of 2109.3 Ma ± 6.0 Ma (MSWD = 1.7) and a lower intercept at 159 Ma ± 110 Ma (Figure 26(A)). A weighted mean $^{207}Pb/^{206}Pb$ age of 2107 Ma ± 6.9 (MSWD = 1.2) (Figure 26(B)) corresponds well to the upper intercept age. The age of magmatic emplacement is best represented by the upper intercept of the discordia, with an age of 2109.3 Ma ± 60 Ma.

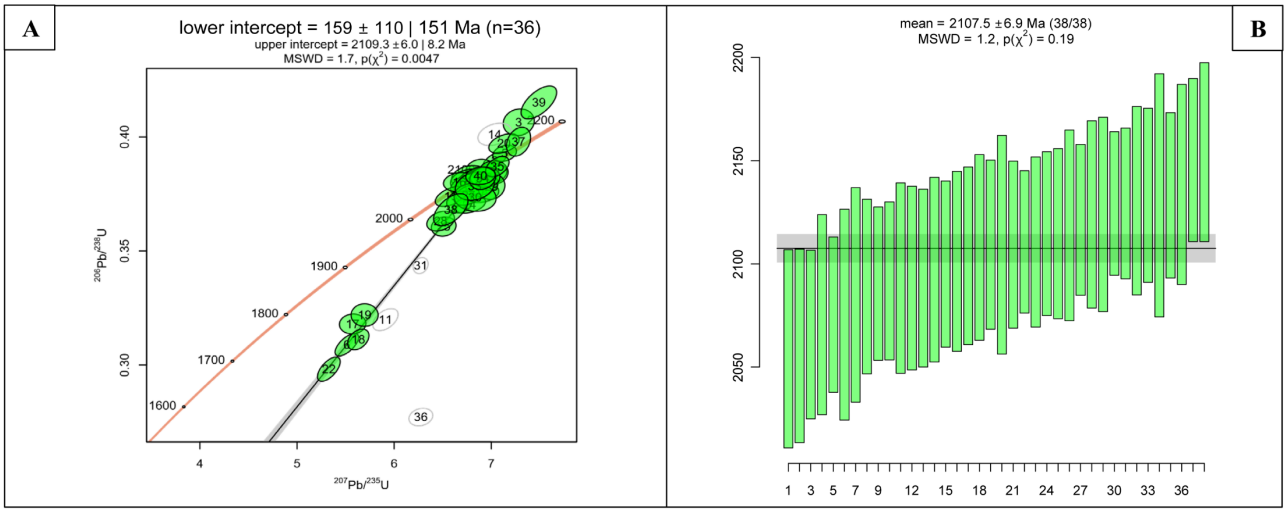

Figure 26. Geochronological diagrams of Tinkoto granite (Ech.85). A: Concordia diagram showing discordia plots; B: The weighted mean 207Pb/206Pb age.

7.3. Koulountou Pluton

Separated zircons from the Koulountou (Ech.98) granite have an appearance varying from prismatic to euhedral grains, with simple growth zoning and complex growth structures. Some euhedral grains contain cores. Thirty-four (34) spot analyses were made on fifteen (15) grains. Some of the spots are discordant. The discordia model yielded an upper intercept of 2106.7 ± 8.1 (MSWD = 1.4; n = 22) and a lower intercept around 13 Ma (**Figure 27(A)**). This age corresponds well to the weighted mean $^{207}Pb/^{206}Pb$ age of 2103.3 Ma ± 9.7 Ma (MSWD = 0.87) (**Figure 27(B)**). No evidence of inheritance in analyzed data.

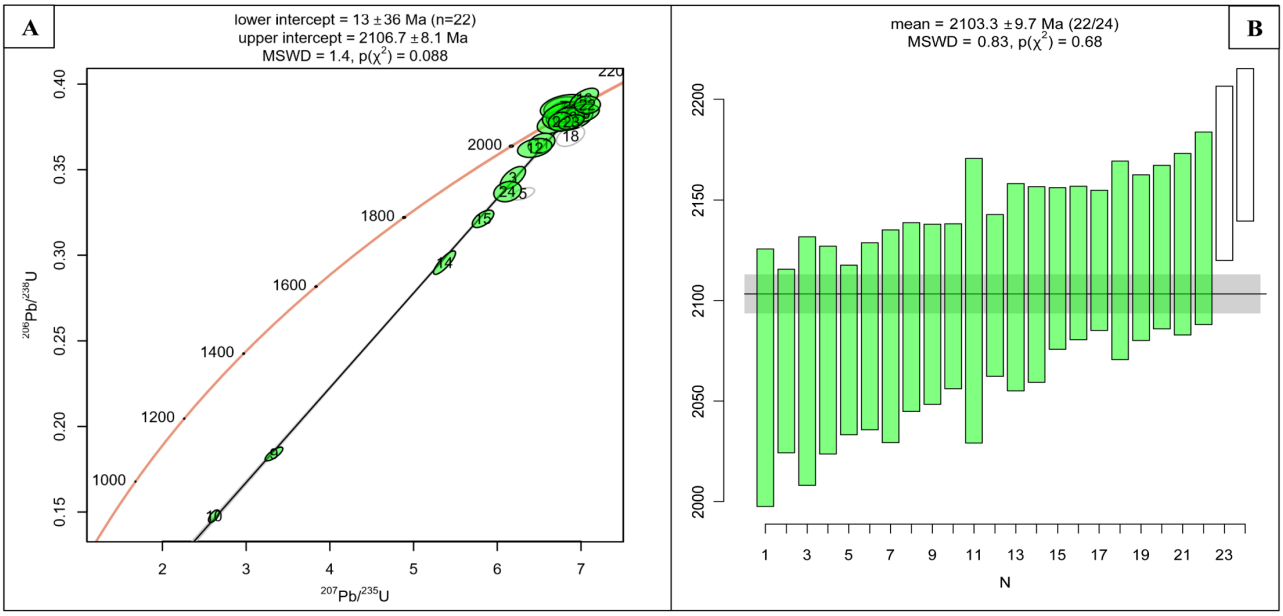

Figure 27. Geochronological diagrams of Koulountou granite (Ech.98). A: Concordia diagram showing discordia plots; B: The weighted mean $^{207}Pb/^{206}Pb$ age.

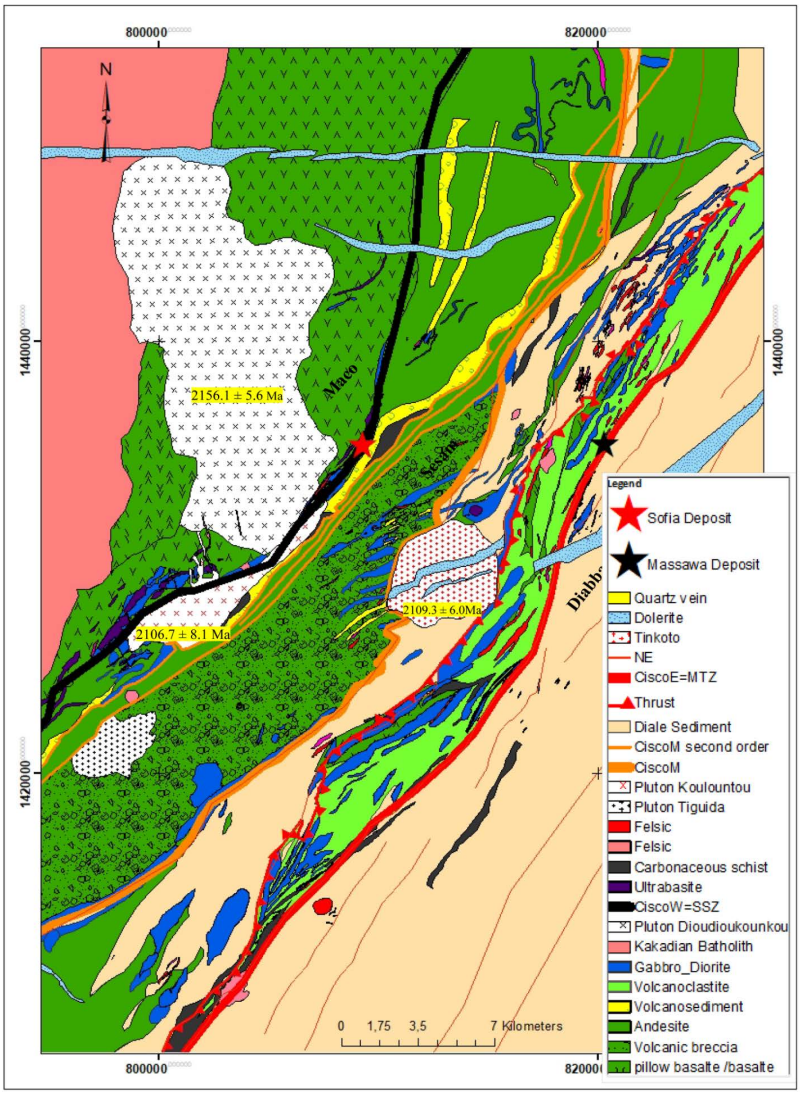

Figure 28. Lithostructural map of Mako-Diale transition zone (Ndiaye et al., 2025) showing radiochronologic data (ages) of plutonic masses within Maco, Sesam, and Diabba. This map also highlights relationships between magmatism and tectonic (especially plutonic masses and major structures). Dioudioukounkou pluton is older and is associated with CiscoW. It is followed by the Tinkoto pluton related to CiscoM main shear. Koulountou is syntectonic to Tinkoto and is related to CiscoM's second-order structures. Maco domain located to the West of the western Shear-contact occidental (CiscoW); Sesam domain limited to the West by CiscoW and to the East by Shear-contact oriental CiscoE; Diabba domain, located to the West of median Shear-contact (CiscoM). Volcanosediments in this map represent andesitic (explosive volcanic) deposited material with facies ranging from coarse to fine (ash) lithic elements.

Geochronological results reveal that the Dioudioukounkou granite yielded a concordant U-Pb zircon age of 2156.1 Ma ± 5.6 Ma. This seems to correspond to the major magmatic activity phase of the Eburnean orogeny and is associated with the early Eburnean deformation CiscoW (SSZ = D1). Tinkoto and Koulountou plutons were emplaced at 2109.3 Ma ± 6.0 Ma and 2106.7 Ma ± 8.1 Ma, respectively. They intruded Sesam and Diabba at the early transpressive tectonic Ebur-

nean deformation phase CiscoM (D_2). Tinkoto pluton predate and is related to CiscoM main shear, while late Koulountou granite is related to CiscoM second-order structures. Plutonic masses from Maco, Sesam, and Diabba were formed predominantly during the Eburnean orogeny, with ages ranging between 2156 Ma and 2106 Ma (Figure 28). This period marks a critical phase of crustal growth and intensive magmatic activity.

8. Discussions

8.1. Geochronological Framework of Kedougou Kenieba Inlier Formations

Geochronological data of Kedougou Kenieba Inlier (integrating new results from this study) formations, according to their position within the tectonomagmatic complexes, are defined in Table 2 and within Figure 29.

Table 2. Geochronological data of Kedougou Kenieba Inlier formations. Data from Gueye et al. (2007); Cissokho (2010), Lambert-Smith et al. (2016) and Ndiaye et al. (2025) or this study. (RT): Total Rock; (Zr): Zircon; (Hb): Hornblende; (Biot): Biotite; (Mo): Monazite.

Series	Tectonomagmatic complexes	Lithologies	Age (Ga)	Methodes	References
Mako	Undefined by this study	Tholeitic Basalt	2063 ± 41	Sm/Nd (RT)	Abouchami et al. (1990)
			2187 ± 13	Sm/Nd (RT)	Dia et al. (1997)
			2195 ± 11	Pb/Pb (RT)	Dia et al. (1997)
		Andesite	2160 ± 16	Sm/Nd (RT)	Boher et al. (1992)
		Medina Foulde Pluton	2138 ± 6	Pb/Pb (Zr)	Dia et al. (1997)
	Maco	Plutonic Layered Complex	2158 ± 8	Pb/Pb (Zr)	Dia et al. (1997)
		Kaourou Pluton	2079 ± 6	Pb/Pb (Zr)	Dia et al. (1997)
		Tonalitic Gneiss of Sandikounda	2194 ± 9	Pb/Pb (Zr)	Gueye et al. (2007)
			2112 ± 12	Ar/Ar (Hb)	Gueye et al. (2007)
			2118 ± 31	K/Ar (Hb)	Gueye et al. (2007)
			2202 ± 6	Pb/Pb (Zr)	Dia et al. (1997)
		Sandikounda Dioritic Gneiss	2205 ± 15	U/Pb (Zr)	Gueye et al. (2007)
		Mamakono Pluton	2067 ± 12	Pb/Pb (Zr)	Gueye et al. (2007)
			2076 ± 3	Pb/Pb (Zr)	Hirdes & Davis (2002)
		Kakadian Batholith	2199 ± 68	Rb/Sr (RT)	Bassot & Caen-Vachette (1984)
		Badon Granodiorite	2198 ± 2	Pb/Pb (Zr)	Gueye et al. (2007)
			2213 ± 3	Pb/Pb (Zr)	Gueye et al. (2007)
			2098 ± 26	Ar/Ar (Biot)	Gueye et al. (2007)
			2090 ± 21	K/Ar (Biot)	Gueye et al. (2007)
		Dioudioukounkou Pluton	2156.1 ± 5.6	U/Pb (Zr)	Ndiaye et al. (2025) or this study
	Sesam	Koulountou Pluton	2106.7 ± 8.1	U/Pb (Zr)	Ndiaye et al. (2025) or this study

Continued

Diale-Dalema	Diabba	Tinkoto Pluton	2074 ± 5	Pb/Pb (Zr)	Gueye et al. (2007)
		Tinkoto Pluton	2109.3 ± 6.0	U/Pb (Zr)	Ndiaye et al. (2025) or this study
		Sediment	2096 ± 8	Pb/Pb (Zr)	Hirdes and Davis (2002)
		Saraya Batholith	2008 ± 35	Rb/Sr (RT)	Bassot & Caen-Vachette (1984)
			1973 ± 33	Rb/Sr (RT)	Bassot & Caen-Vachette (1984)
			2008 ± 16	Rb/Sr (RT)	Ndiaye et al. (1997)
			2079 ± 2	U/Pb (Zr)	Hirdes & Davis (2002)
			2064 ± 4	U/Pb (Mo)	Hirdes & Davis (2002)
	Faleme	Andesite	2070 ± 10	Pb/Pb (Zr)	Milesi et al. (1989)
			2072 ± 9	Pb/Pb (Zr)	Calvez et al. (1990)
		Balangouma Pluton	2118 ± 16	U/Pb (Zr)	Lambert-Smith et al. (2016)
			2105 ± 9.8	U/Pb (Zr)	Lambert-Smith et al. (2016)
		Boboti Granodiorite	1989 ± 28	Rb/Sr (RT)	Bassot & Caen-Vachette (1984)
			2080 ± 0.9	U/Pb (Zr)	Hirdes & Davis (2002)
			2008 ± 16	Rb/Sr (RT	Ndiaye et al. (1997)
			2088 ± 8	U/Pb (Zr)	Lambert-Smith et al. (2016)
		Rhyolite from South of Faleme River	2082 ± 1	U/Pb (Zr)	Hirdes & Davis (2002)
			2099 ± 4	U/Pb (Zr)	Hirdes & Davis (2002)
Kofi	Kofi	Sediment	2093 ± 7	Pb/Pb (Zr)	Boher et al. (1992)
			2125 ± 27	Pb/Pb (Zr)	Boher et al. (1992)
		Gamaye Granite	2045 ± 27	Rb/Sr (RT)	Bassot & Caen-Vachette (1984)

The Mako volcanic belt and the Sandikounda amphibolite-gneiss complex (SAG) were intersected by the Sandikounda Layered Plutonic Complex (SLPC) 2158 Ma ± 8 Ma ago (Dia et al., 1997). This intrusion was followed by those of the Dioudioukounkou granite at 2156.1 Ma ± 5.6 Ma and Soukouta granite at 2142 Ma ± 7 Ma (Lambert-Smith et al., 2016).

The Laminia Kaourou Complex (LKC) is thought to have been formed between 2138 Ma ± 6 Ma and 2105 Ma ± 8 Ma (Dia et al., 1997). The SAG cooled below 550˚C at 2112 Ma ± 12 Ma. The intrusion of the SLPC and LKC led to the migmatization of the SAG and Badon pluton (Gueye et al., 2008). The SAG protolith represents the initial stage of Paleoproterozoic crustal growth in the region (Dia et al., 1997). The SAG and Badon pluton represent early magmatism in the KKI and predate the major D2 deformation phase (Gueye et al., 2008).

The D1 phase is synchronous with the intrusion of large Tonalite-Trondhjemite-Granodiorite (TTG) batholiths within the Mako belt (Gueye et al., 2008; Diene et al., 2012). Conversely, Ledru et al. (1991) proposed that the D1 phase only affected

the metasedimentary rocks of the Diale-Dalema series. The D1 phase, dated between 2200 and 2120 Ma (Lompo, 2010; Feybesse et al., 1990), corresponds to intense crustal accretion linked to the emplacement of the Birimian magmatic units. Large quantities of magma were transferred through the crust during this deformation phase, which corresponds to a period of crustal thickening (Gueye et al., 2008). Dioudioukounkou granite intruded Maco and yielded a concordant U-Pb zircon age of 2156.1 Ma ± 5.6 Ma. This seems to correspond to the major magmatic activity phase of the Eburnean orogeny and is associated with the early Eburnean deformation D1, corresponding in this area of study to CiscoW or SSZ.

The D2 phase, around 2130 to 2100 Ma, marks a transition to an extensional regime in a subduction context, with the opening of a back-arc basin behind the active magmatic arc (Milesi et al., 1992; Hirdes et al., 1992). This extension is linked to the dynamics of the subducting plate and promotes the formation of volcanics and sedimentary sequences in a distensive environment. The D2 phase is characterized by large N-S strike-slip faults and shear zones (Diene et al., 2012; Masurel et al., 2017) and marks a change in tectonic style from collisional to transcurrent deformation (Dabo & Aifa, 2010; Diene et al., 2012). In the field of study, the D2 phase corresponds to CiscoM and is a ductile then brittle shear zone with a schistosity showing two main directions, North-south and North-east, with fairly steep dips. It consists of a main structure associated with other second-order structures. The main structure has two branches: the main branch to the North of the study area is oriented N010 to N0180 and dips 56˚C to 85˚C. The northeast branch is located to the South, trending N044 to N080 and dipping between 63˚C and 90˚C (Ndiaye et al., 2025). The Tinkoto and Koulountou plutons were emplaced at 2109.3 Ma ± 6.0 Ma and 2106.7 Ma ± 8.1 Ma, respectively. They intruded Sesam and Diabba during the early transpressive tectonic Eburnean deformation phase CiscoM (D2). The Tinkoto pluton predates and is related to the CiscoM main shear, while the Koulountou granite is related to CiscoM North-east second-order structures located to the West of the Main shear and within the Sesam complex (**Figure 29**). The Laminia Kaourou Complex, the Tinkoto and Koulountou plutons represent the syntectonic plutonic group.

Phase D3, between 2100 and 2070 Ma, corresponds to a continental collision with crustal thickening, the development of tangential structures, and regional metamorphism (Pons et al., 1995). In the study area, phase D3 corresponds to CiscoE, representing the MTZ. The D3 phase is characterized by the reactivation of early structures and the activation of ductile brittle North-South to North East-South West trending sinistral shear zones accommodating NNW-SSE horizontal shortening (Diene et al., 2012; Lawrence et al., 2013; Dabo et al., 2017; Masurel et al., 2017). The calc-alkaline Mamakono pluton invaded the Mako volcanic belt 2076 ± 3 Ma ago (Hirdes and Davis, 2002). This small circular intrusion represents the late phase of Eburnean magmatism associated with a dextral transtensional deformation D3. The late Saraya batholith intruded the Diabba sedimentary basin at 2079 Ma ± 2 Ma (monazite) according to Hirdes and Davis (2002).

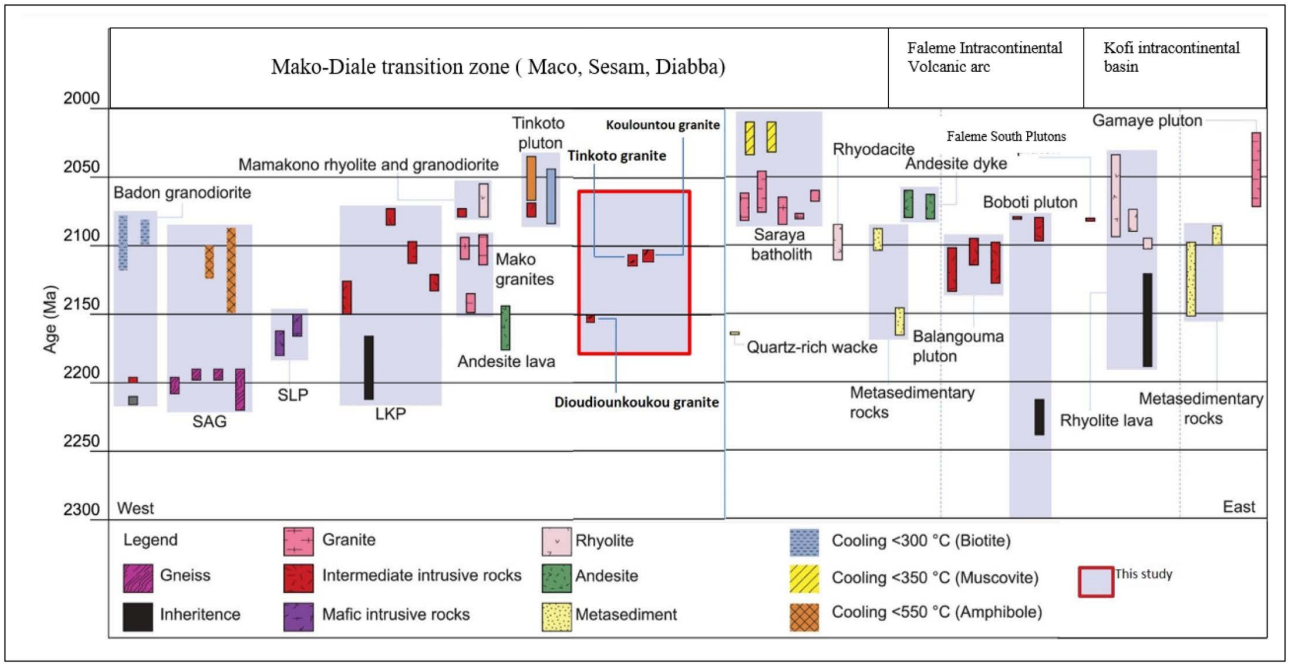

Figure 29. Summary diagram of published age data for the KKI. SAG: Sandikounda amphibolite-gneiss complex. SLP: Sandikounda Layered Plutonic. LKC: Laminia Kaourou Complex. The new age data from this study are shown in the red box, modified from Lambert-Smith et al. (2016).

Finally, phase D4 (standing in this study as CiscoF), between 2050 and 2030 Ma, reflects intracontinental tectonic reactivation, marked by the formation of post-orogenic sedimentary basins and late gold mineralization (Baratoux et al., 2011; Billa et al., 1999). The Gamaye pluton is dated to 2045 Ma ± 27 Ma (Bassot & Caen-Vachette, 1984) and is related to Phase D4.

Plutonic masses from Maco, Sesam, and Diabba were formed predominantly during the Eburnean orogeny, with ages ranging between 2156 Ma and 2106 Ma. Based on geochronological data, we can establish that the granitoid suites of the Kedougou Kenieba Inlier were formed between approximately 2160 Ma and 2040 Ma.

8.2. The Latest Lithostratigraphic Architecture of Kedougou Kenieba Inlier

The geological formations of the Kedougou Kenieba inlier are characterized by alternating volcano-plutonic, volcano-sedimentary, and sedimentary rocks, intruded by different generations of granitoids. Results from this study show that the lithostructural architecture of Kedougou-Kenieba Inlier is formed by succession of lithostructural domains evolving to tectonomagmatic complexes heavily affected by tectonic (and magmatic) events, notably the Eburnean orogeny. The Eburnean orogeny is characterized by a complex tectonomagmatic evolution (Ledru et al., 1989; Ledru et al., 1991; Milesi et al., 1992; Feybesse & Milesi, 1994; Pons et al., 1995; Dabo & Aïfa, 2010; Lompo, 2010; Vidal et al., 2010).

Apart from the undefined complex setting at the West of Maco in **Table 2**, Paleoproterozoic Birimian terrains of the Kedougou-Kenieba Inlier reveal tectonomag-

matic complexes characterized by signatures reflecting a succession of tectonovolcanic arcs and sedimentary basins. The tectonovolcanic arcs are represented by strong magnetic signatures zones corresponding from West to East, to tectonovolcanic arc within oceanic volcanic arc context associated to CiscoW (SSZ = D1), the tectonovolcanic arc within Island arc context associated to CiscoM (D2), the tectonovolcanic arc within Back-arc basin context associated to CiscoE (MTZ = D3), and the Faleme tectonovolcanic arc within intra-continental volcanic arc context associated to CiscoF (= D4). Basins defined within low to medium magnetic zones are mainly represented by the Diale back-arc basin (Diabba) and the Kofi intra-continental basin. The latest architecture of Kedougou Kenieba inlier is described as follows (**Figure 30**):

8.2.1. The Tectonovolcanic Arc Within Oceanic Volcanic Arc Context (Main Arc)

This tectonovolcanic arc (**Figure 30**) is bounded to the East by the CiscoW. The formations of this arc belong to the Maco tectonomagmatic complex, which is characterised by orogenic to late to post-orogenic mafic magmatic rocks, mainly calc-alkaline basalts of the compressed active margin type with volcanic arc affinity, gabbros and tholeiitic diorites, calc-alkaline diorites and the granites of Dioudioukounkou, Badon-Kakadian, Soukouta and Falombo. The high-intensity magnetic signature of the Maco tectonomagmatic complex includes a fluid texture (mainly correlated with weakly metamorphosed calc-alkaline basalts) and locally concentric or curvilinear lines that have a high magnetic intensity, defining late to post-tectonic granitic bodies.

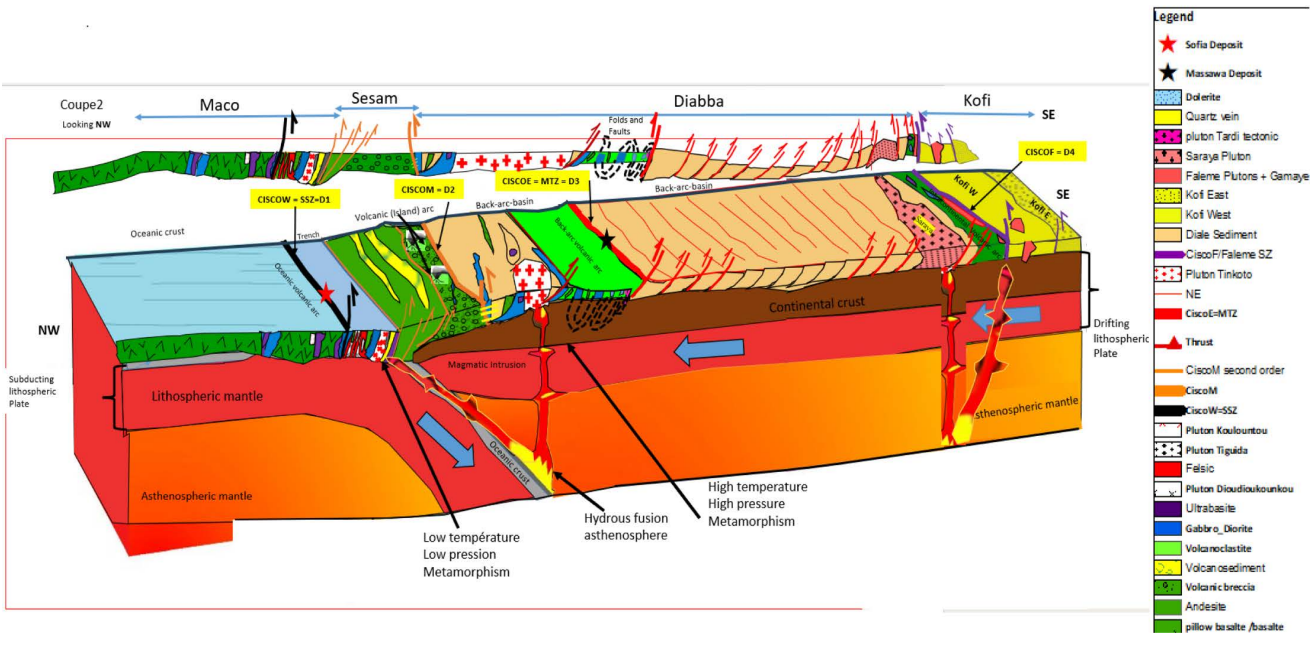

Figure 30. 3D model and 2D section of tectonomagmatic complexes of Kedougou Kenieba Inlier.

The Maco formations show three (3) geotectonic fields associated with different

geodynamic environments: an ocean ridge and floor environment, a volcanic arc granitoid (VAG) zone, and an orogenic zone.

The ocean ridge and floor zone is marked by a compressive active margin environment associated with calc-alkaline volcanic arc basalts. These calc-alkaline basalts (Ech.70) with an alkaline content ($Na_2O + K_2O$) of 5.54 are marked by a slight enrichment in light rare earth elements (∑REE = 81.9%) and a LaN/SmN ratio of 2.79.

The orogenic zone is marked by a compressive active margin environment associated with volcanic arc basalts. This orogenic zone is represented by calc-alkaline basalts (Ech.89) associated with a volcanic arc environment, associated with the CiscoW contact shear zone constituting the eastern limit of the Maco domain. These formations show a LaN/SmN ratio below the detection limit, with low enrichment in light rare earths and an alkaline content ($Na_2O + K_2O$) of 5.1%.

The volcanic arc granitoid zones are marked by three geodynamic environments associated with basic to intermediate plutonic formations: a pre-plateau collision zone, an active margin fractionates mantle zone, and an intra-continental fractionates mantle zone.

The pre-plate collision zone is marked by a compressive to distensive intra-continental environment associated with tholeiitic gabbros; the active margin fractionates mantle zone is characterized by a compressive active margin environment associated with tholeiitic diorites.

The intra-continental fractionates mantle zone is marked by a compressive to distensive intra-continental environment associated with calc-alkaline diorites.

8.2.2. The Tectonovolcanic Arc Within Island Arc Context

It is bounded to the East by the CiscoM (**Figure 30**). The formations this arc belong to Sesam tectonomagmatic complex marked by basic to intermediate orogenic, syncollisional to post-collisional uplift volcanism, essentially marked by tholeiitic andesitic basalts, tholeiitic and calc-alkaline andesites, and tholeiitic and calc-alkaline volcanosediments. Sesam's high-intensity magnetic signature is mainly marked toward the South-east and shows a locally disconformed semi-linear orientation, broad and mainly correlated with tholeiitic andesitic basalts, weakly metamorphosed tholeiitic and calc-alkaline andesites. Northeast-trending curvi-linear lines show high magnetic intensity defining syn to post-tectonic granitic bodies (syn-collisional Tiguida granite, Bouroumbourou, Koulountou active margin plutonic episodes: the first represented by calc-alkaline granodiorites and the second by post-collisional Koulountou granite...). The Sesam formations are associated with six (6) geotectonic fields associated with geodynamic environments: ocean ridge and floor, spreading center of island, orogenic zone, fractionated mantle, syn-collisional and post-collisional uplift environment.

The Ocean Ridge and floor zone is marked by a compressive active margin geodynamic environment associated with tholeiitic andesitic basalts with MORBs affinity (Ech.18) with a LaN/SmN ratio below the detection limit, indicating low

enrichment in light rare earths. This area is also marked by a compressive active margin geodynamic environment associated with calc-alkaline volcanosediments (Ech.15) with andesitic lithic elements showing an affinity with island arc lavas.

The Spreading center of island zone is marked by a compressive to distensive intra-continental geodynamic environment associated with tholeiitic andesites showing an affinity with within-plate lavas. This domain is also marked by a compressive active margin geodynamic environment associated with tholeiitic volcanosediments (Ech.3) showing affinity with island arc lavas.

The orogenic zone is marked by a geodynamic environment of island arc lavas associated with calc-alkaline andesites (Ech.21). These andesites are marked by a LaN/SmN ratio below the detection limit, indicating low enrichment in light rare earths.

The island arc granitoid zones are marked by three geodynamic environments associated with intermediate to acidic plutonic formations: the Fractionates mantle zone is marked by a compressive to distensive intracontinental environment associated with calc-alkaline Koulountou granodiorites (Ech.92) showing a "VAG + Syn COLG" affinity; the Syn-collisional granite environment marked by the Tiguida calc-alkaline granite (Ech.59) of the active compressive margin showing a VAG + Syn COLG affinity; and he post-collision uplift environment is marked by the calc-alkaline granite of the active compressive margin associated with the Koulountou granite (Ech.97) showing an affinity with the geodynamic pointriple VAG + Syn COLG - WPG - ORG environment.

8.2.3. The Tectonovolcanic Arc Within Back-Arc Basin Context

This tectonovolcanic arc (**Figure 30**) is delineated to the East by the CiscoE. The formations of this arc belong to the Diabba tectonomagmatic complex, which is marked by a magnetic signature represented by a distinct, narrow, and continuous linear trend along the main shear zone. Lithologies are represented by volcanoclastites, mainly ranging from coarse facies to volcaniclastic ash facies.

The Diabba formations are divided into four (4) geotectonic fields associated with different geodynamic environments: the continental zone, the ocean island zone, the orogenic zone, and the pre-plate collision zone.

The continental zone is marked by a compressive geodynamic environment of active margins associated with tholeiitic basalts with an affinity for within-plate lavas. The rare earth content (∑REE) of these spinifex basalts from Diabba (Ech.375) is 122.4 ppm. These rocks show high fractionation rates with a LaN/YbN ratio of 11.9. They are enriched in light rare earths, with a LaN/SmN ratio of 3.

The Ocean Island area is marked by a compressive active margin geodynamic environment associated with tholeiitic andesitic basalts showing an affinity for MORBs. The rare earth content (∑REE) of the andesitic basalts is 34.2 ppm. These rocks show low fractionation rates with a LaN/YbN ratio below the detection limit. Rare earth enrichment is low, with the LaN/SmN ratio below the detection limit.

The orogenic zone is marked by a compressive active margin geodynamic en-

vironment associated with calc-alkaline andesites showing an affinity with island arc lavas, and calc-alkaline dacites showing an affinity with island arc lavas.

The Pre-plate collision zone is characterized by a compressive active margin environment associated with VAG-Syncollisional granitoids.

8.2.4. The Tectonovolcanic Arc Within Intra-Continental Volcanic Arc Context (Secondary or Collusional Arc)

The tectonovolcanic arc of the Faleme (CiscoF) is bounded to the East by the CiscoF **(Figure 30)**. The formations of the Faleme volcanic arc consist of metamorphosed volcanic and sedimentary rocks intruded by granitic and tonalitic plutons. In the past, some authors did not consider the Faleme volcanic formations to be an entity distinct from the Diale-Dalema Basin. Hirdes and Davis (2002) attribute this confusion to the fact that these rocks rarely outcrop in this area. The airborne geophysical survey clearly revealed the presence of a distinct faleme volcanic belt. The formations of this arc belong to the Kofi tectonomagmatic complex. The Faleme volcanic sequence consists of pillow andesites (the most abundant) overlain by a series of bedded rhyolites. Volcanic-clastic rocks and sediments (schists, wackes, siltstones, and conglomerates) are also present in the marginal region between the Faleme belt and the Diale-Dalema sedimentary basin (Hirdes and Davis, 2002). Plutonic intrusions of the Faleme formations are represented by the Balangouma, Faleme Sud, and Boboti plutons. The magnetic signature of the Faleme plutonovolcanic arc is defined by a region of high magnetic intensity along the Eastern margin of the study area. The areas of higher magnetic intensity generally correlate with pyroxene granodiorite and microdiorite intrusions. Extensive zones have a negative correlation. The latter zones are attributed to magnetic skarns associated with microdiorites (Technical report by the Fugro Airborne Surveys Interpretation Team, Airborne Geophysical Project 9ACP/SE/009). Magmatic intrusions on the Eastern edge of the Diale-Dalema basin were formed in a mainly active continental margin and within-plate volcanic zone setting (Faye et al.,2023). According to Ndiaye et al. (1997), the Dalema granitoids are potassium-rich, calc-alkaline in nature and similar to collision-type granitoids, with low YbN values (1.82 - 9.4) and high LaN/YbN ratios of up to 137. They are 2008 Ma ± 16 Ma old and have a low initial strontium ratio (Sri) of around 0.702, consistent with a mantle source. According to these authors (Ndiaye et al., 1997), these data seem to show that granodiorites and syenogranites originate from the same source but with different evolution. Their protolith is of mantle origin in view of the values (Dabo, 2011).

8.2.5. Sedimentary Basins of Kedougou Kenieba Inlier

1) Diale back arc basin (Diabba) = Main basin

Diabba represents the back-arc basin of the Kedougou Inlier. It is bounded to the West by the CiscoM and to the East by the CiscoF. The predominantly sedimentary formations of the Diale back-arc basin consist of detrital and silicocarbonate formations intersected by highly developed acid magmatism. The Diale-Dalema sedi-

mentary basin consists of a sedimentary pile interspersed with calc-alkaline volcanic rocks (Bassot, 1966; Dioh et al., 2006; Gueye et al., 2008). This sedimentary pile includes grauwackes, sandstones, pelites, and limestones at the base, surmounted by a pelitic and siliceous unit. Previous publications have divided the Diale Dalema basin into two distinct formations: Diale sediments (more pelitic) to the West of the Saraya batholith, and the Dalema sediments to the East (more calcareous). However, the geophysical data from this study do not confirm this segmentation.

In this study, Diabba consists of a single lithostructural unit associated with volcanoplutonic formations. Deformation in the Diale-Dalema meta-sediments is characterised by extensive arcuate to linear shear zones (Fugro Airborne Surveys Interpretation Team, 2000). The dykes represented by thin linear magnetic signatures intersect lithologies showing linear texture of Diabba; Diabba is assimilated to an overturned funnel-shaped geosynclinal megacomplex (**Figure 31**) that overlies basic, intermediate, and acid volcanism. The Diabba formations are mainly intersected by the Tinkoto and Saraya massifs, the Diabba granite near Massawa, and the Faleme plutons. The low magnetic response of the Saraya Batholith (including associated late marginal plutons) is only subtly differentiated from the Diale-Dalema metasediments. The weak magnetic response of the Saraya Batholith is in complete contrast to the high magnetic intensity characteristic of the granitic intrusions associated with the Mako and Faleme Belts, which reflect the distinct source of protoliths indicated by their peraluminous and metaluminous geochemical characteristics (e.g., Schwartz & Melcher, 2004; Dioh et al., 2006; Gueye et al., 2008). On this basis, the weak magnetic response of the Dar Salam Granodiorite (Schwartz & Melcher, 2004) on the South-western margin of the Faleme Belt indicates that it is associated with the Saraya Batholith.

The absence of penetrative deformation and the tonalitic to dioritic intrusions reflect a distinct deep crustal character, the margin along which the Saraya Batholith intruded. The strong deformation in the western metasediments reflects the buttress-like shape of the Saraya Batholith. This marginal zone was consequently a focal point for the emplacement of a series of dense mafic dykes in the Western part of the Diale-Dalema metasedimentary basin and the Western part of the Saraya Batholith. To the West, localized anastomosing deformation of calc-alkaline granites and greenstones in the Mako Belt may reflect a stiffer crustal character of a relatively old terrane arc (Fugro Airborne Surveys Interpretation Team, 2000). Certain features, such as the dykes identified by magnetic trends in the Diale-Dalema Basin and the Saraya Batholith, were never fully mapped before the acquisition of magnetic data. Their presence in the Birimian units and their absence in the Mauritanides branch indicate that they must predate the Mauritanides. Similarly, the contrast between the high intensity of the late post-tectonic granites in the volcanic belts and the discrete magnetism of the attached sediments (especially Faleme) means that this study is the first in which they have been mapped so distinctively. The negative correlation zones in the Faleme Belt are interpreted as resulting from the remanence of magnetic skarns. Comparison of the

magnetic characteristics of the Faleme Volcanic Belt intrusions with those of the Saraya Batholith (of low to moderate intensity) indicates differences reflecting the iron abundance of their respective linear protolith sources (Fugro Airborne Surveys Interpretation Team, 2000).

2) Kofi intra-continental basin (secondary basin)

Kofi basin consists of detrital metasedimentary rocks, metacarbonate rocks, and breccias (Lawrence et al., 2013; Lambert-Smith, 2016; Masurel et al., 2017). It is intruded by monzodiorites, monzogranites, and post-Paleoproterozoic mafic dykes (Baratoux et al., 2019). The Kofi series is made of metasedimentary rocks alternating with calc-alkaline volcanic flows and pyroclastics (Masurel et al., 2017).

The weak magnetic response of the Kofi Formation is reflected in two distinct sedimentary formations associated with volcanoplutonic units. The formation located on the Western side corresponds to the West Kofi series, while the second, located on the Eastern side, represents the East Kofi unit. The Kofi basin is a narrow post-Eburnian hemi-graben (**Figure 31**) opened at the end of the late Orogenic phase.

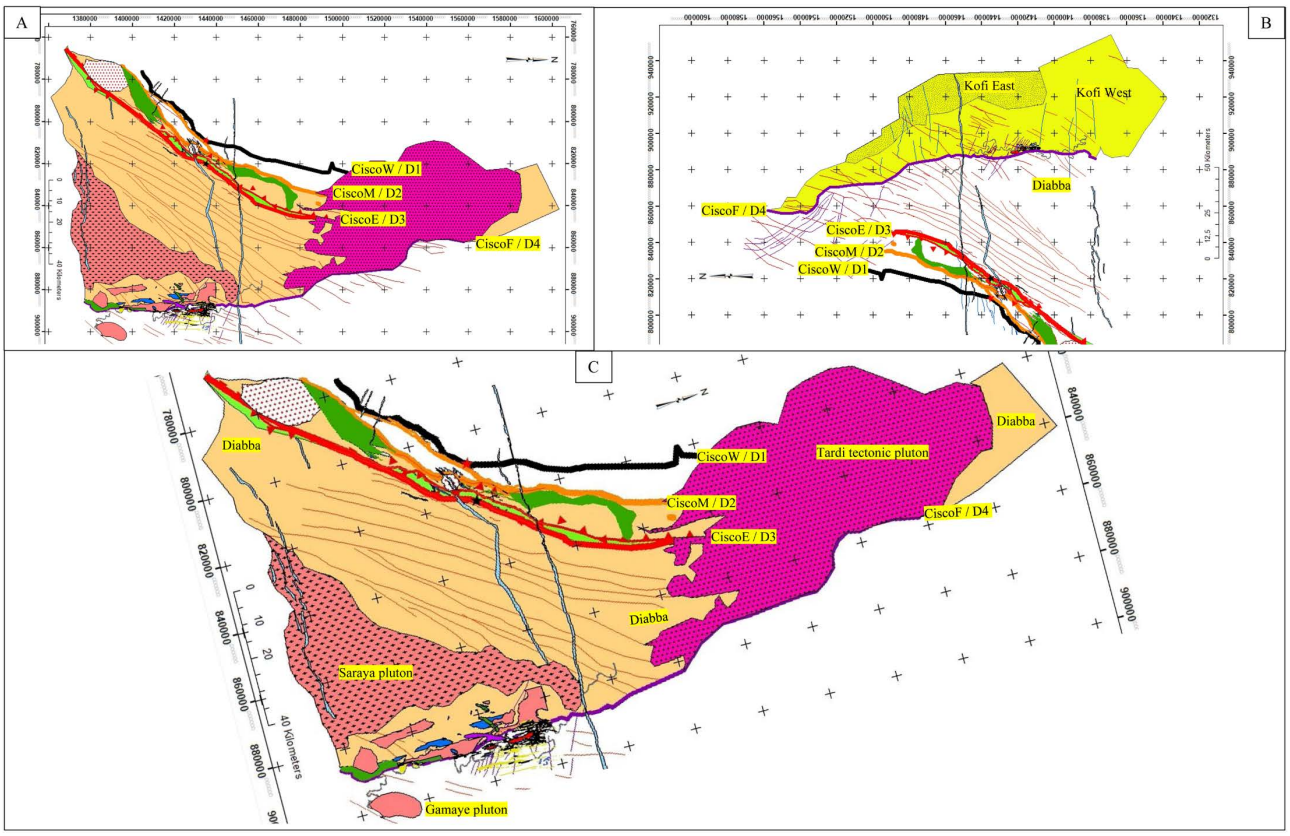

Figure 31. Kedougou Kenieba Inlier Back-arc basin and intracontinental basin. A, C: Diabba, overturned funnel-shaped basin; B: Lithostructural framework of the Diabba next to the Kofi basin.

The northern, central, and eastern parts of the Gamaye pluton are almost isotropic. However, the study of the microstructures show that these parts of the Ga-

maye pluton have also undergone solid-state deformation and dynamic recrystallization. Measurements of the anisotropy of magnetic susceptibility, conducted on about 50 samples, reveal paramagnetic signatures, with bulk susceptibilities lower than 0.5×10^{-3} SI. The shape of the magnetic fabric ranges from oblate to prolate, and the degree of anisotropy increases towards the Western limit of the pluton and the SMSZ, together with the rock strain intensity. There is also a deflection of the magnetic foliation and lineation in that direction: in particular, when approaching the western border, the magnetic fabric is dominated by NNW-SSE-trending, steeply dipping foliations (parallel to the C plane of the S-C fabrics) and gently plunging lineations (concordant with the strike-slip movement of the SMSZ). It is concluded that the Gamaye pluton has been emplaced along the SMSZ and/or has been deformed by this transcurrent regional discontinuity (Dembele et al., 2023). **Table 3** summarizes the evolution of tectonomagmatic complexes leading to the formation of arcs and basins.

Table 3. Summary of the evolution phases of Kedougou Kenieba Inlier's tectonomagmatic complexes.

Order	Context	Essential Description
1	Oceanic volcanic arc	First volcanoes formed in an oceanic context, above subduction
2	Island arc	Volcanic island chain that develops after volcanic accumulation
3	Back-arc basin	Extension zone behind island arc, sedimentary (Diabba)
4	Intracontinental volcanic arc	Magmatic activity on the continent, linked to thermal anomalies and rift (CiscoF)
5	Intracontinental basin	Internal and post-orogenic movements (Kofi)

The lithostructural architecture of Kedougou Kenieba Inlier highlights Maco, Sesam, Diabba, and Kofi tectonomagmatic complexes. The geodynamic evolution of Kedougou-Kenieba Inlier tectonomagmatic complexes (**Figure 32**) is linked to a single magmatic event associated with tectonomagmatic episodes resulting in a succession of tectonovolcanic arcs (four) associated with plutonic formations and sedimentary (two basins, Diabba and Kofi) settings. The Diale back-arc basin's architecture highlights an overturned funnel-shaped geosynclinal complex, while the Kofi basin's design reveals a hemigraben configuration that opened at the end of late orogenic phase. These arcs and basins form the belt. The volcanic arcs of Maco and the island arc of Sesam stand as belt arcs, while the arc of the back basin and the arc of the intracontinental arc represent basins' arcs. The model reflects the following tectonic progression: **Oceanic subduction** → **Volcanic formation** → **Backward extension** → **Continental reactivation** → **Continental subsidence**. Geochronological data show that the magmatic and tectonic system of the Kedougou Kenieba Inlier evolved from ocean to the heart of the continent, combining volcanism, extension, and subsidence. This architecture is very similar to that observed in active zones such as the Pacific or the margins of Asia.

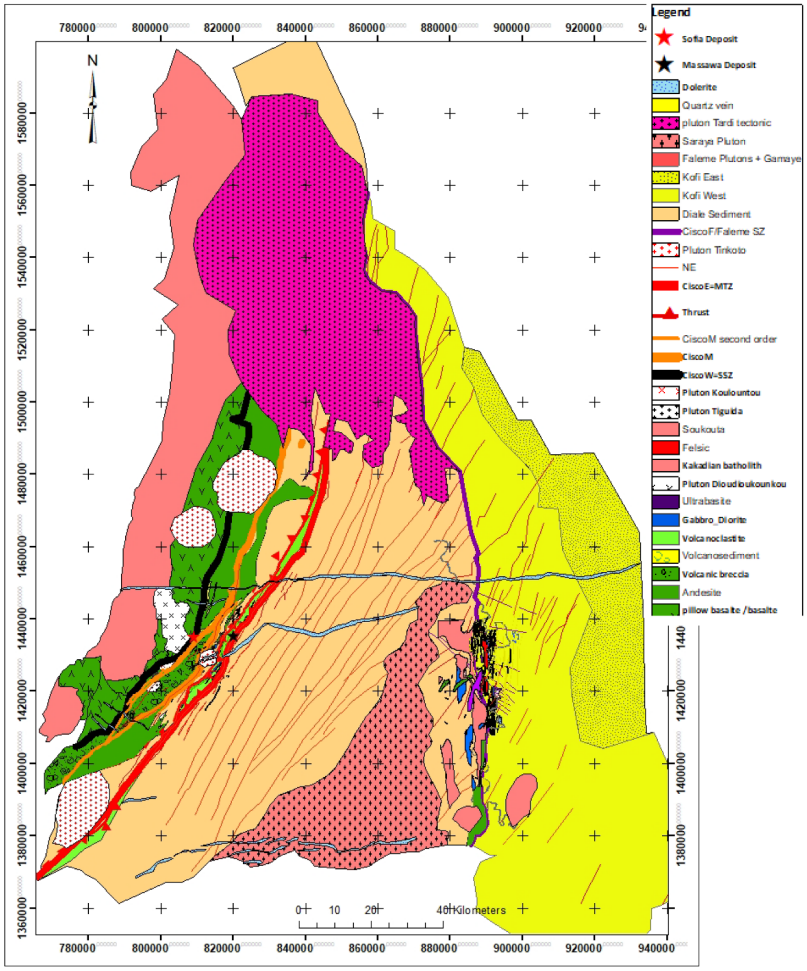

Figure 32. Latest lithostructural architecture of Kedougou-Kenieba Inlier.

9. Conclusion

The characterization of Paleoproterozoic plutonic masses, their host rocks and their implications on lithological and tectonic structuring of Kedougou-Kenieba inlier were defined in this study through an approach integrating geological mapping, petrography, structural analysis, geochemistry, geophysics, and geochronology. Results highlight a lithostructural architecture, offering a new reading of crustal evolution in Paleoproterozoic and perspectives for metallogenic analysis of the Kedougou Kenieba Inlier.

Indeed, the lithostructural and geochemical characterization of the plutonic masses shows that Dioudioukounkou is a calc-alkaline volcanic arc granite setting in an oceanic context. It is marked by a compressive active margin environment. Koulountou met aluminous granite and Tiguida peraluminous granite represent island arc granites. Tiguida is syncollisional and associated with a low percentage of light rare earths with a LaN/SmN ratio below the detection limit and a content ($Na_2O + K_2O$) of 6.89%, representing the highest alkaline content within Sesam domain. Koulountou is a post-collision uplift granite marked by a compressive active margin environment. The Tinkoto and Diabba granitoids are hosted by tholeiitic and calc-alkaline volcanic

formations intersected by calc-alkaline plutonic formations.

Maco, Sesam, and Diabba constitute, respectively, host rocks of Dioudiou-kounkou, Koulountou, Tiguida, and Tinkoto. Maco's lithologies are mainly rep-resented by metabasalts, serpentinites in tectonic contact with CiscoW (D1 = SSZ), and basic, intermediate, and acidic plutonites. Sesam is marked by a volcanic sequence formed of large andesitic rock flows alternating with volcano sedimentary facies with andesitic lithic elements, ultramafic rocks in the context of an island arc delineated to the East by the tectonic contact with CiscoM (D2) and acidic, intermediate to basic plutonites; Diabba shows a sedimentary unit associated with a volcanic sequence represented by volcanoclastites, andesitic formations. These formations are intersected by large plutonic masses and small plutonites, such as serpentinite lenses in tectonic contact with the CiscoE (MTZ=D3). Diabba formation is limited to the East by the CiscoF (D4), defined at the level of Faleme shear.

The magmatism behavior was defined from a comparative geochemical study of the large plutonic masses of Maco, Sesam, and Diabba and their country rocks. Results reveal calc-alkaline volcanism, calc-alkaline plutonism, tholeiitic volcanism, and tholeiitic plutonism. Calc-alkaline volcanism occurs at Maco, Sesam, and Diabba. Calc-alkaline plutonism is notable in Maco, Sesam, and Diabba. The tholeiitic volcanism of the Mako-Diale Transition Zone (ZTMD) has not been intersected at Maco. It is represented in the Sesam and Diabba domains. Tholeiitic plutonism is found exclusively in Maco. All large plutonic masses show calc-alkaline signatures.

Geochronological results show that the Dioudioukounkou granite yielded a concordant U-Pb zircon age of 2156.1 Ma ± 5.6 Ma. This seems to correspond to the major magmatic activity phase of the Eburnean orogeny and is associated with the early Eburnean deformation CiscoW (SSZ=D1). Tinkoto and Koulountou plutons were emplaced at 2109.3 Ma ± 6.0 Ma and 2106.7 Ma ± 8.1 Ma, respectively. They intruded Sesam and Diabba at the early transpressive tectonic Eburnean deformation phase CiscoM (D2). Tinkoto pluton predates and is related to CiscoM main shear, while Koulountou granite is related to CiscoM second-order structures. Plutonic masses from Maco, Sesam, and Diabba were formed predominantly during the Eburnean orogeny, with ages ranging between 2156 Ma and 2106 Ma. A period associated to a critical phase of crustal growth and intensive magmatic activity.

Geophysical signatures reflect the succession of tectonovolcanic arcs and sedimentary basins. The tectonovolcanic arcs are represented by strong magnetic signatures zones corresponding from West to East, to tectonovolcanic arc within oceanic volcanic arc context associated to CiscoW(SSZ=D1), the tectonovolcanic arc within Island arc context associated to CiscoM (D2), the tectonovolcanic arc within Back-arc basin context associated to CiscoE (MTZ = D3), and the Faleme tectonovolcanic arc within intra-continental volcanic arc context associated to CiscoF (= D4). These tectonovolcanic arcs and plutonites form together the belt

Basins defined within low to medium magnetic zones are mainly represented

by Diale back-arc basin (Diabba) and Kofi intra-continental basin.

The latest lithostructural architecture of Kedougou Kenieba Inlier highlights Maco, Sesam, Diabba, and Kofi tectonomagmatic complexes. The geodynamic evolution of these complexes is linked to a single magmatic event associated with tectonomagmatic episodes resulting from the succession of tectonovolcanic arcs associated with plutonites and a sedimentary setting. Diabba, representing the back-arc basin, highlights an overturned funnel-shaped geosynclinal architecture, while the Kofi intracontinental basin reveals a hemi-graben design opened at the end of the late Orogenic phase.

Kedougou-Kenieba Inlier is a great example of the close links between metamorphism, regional scale deformation, and granite generation and emplacement. A cross-analysis of plutonic masses and hosted formations of Kedougou Kenieba Inlier reveals a lithostructural architecture shaped by interconnected magmatic and tectonic mechanisms. Global data from this study highlights a geodynamic architecture integrating the constraints associated with pluton emplacement and regional deformation. This design reflects following tectonic progression: **Oceanic subduction → Volcanic formation → Backward extension → Continental reactivation → Continental subsidence** and is strengthened by geochronological data showing that magmatic and tectonic system of Kedougou Kenieba Inlier evolved from ocean to the heart of the continent, combining volcanism, extension, and subsidence. This architecture is very similar to that observed in active zones such as Pacific or margins of Asia.

Acknowledgements

The authors thank the Department of Earth Sciences at the University of Geneva for QUEMSCAN analysis, the University of Lausanne for carrying out the geochemical analyses via XRF or X-ray fluorescence spectrometry and LA-ICP-MS zircon analysis, and finally, thanks the laboratory of the UFR Earth Sciences and mineral resources of Félix Houphouët-Boigny University for the production of the thin and polished sections samples. Authors also would like to thank the three anonymous reviewers for their technical comments and useful observations, which helped to improve the scientific quality of the manuscript.

Conflicts of Interest

The authors declare no conflicts of interest regarding the publication of this paper.

References

Abouchami, W., Boher, M., Michard, A., & Albarede, F. (1990). A Major 2.1 Ga Event of Mafic Magmatism in West Africa: An Early Stage of Crustal Accretion. *Journal of Geophysical Research: Solid Earth, 95,* 17605-17629. https://doi.org/10.1029/jb095ib11p17605

Allibone, A., Lawrence, D., Scott, J., Fanning, M., Lambert-Smith, J., Stenhouse, P. et al. (2020). Chapter 7: Paleoproterozoic Gold Deposits of the Loulo District, Western Mali. In R. H. Sillitoe et al. (Eds.), *Geology of the World's Major Gold Deposits and Provinces*

(pp. 141-162). Society of Economic Geologists. https://doi.org/10.5382/SP.23.07

Attoh, K., Evans, M. J., & Bickford, M. E. (2006). Geochemistry of an Ultramafic-Rodingite Rock Association in the Paleoproterozoic Dixcove Greenstone Belt, Southwestern Ghana. *Journal of African Earth Sciences, 45,* 333-346. https://doi.org/10.1016/j.jafrearsci.2006.03.010

Baratoux, L., McFarlane, H. B., Ailleres, L., Betts, P., Ganne, J., Jessell, M. W. et al. (2019). Episodic Collisional Orogenesis and Lower Crust Exhumation during the Palaeoproterozoic Eburnean Orogeny: Evidence from the Sefwi Greenstone Belt, West African Craton. *Precambrian Research, 325,* 88-110. https://doi.org/10.1016/j.precamres.2019.02.012

Baratoux, L., Metelka, V., Naba, S., Jessell, M. W., Grégoire, M., & Ganne, J. (2011). Juvenile Paleoproterozoic Crust Evolution during the Eburnean Orogeny (~2.2-2.0ga), Western Burkina Faso. *Precambrian Research, 191,* 18-45. https://doi.org/10.1016/j.precamres.2011.08.010

Bassot, J. P. (1963). *Etude géologique du Sénégal oriental et des confins guinéo-maliens.* Ph.D. Thesis, Clermont Auvergne University.

Bassot, J. P. (1966). Etude géologique du Sénégal Oriental & de ses confins Guinéo-maliens. *Mémoire BRGM, n˚40,* 332.

Bassot, J. P. (1987). Le complexe volcano-plutonique calco-alcali de la rivière daléma (Est Sénégal): Discussion de sa signification géodynamique dans le cadre de l'orogénie eburnéenne (protérozoïque inférieur). *Journal of African Earth Sciences (1983), 6,* 505-519. https://doi.org/10.1016/0899-5362(87)90091-1

Bassot, J. P., & Caen-Vachette, M. (1984). *Données géochronologiques nouvelles sur les granitoïdes de l'EST du Sénégal: Implication sur l'histoire du Birimien de cette region* (pp. 191-209). Géologie Africaine Tervuren.

Batchelor, R. A., & Bowden, P. (1985). Petrogenetic Interpretation of Granitoid Rock Series Using Multicationic Parameters. *Chemical Geology, 48,* 43-55.

Bessoles, B. (1977). *Géologie de l'Afrique, Craton Ouest Africain* (p. 404). BRGM.

Beziat, D., Bourges, F., Debat, P., Lompo, M., Martin, F., & Tollon, F. (2000). A Paleoproterozoic Ultramafic-Mafic Assemblage and Associated Volcanic Rocks of the Boromo Greenstone Belt: Fractionates Originating from Island-Arc Volcanic Activity in the West African Craton. *Precambrian Research, 101,* 25-47. https://doi.org/10.1016/s0301-9268(99)00085-6

Billa, M., Feybesse, J., Bronner, G., Lerouge, C., Milesi, J., Traoré, S. et al. (1999). Les formations à quartzites rubanés ferrugineux des Monts Nimba et du Simandou: Des unités empilées tectoniquement, sur un « soubassementplutonique Archéen (craton de Kénéma-Man), lors de l'orogène Éburnéen. *Comptes Rendus de l'Académie des Sciences—Series IIA—Earth and Planetary Science, 329,* 287-294. https://doi.org/10.1016/s1251-8050(99)80248-1

Bodin, L. (1951). Contribution à l'étude des granites birimiens de l'A.G.F. *Bulletin de la Direction des Mines de l'A.O.F., Dakar, No. 6,* 24-62.

Boher, M., Abouchami, W., Michard, A., Albarede, F., & Arndt, N. T. (1992). Crustal Growth in West Africa at 2.1 Ga. *Journal of Geophysical Research: Solid Earth, 97,* 345-369. https://doi.org/10.1029/91jb01640

Bundesanstalt für Geowissenschaften und Rohstoffe, Hannover (1998). Geologie de la Region Haute Comoe Nord: *Projet de Cooperation geologique Ivoiro-Allemande* (1992-1994 & 1995-1996). Republique de cote d'Ivoire, Ministère des.../Direction de la Geologie. Bulletin No. 1 + 2.

Cabanis, B., & Lecolle, M. (1989). Le diagramme La/10-Y/15-Nb/8: Un outil pour la dis

crimination des séries volcaniques et la mise en évidence des processus de mélange et/ou de contamination crustale. *Sciences de la Terre, 309,* 2023-2029.

Calvez, J.Y., Feybesse, J.L., Ledru, P., & Milesi, J.P. (1990). Géochronologie du Protérozoïque inférieur du craton ouest-africain (Méthode d'évaporation directe de zircons isolés). In *13ème Réunion des Sciences de la Terre* (p. 26).

Castaing, C., Billa, M., Milesi, J. P., Thiéblemont, D., Le Metour, J., Egal, E., Donzeau, M., Guerrot, C., Cocherie, E. A., Chevremont, P., Tegyey, M., Itard, Y., Zida, B., Ouédraogo, I., Koté, S., Kaboré, B. E., Ouédraogo, C., Ki, J. C., & Zunino, C. (2003). *Notice explicative de la Carte géologique et minière du Burkina Faso à 1/1 000 000*. Bureau de Recherches Géologiques et Minières.

Cissokho, S. (2010). *Etude géologique du secteur de Mako (partie méridionale du supergroupe de Mako, boutonnière de Kédougou-Kéniéba, Sénégal oriental): Implications sur la diversité magmatique.* Master's Thesis, Cheikh Anta Diop University.

Cox, K. G., Bell, J. D., & Pankhurst, R. J. (1979). *The Interpretation of Igneous Rocks* (p. 450). Unwin Hyman Ltd.

Dabo, M. (2011). *Tectonique et minéralisations aurifères dans les formations birimiennes de Frandi-Boboti, boutonnière de Kédougou-Kéniéba, Sénégal.* Ph.D. Thesis, University of Rennes 1, 233 p.

Dabo, M., & Aïfa, T. (2010). Structural Styles and Tectonic Evolution of the Kolia-Boboti Sedimentary Basin, Kédougou-Kéniéba Inlier, Eastern Senegal. *Comptes Rendus. Géoscience, 342,* 796-805. https://doi.org/10.1016/j.crte.2010.06.002

Dabo, M., & Aïfa, T. (2013). Pure Shear to Simple Shear-Dominated Transpression during the Eburnean Major D_2 Deformation, Daléma Sedimentary Basin, Eastern Senegal. *International Geology Review, 55,* 1073-1086. https://doi.org/10.1080/00206814.2012.760711

Dabo, M., Aïfa, T., Gassama, I., & Ngom, P. M. (2018). Thrust to Transpression and Transtension Tectonics during the Paleoproterozoic Evolution of the Birimian Greenstone Belt of Mako, Kédougou-Kéniéba Inlier, Eastern Senegal. *Journal of African Earth Sciences, 148,* 14-29. https://doi.org/10.1016/j.jafrearsci.2018.05.010

Dabo, M., Aïfa, T., Gning, I., Faye, M., Ba, M. F., & Ngom, P. M. (2017). Lithological Architecture and Petrography of the Mako Birimian Greenstone Belt, Kédougou-Kéniéba Inlier, Eastern Senegal. *Journal of African Earth Sciences, 131,* 128-144. https://doi.org/10.1016/j.jafrearsci.2017.04.005

Dampare, S. B., Shibata, T., Asiedu, D. K., Okano, O., Osae, S. K. D., Atta-Peters, D. et al. (2019). Ultramafic-Mafic and Granitoids Supra-Subduction Magmatism in the Southern Ashanti Volcanic Belt, Ghana: Evidence from Geochemistry and Nd Isotopes. *Geological Journal, 55,* 2495-2531. https://doi.org/10.1002/gj.3512

Dembele, A., Bolle, O., Pujol, M., Dabo, M., & Bouaré, M. L. (2023). The Gamaye Pluton: A Tectonic Marker of the Early Eburnean (Birimian) Orogeny in the Kédougou-Kéniéba Inlier (West African Craton). In *The GBL Meeting 2024*. Université de Liège.

DePaolo, D. J. (1981). Nd Isotopic Studies: Some New Perspectives on Earth Structure and Evolution. *Eos, Transactions American Geophysical Union, 62,* 137-137. https://doi.org/10.1029/eo062i014p00137-01

Dessimoulie, L. (2019). *Apports de la géochimie élémentaire et isotopique pour la compréhension des processus de serpentinisation: Cas de la dorsale sud-ouest indienne.* Master's Thesis, Université Clermont Auvergne.

Dia, A. (1988). *Caractère et signification des complexes magmatiques et métamorphiques du secteur de Sandikounda-Laminia (Nord de la boutonnière de Kédougou, Est du Sénégal): Un modèle géodynamique du Birimien de l'Afrique de l'Ouest.* Master's Thesis,

Cheikh Anta Diop University.

Dia, A., Van Schmus, W. R., & Kröner, A. (1997). Isotopic Constraints on the Age and Formation of a Palaeoproterozoic Volcanic Arc Complex in the Kedougou Inlier, Eastern Senegal, West Africa. *Journal of African Earth Sciences, 24,* 197-213. https://doi.org/10.1016/s0899-5362(97)00038-9

Diallo, M., Baratoux, L., Dufréchou, G., Jessell, M. W., Vanderhaeghe, O., Ly, S. et al. (2020). Structure of the Paleoproterozoic Kédougou-Kéniéba Inlier (Senegal-Mali) Deduced from Gravity and Aeromagnetic Data. *Journal of African Earth Sciences, 162,* 103732. https://doi.org/10.1016/j.jafrearsci.2019.103732

Diene, M., Gueye, M., Diallo, D. P., & Dia, A. (2012). Structural Evolution of a Precambrian Segment: Example of the Paleoproterozoic Formations of the Mako Belt (Eastern Senegal, West Africa). *International Journal of Geosciences, 3,* 153-165. https://doi.org/10.4236/ijg.2012.31017

Dioh, E. (1986). *Etude des roches magmatiques Birimiennes de la région de Sonfara-Laminia—Médina Foulbé (Sénégal Oriental).* Master's Thesis, University of Nancy I.

Dioh, E., Beziat, D., Debat, P., Grégoire, M., & Ngom, P. M. (2006). Diversity of the Palaeoproterozoic Granitoids of the Kédougou Inlier (Eastern Sénégal): Petrographical and Geochemical Constraints. *Journal of African Earth Sciences, 44,* 351-371. https://doi.org/10.1016/j.jafrearsci.2005.11.024

Dioh, E., Debat, P., Dia, A., Pons, J., Rocci, G., & Rollet, M. (1990). Caractérisation d'un complexe rubané dans les formations Birimiennes de la partie septentrionale de la boutonnière de Kédougou—Kéniéba. *Comptes Rendus de l'Académie des Sciences, Série II, 310,* 935-940.

Escario Perez, S. (2018). *Flux hydrothermaux dans le manteau lithosphérique: Étude expérimentale du processus de serpentinisation*. Thèse de doctorat, Université de Montpellier.

Fabre, R., Matheis, G., & Utke, A. W. (1987). Caractérisation géochimique du magmatisme birimien dans le centre de la Côte d'Ivoire (Afrique de l'Ouest). Ses implications géodynamiques. In G. Matheis, & H. Schandelmeier (Eds.), *Current Research in African Earth Sciences: Extended Abstracts of the 14th Colloquium on African Geology* (pp. 21-24). CRC Press.

Faye, C. I., Ndiaye, A. A., Dia, I., Diene, M., Gueye, M., Grosjean, M. et al. (2023). Magmatic Arc Construction within the Kedougou-Kenieba Inlier, Eastern Senegal: Petrographic, Lithogeochemical and Radiogenic Isotope Constraints. *Journal of African Earth Sciences, 208,* Article ID: 105076. https://doi.org/10.1016/j.jafrearsci.2023.105076

Feybesse, J., & Milesi, J. (1994). The Archaean/Proterozoic Contact Zone in West Africa: A Mountain Belt of Décollement Thrusting and Folding on a Continental Margin Related to 2.1 Ga Convergence of Archaean Cratons? *Precambrian Research, 69,* 199-227. https://doi.org/10.1016/0301-9268(94)90087-6

Feybesse, J.-L., Milesi, J.-P., Ouedraogo, M., & Prost, A. (1990). La «ceinture» proté-rozoïque inférieur de Boromo-Goren (Burkina Faso), un exemple d'interférence entre deux phases transcurrentes éburnéennes. *Comptes Rendus de l'Académie des Sciences, Série 2, Mécanique, Physique, Chimie, Sciences de l'univers, Sciences de la Terre, 310,* 1353-1360.

Fugro Airborne Surveys Interpretation Team (2000). *Technical Report of the Fugro Airborne Surveys Interpretation Team: Airborne Geophysical Project 9ACP/SE/009*. Ministère des Mines, de l'Énergie et de l'Hydraulique, République du Sénégal.

Gasquet, D., Barbey, P., Adou, M., & Paquette, J. L. (2003). Structure, Sr–nd Isotope Geo-

chemistry and Zircon U–pb Geochronology of the Granitoids of the Dabakala Area (côte d'Ivoire): Evidence for a 2.3 Ga Crustal Growth Event in the Palaeoproterozoic of West Africa? *Precambrian Research, 127,* 329-354. https://doi.org/10.1016/s0301-9268(03)00209-2

Gueye, M. (1995). *Étude géologique et géochronologique du secteur Saraya-Moussala (Sud-Est du Sénégal): Implications sur l'évolution géodynamique du Birimien.* Ph.D. Thesis, Université Cheikh Anta Diop, 245 p.

Gueye, M., Ngom, P. M., Diène, M., Thiam, Y., Siegesmund, S., Wemmer, K. et al. (2008). Intrusive Rocks and Tectono-Metamorphic Evolution of the Mako Paleoproterozoic Belt (Eastern Senegal, West Africa). *Journal of African Earth Sciences, 50,* 88-110. https://doi.org/10.1016/j.jafrearsci.2007.09.013

Gueye, M., Siegesmund, S., Wemmer, K., Pawlig, S., Drobe, M., Nolte, N. et al. (2007). New Evidences for an Early Birimian Evolution in the West African Craton: An Example from the Kedougou-Kenieba Inlier, Southeast Senegal. *South African Journal of Geology, 110,* 511-534. https://doi.org/10.2113/gssajg.110.4.511

Guillou, J.-J., Ndiaye, P. M., & Samama, J.-C. (2009) Critères de reconnaissance et rôle métallogénique d'une paleo-surface à un milliard d'années: Cas de la boutonnière de Kédougou-Kéniéba (Sénégal, Mali). *Journal des Sciences et Technologies, No. 7,* 1-15.

Hirdes, W., & Davis, D. W. (2002). U-Pb Geochronology of Paleoproterozoic Rocks in the Southern Part of the Kédougou-Kénieba Inlier, Senegal, West Africa: Evidence for Diachronous Accretionary Development of the Eburnean Province. *Precambrian Research, 118,* 83-99. https://doi.org/10.1016/S0301-9268(02)00080-3

Hirdes, W., Davis, D. W., & Eisenlohr, B. N. (1992). Reassessment of Proterozoic Granitoid Ages in Ghana on the Basis of U/Pb Zircon and Monazite Dating. *Precambrian Research, 56,* 89-96. https://doi.org/10.1016/0301-9268(92)90085-3

https://doi.org/10.1016/0009-2541(85)90034-8

Irvine, T. N., & Baragar, W. R. A. (1971). A Guide to the Chemical Classification of the Common Volcanic Rocks. *Canadian Journal of Earth Sciences, 8,* 523-548. https://doi.org/10.1139/e71-055

Junner, N. R. (1940). Geology of the Gold Coast and Western Togoland. *Gold Coast Geological Survey Bulletin, No. 11,* 40.

Labou, I., Benoit, M., Baratoux, L., Grégoire, M., Ndiaye, P. M., Thebaud, N. et al. (2019). Petrological and Geochemical Study of Birimian Ultramafic Rocks within the West African Craton: Insights from Mako (Senegal) and Loraboué (Burkina Faso) Lherzolite/harzburgite/wehrlite Associations. *Journal of African Earth Sciences, 162,* Article ID: 103677. https://doi.org/10.1016/j.jafrearsci.2019.103677

Lambert-Smith, J. S., Lawrence, D. M., Müller, W., & Treloar, P. J. (2016). Palaeotectonic Setting of the South-Eastern Kédougou-Kéniéba Inlier, West Africa: New Insights from Igneous Trace Element Geochemistry and U-Pb Zircon Ages. *Precambrian Research, 274,* 110-135. https://doi.org/10.1016/j.precamres.2015.10.013

Laurent, O., Zeh, A., & Gerdes, A. (2014). Petrogenesis and Geochronology of a Post-Orogenic Calc-Alkaline Magmatic Association: The Žulová Pluton, Bohemian Massif. *Journal of Geosciences, 59,* 415-440. https://doi.org/10.3190/jgeosci.176

Lawrence, D. M., Treloar, P. J., Rankin, A. H., Harbidge, P., & Holliday, J. (2013). The Geology and Mineralogy of the Loulo Mining District, Mali, West Africa: Evidence for Two Distinct Styles of Orogenic Gold Mineralization. *Economic Geology, 108,* 199-227. https://doi.org/10.2113/econgeo.108.2.199

Le Bas, M. J., Le Maitre, R. W., Streckeisen, A., & Zanettin, B. (1986). A Chemical Classification of Volcanic Rocks Based on the Total Alkali-Silica Diagram. *Journal of Petrology,*

27, 745-750. https://doi.org/10.1093/petrology/27.3.745

Ledru, P., Pons, J., Milesi, J. P., Dommanget, A., Johan, V., Diallo, M., et al. (1989). Tec tonique transcurrente et évolution polycyclique dans le birimien, protérozoïqueinféri eur, du Sénégal-Mali (Afrique de l'ouest). *Comptes rendus de l'Académie des Sciences, 308,* 117-122.

Ledru, P., Pons, J., Milesi, J. P., Feybesse, J. L., & Johan, V. (1991). Transcurrent Tectonics and Polycyclic Evolution in the Lower Proterozoic of Senegal-Mali. *Precambrian Research, 50,* 337-354. https://doi.org/10.1016/0301-9268(91)90028-9

Loh, G., & Hirdes, W. (1996). The Structural Development of the Paleoproterozoic Birmian and Tarkwaian Rocks of Southwestern Ghana. *Geologisches Jahrbuch D, 100,* 517-546.

Loh, G., & Hirdes, W. (1999). Explanatory Notes for the Geological Map of Southwest Ghana 1:100,000 Sekondi (0402A) and Axim (0403B) Sheets. *Bulletin of the Ghana Geological Survey, 49,* 149.

Lompo, M. (2010). Paleoproterozoic Structural Evolution of the Man-Leo Shield (West Africa). Key Structures for Vertical to Transcurrent Tectonics. *Journal of African Earth Sciences, 58,* 19-36. https://doi.org/10.1016/j.jafrearsci.2010.01.005

Masurel, Q., Thébaud, N., Miller, J., Ulrich, S., Hein, K. A. A., Cameron, G. et al. (2017). Sadiola Hill: A World-Class Carbonate-Hosted Gold Deposit in Mali, West Africa. *Economic Geology, 112,* 23-47. https://doi.org/10.2113/econgeo.112.1.23

Meschede, M. (1986). A Method of Discriminating between Different Types of Mid-Ocean Ridge Basalt and Continental Tholeiites with the Nb-Zr-Y Diagram. *Chemical Geology, 56,* 207-218. http://dx.doi.org/10.1016/0009-2541(86)90004-5

Milesi, J. P., Dommanget, A., Johan, V., & Diallo, M. (1989). Lower Proterozoïc Succession in Senegal and Mali (West Africa): Position of Sediment-Hosted Au and Fe Deposits of Loulo Area and Significance in Terms of Crustal Evolution. In *The 28th International Geological Congress* (pp. 2-3).

Milesi, J., Ledru, P., Feybesse, J., Dommanget, A., & Marcoux, E. (1992). Early Protero-Zoic Ore Deposits and Tectonics of the Birimian Orogenic Belt, West Africa. *Precambrian Research, 58,* 305-344. https://doi.org/10.1016/0301-9268(92)90123-6

Ndiaye, M. C., Ndiaye, M., Ngom, P. M., Diagne, M., Moscariello, A., & Haller, A. D. (2025). Sesam, toward a Mature Magmatic Arc Sourced from Tholeiitic Volcanisms and Calc-Alkaline Volcanoplutonism within Kedougou-Kenieba Inlier, South-East Senegal/West Africa. *Journal of Geoscience and Environment Protection, 13,* 331-386. https://doi.org/10.4236/gep.2025.131018

Ndiaye, P. M., Dia, A., Vialette, Y., Diallo, D. P., Ngom, P. M., Sylla, M. et al. (1997). Données pétrographiques, geochimiques et géochronologiques nouvelles sur les granitoïdes du Paléoprotérozoïque du Supergroupe de Dialé-Daléma (Senégal Oriental): Implications pétrogénétiques et géodynamiques. *Journal of African Earth Sciences, 25,* 193-208. https://doi.org/10.1016/s0899-5362(97)00098-5

Ngom, P. M. (1995). *Caractérisation de la croûte Birimienne dans les parties centrale et méridionale du super-groupe de Mako. Implications géochimiques et pétrogénétiques.* Master's Thesis, Cheikh Anta Diop University.

Ngom, P. M., Cordani, U. G., Teixeira, W., & Janasi, V. D. A. (2010). Sr and Nd Isotopic Geochemistry of the Early Ultramafic-Mafic Rocks of the Mako Bimodal Volcanic Belt of the Kedougou-Kenieba Inlier (Senegal). *Arabian Journal of Geosciences, 3,* 49-57. https://doi.org/10.1007/s12517-009-0051-3

Ngom, P. M., Guèye, M., Cissokho, S., Joron, J. L., Treuil, M., & Dabo, M. (2008). Étude géochimique et pétrographique des roches vertes du supergroupe de Mako: Implications pour les interactions fluide-roche et la métallogénie régionale. *Journal des Sciences et*

Technologies, 4, 52-71.

Ngom, P. M., Rocci, G., Debat, P., Dia, A., Diallo, D. P., Dioh, E., & Sylla, M. (1998). Les massifs basiques et ultrabasiques Birimiens du super-groupe de Mako (Sénégal Orien tal): Pétrographie, géochimie et signification pétrogénétique. *Bull. L'IFAN Cheikh Anta Diop, Dakar, Sénégal, T. 49, Sér. A, No. 2,* 33-54.

Ouedraogo, A. (1985). *Etude de quelques unités plutoniques basiques éburnéennes dans le sillon de Bouroum Yalogo au NE du Burkina Faso.* Master's Thesis, University of Nancy I.

Pawlig, S., Gueye, M., Klischies, R., Schwarz, S., Wemmer, K., & Siegesmund, S. (2006). Geochemical and Sr-Nd Isotopic Data on the Birimian of the Kedougou-Kenieba Inlier (Eastern Senegal): Implications on the Palaeoproterozoic Evolution of the West African Craton. *South African Journal of Geology, 109,* 411-427. https://doi.org/10.2113/gssajg.109.3.411

Pearce, J. A. (1982). Trace Elements Characteristics of Lavas from Destructive Plate Bound Aries. In R. S. Thorpes (Ed.), *Andesites* (pp. 525-548). Wiley.

Pearce, J. A., & Gale, G. H. (1977). Identification of Ore-Deposition Environment from Trace-Element Geochemistry of Associated Igneous Host Rocks. *Geological Society, London, Special Publications, 7,* 14-24. https://doi.org/10.1144/gsl.sp.1977.007.01.03

Pearce, J. A., Harris, N. B. W., & Tindle, A. G. (1984). Trace Element Discrimination Diagrams for the Tectonic Interpretation of Granitic Rocks. *Journal of Petrology, 25,* 956-983. https://doi.org/10.1093/petrology/25.4.956

Pons, J., Barbey, P., Dupuis, D., & Léger, J. M. (1995). Mechanisms of Pluton Emplacement and Structural Evolution of a 2.1 Ga Juvenile Continental Crust: The Birimian of South-western Niger. *Precambrian Research, 70,* 281-301. https://doi.org/10.1016/0301-9268(94)00048-v

Pouclet, A., Doumbia, S., & Vidal, M. (2006). Geodynamic Setting of the Birimian Volcanism in Central Ivory Coast (Western Africa) and Its Place in the Palaeoproterozoic Evolution of the Man Shield. *Bulletin de la Société Géologique de France, 177,* 105-121. https://doi.org/10.2113/gssgfbull.177.2.105

Pouclet, A., Vidal, M., Delor, C., Siméon, Y., & Alric, G. (1996). Le volcanisme birimien du nord-est de la Côte d'Ivoire, mise en évidence de deux phases volcanotectoniques distinctes dans l'évolution géodynamique du Paléoprotérozoïque. *Bulletin de la Société Géologique de France, 167,* 529-541.

Roques, J. (1986). *In Dioh, M. Étude géologique du secteur de Tomboronkoto (Sénégal oriental).* Mémoire de maîtrise, Université Cheikh Anta Diop.

Roques, M. (1948). Le Precambrien de l'Afrique occidentale francaise. *Bulletin de la Société Géologique de France, 5,* 589-628. https://doi.org/10.2113/gssgfbull.s5-xviii.8-9.589

Sangare, A. (2008). *Les roches ultramafiques et mafiques Paléoprotérozoïques de la ceinture de roches vertes de Kadiolo (Mali). Pétrologie, évolution et ressources minérales associées.* Ph.D. Thesis, Sidi Mohamed Ben Abdellah University.

Schwartz, M. O., & Melcher, F. (2004). The Falémé Iron District, Senegal. *Economic Geology, 99,* 917-939. https://doi.org/10.2113/gsecongeo.99.5.917

Shand, S. J. (1943). *Eruptive Rocks: Their Genesis, Composition, Classification, and Their Relation to Ore Deposits with a Chapter on Meteorites*. John Wiley and Sons.

Sun, S. S., & McDonough, W. F. (1989). Magmatic Differentiation and Mineralization of Iron-Rich Tholeiites from the Archean Komati Formation, Barberton Mountain Land, South Africa. *Chemical Geology, 75,* 35-57.

Sun, S., & McDonough, W. F. (1995). Chemical and Isotopic Systematics of Oceanic Bas-

alts: Implications for Mantle Composition and Processes. *Geological Society, London, Special Publications, 42,* 313-345. https://doi.org/10.1144/gsl.sp.1989.042.01.19

Taylor, P. N., Moorbath, S., Leube, A., & Hirdes, W. (1992). Early Proterozoic Crustal Evolution in the Birimian of Ghana: Constraints from Geochronology and Isotope Geochemistry. *Precambrian Research, 56,* 97-111.

Taylor, S. R., McLennan, S. M., & McCulloch, M. T. (1988). Geochemical Constraints on the Growth of the Continental Crust. *Chemical Geology, 70,* 1-24.

Vidal, L., Ménot, G., Joly, C., Bruneton, H., Rostek, F., Çağatay, M. N. et al. (2010). Hydrology in the Sea of Marmara during the Last 23 Ka: Implications for Timing of Black Sea Connections and Sapropel Deposition. *Paleoceanography, 25,* PA1205. https://doi.org/10.1029/2009pa001735

Witschard, F. (1965). *Contribution à l'étude géologique, pétrographique et métallogénique des massifs granitiques du Sénégal oriental.* B.R.G.M. No. 44.

Zonou, S. (1987). *Les formations leptino-amphibolitiques et le complexe volcanique et volcano-sédimentaire du Protérozoïque inférieur de Bouroum-nord (Burkina-Faso, Afrique de l'Ouest): Etude pétrographique, géochimique, approche pétrogénétique et évolution géodynamique.* Ph.D. Thesis, University of Nancy 1.